A statically balanced mobile arm support

Based on a novel spring system

M. P. Lustig

Faculty Mechanical, Maritime and Materials Engineering

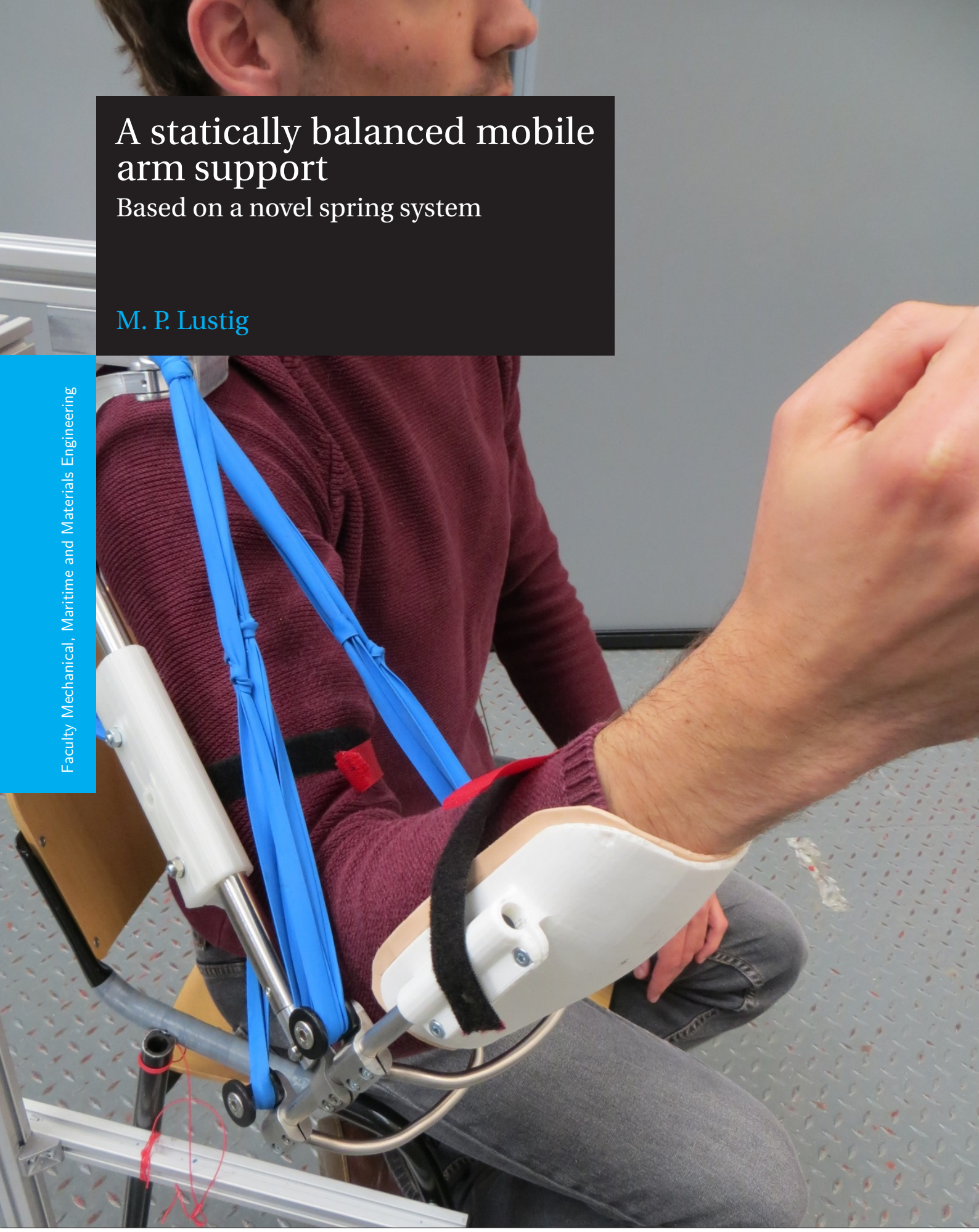

TU Delft Delft University of Technology

Challenge the future

A STATICALLY BALANCED MOBILE ARM SUPPORT

BASED ON A NOVEL SPRING SYSTEM

by

M. P. Lustig

in partial fulfillment of the requirements for the degree of

Master of Science
in Mechanical Engineering

at the Delft University of Technology,
to be defended publicly on Tuesday July 10, 2015 at 13:30.

Supervisors:	Prof. dr. ir. J. L. Herder,	TU Delft
	Ir. A. G. Dunning,	TU Delft
Thesis committee:	Dr. S. H. Hossein Nia Kani,	TU Delft
	Prof. dr. ir. H. van der Kooij,	TU Delft

An electronic version of this thesis is available at http://repository.tudelft.nl/.

TU Delft Delft University of Technology

CONTENTS

INTRODUCTION

In this thesis, the research I performed on the topic of a statically balanced arm support is reported. The main contribution is presented in two papers. The first is focused on a method for designing statically balanced serial linkages, using zero-free-length springs, without the need for auxiliary links. In this paper design equations for a statically balanced system are obtained from energy equations, by obeying these equations balance is ensured. Additionally, a graphical representation of the behavior is made, providing insight in the underlying principles of balancing serial linkage. The second paper is on designing a statically balanced mobile arm support based on a spring system obtained with the method described in the first paper. To realize a close-to-body fit new technology is introduced for creating hollow spring structures that fit around the human body. The resulting system is evaluated in an experiment. In addition to the papers multiple appendices are included in this report. In these appendixes different topics like new principles, statically balancing, prototypes, experimental results and Matlab code are presented.

1

PAPER 1

1.1. CARTESIAN BASED STIFFNESS MATRIX APPROACH AND GRAPHICAL REPRESENTATION FOR DESIGNING STATICALLY BALANCED LINKAGES

This paper is focused on designing statically balanced serial linkages and has two main objectives.

The first is to create stiffness matrix method, based on Cartesian coordinates, for designing statically balanced serial linkages, without auxiliary links. This method is created because current methods focused on this task are not user friendly and obtained design equations are relatively complex. As a result the obtained solutions found in literature are all in a limited selection of the full solution space. All having fixed world spring attachments on a vertical line through the fixed world joint point. In the present paper the method is set up using a different, Cartesian coordinate system. The resulting design equations are ore suitable for utilizing the whole design space.

The second objective is to provide illustrative examples of solutions in this complete design space. Relations are provided of how and why spring attachments can be placed anywhere in a 2D plane. The found behavior is visualized.

This paper has been submitted to the journal Mechanism and Machine Theory. A slightly shorter, altered version is accepted for the IFToMM World Congress 2015 (Chapter F).

Cartesian based stiffness matrix approach and graphical representation for designing statically balanced serial linkages

M. P. Lustig[a], A. G. Dunning[a,b,*], J. L. Herder[b]

Delft University of Technology, Faculty of Mechanical, Maritime and Materials Engineering, Delft, The Netherlands

[a] *Department of Biomechanical Engineering,*
[b] *Department of Precision and Microsystems Engineering*

Abstract

A statically balanced system is in equilibrium in every pose, by maintaining a constant potential energy level. In classical solutions for balancing serial linkages, each DOF is balanced by an independent element (counter-mass or mono-articular spring). Disadvantages are increased mass and inertia for counter-mass elements, and the need for auxiliary links for spring solutions. Recent literature presents a method for balancing serial linkages without auxiliary links; using multi-articular springs. This method obtains constraint equations from the stiffness matrix. Downsides are different coordinate systems for describing locations and states, and set criteria constraining attachments to fixed lines. In the presented paper the stiffness matrix approach is implemented using a consistent Cartesian coordinate system. Goal is to compare the use of this single coordinate system to the use of multiple coordinate systems for this method, and to obtain an increased insight and a visualization of the relations between different parameters. The Cartesian coordinates are implemented successfully, resulting in a simpler, more intuitive method for designing statically balanced serial linkages. Furthermore, obtained parameter relations are visualized in two examples providing knowledge about how systems parameters can be changed while balance is maintained.

Keywords: Static balance, Zero-free-length spring, Serial linkage, Constant potential energy

1. Introduction

A system which is in equilibrium in every motionless state is called statically balanced. For such systems the potential energy level remains constant in every pose [1]. This constant energy level greatly reduces operational effort as only dynamic effects remain to be overcome during motion. Many applications for static balancing exist due to these benefits [1, 2, 3, 4].

Different techniques exist to statically balance the rotation of a rigid pendulum. A simple option is adding a counter-mass [1], downside of which is the increased mass and inertia [5]. A second option is connecting a zero-free-length spring (ZFLS) between the link and fixed world [1]. For a ZFLS the spring force is proportional to its length. Other less common solutions use a non-circular cam [6] or compliant flexure elements [7]. These solutions are all designed to balance a single degree of freedom (DOF).

Solutions for balancing a serial linkage with multiple DOFs make use of counter-mass or ZFLSs. In the first case a counter-mass is added to each link [8, 9], additional auxiliary links allow counter-mass relocation [10]. Inertia increase becomes a greater problem as added weights of distal counter-masses must be balanced as well. Classical ZFLS solutions require a parallel beam construction providing a link with fixed orientation at each joint [1, 11, 12]. Each link is balanced by a single ZFLS that spans the joint of the respective link, a mono-articular spring. The disadvantage of parallel beams are an increased complexity and added inertia. In these systems each DOF is balanced by an independent balancing element.

Recent literature presents two methods in which ZFLSs can span multiple joints to balance serial linkages without parallel beams. The first method is the stiffness matrix approach by Lin et al. [12, 13, 14, 15]. Energy equations are set up in a general form $U = \frac{1}{2}\boldsymbol{Q}^T\boldsymbol{K}\boldsymbol{Q}$, separating states $\boldsymbol{Q}$ and parameters in a stiffness matrix $\boldsymbol{K}$. Off-diagonal elements of $\boldsymbol{K}$ contain state dependent energy terms, constraining these terms equal to zero results in a statically balanced system [13]. The second method is an iterative method developed by Deepak and Ananthasuresh [16]. Balance is ensured link by link, in steps, starting at the most distal link. At each step, balance of a specific link is acquired by adding up to two ZFLSs between this link and fixed world. For each link only energy terms of the current and previous step links affect its constraint equations [16]. In these two methods each DOF is balanced by combined efforts of multiple ZFLSs.

*Corresponding author. E-mail adress: a.g.dunning@tudelft.nl; Postal address: Mekelweg 2, 2628CD Delft, The Netherlands

Both methods can create statically balanced serial linkages and are based on an energy approach. Nevertheless multiple differences exist in ease of implementation and capabilities. The first is that in Lin's method all constraints are obtained at once for a chosen spring configuration, whereas in Deepak's method only a selection of the constraints is evaluated at once. If no straightforward solution is found, Deepak's method explains which spring(s) can be added for a solvable system, Lin's method does not directly. However, information on which links are unbalanced and thus require additional springs can be extracted from the stiffness matrix [15]. Another difference is that all springs are connected to the fixed world in Deepak's method while in Lin's method springs can be attached in between any two links, i.e. additional constraints are provided considering these springs. Finally, Deepak's method allows planar placement of spring attachments while in Lin's method criteria are set up constraining attachments to be located on fixed straight lines [15].

In the presented work the stiffness matrix approach is selected for calculating balanced linkages as it provides all constraints at once and allows additional spring placement options. The exact implementation however is altered. Current literature describes locations on links using polar coordinate systems, while states are described using unit vectors (xy-components). In the presented work Carthesian (xy-) coordinates are used describing link locations as well as the states.

Three goals are formulated in the presented paper. The first goal is to implement Cartesian coordinates in the stiffness matrix approach for balanced serial linkages to investigate its benefits over using a polar coordinate system. The second goal is to gain more insight in the relations between different parameters of this method in the design space, for instance it will be investigated if placement of springs outside the vertical straight lines is allowed. The third goal is to visualize these behavioral relations in two examples.

The structure of this paper is as follows. First, in 'Method' the Cartesian coordinate stiffness matrix approach is derived. Next, in 'Application and behavior' two examples of balanced linkages are presented of which the behavior is analyzed. Third, in 'Discussion' the use of Cartesian and polar coordinates are compared. Finishing with the obtained conclusions concerning the set goals.

2. Method

We propose the use of Cartesian coordinates in the stiffness matrix approach for designing serial statically balanced linkages. This is in contrast to the polar coordinate system used in current literature on this method [12, 13, 14, 15]. In the presented paper the location of spring attachments, joints and COMs is described using (local) x- and y- coordinates on the respective links they are located on. In this section the assumptions are explained first, followed by the full derivation of the stiffness matrix approach using xy-coordinates.

2.1. Assumptions and limitations

The presented method is set up for planar linkages, the gravitational field acting in this plane has constant magnitude and direction. The links are connected to each other and/or the fixed world using revolute joints. All springs have linear ZFLS behavior and the mass of these springs is neglected. Mechanical limits of links/springs colliding with one another are not taken into account. The fixed world is assumed to be rigid and static.

2.2. Derivation of stiffness matrix

The stiffness matrix approach is derived in five steps. First all coordinate points are described as a function of the link states and parameter values. The second step is setting up potential energy equations for all spring and mass components and writing these equations in a generalized form. The third step is to combine the energy equations of the different components to obtain the total stiffness matrix. The fourth step is obtaining the constraint equations for balance from the stiffness matrix. The fifth and final step is focused on how to solve the obtained equations. The equations are set up for an n link system where the fixed world is link 1, as a result the system has $n-1$ moving links.

2.2.1. Step 1: Coordinate vectors

The state of link u is described by global unit vector $\boldsymbol{q}_u$ (Figure 1a). The fixed world vector $\boldsymbol{q}_1$ is constant, aligned with the global x-axis. For moving links ($u = 2 \cdots n$) vector $\boldsymbol{q}_u$ is aligned with the local x_u-axis. The origin of each local coordinate system is located at the proximal joint J_{u-1}. The y_u-axis are orientated perpendicular to the respective x_u-axis. A unit vector in this y_u direction is obtained by rotating the state vector $\boldsymbol{q}_u$ by 90° using rotation matrix $\boldsymbol{R}$. Combined state vector $\boldsymbol{Q}$ holds the states of all n-links.

$$\boldsymbol{q}_1 = \begin{bmatrix}1\\0\end{bmatrix} \tag{1a}$$

$$\boldsymbol{q}_u = \begin{bmatrix}q_{xu}\\q_{yu}\end{bmatrix} \tag{1b}$$

$$\boldsymbol{Q} = \begin{bmatrix}\boldsymbol{q}_1\\\vdots\\\boldsymbol{q}_n\end{bmatrix} \tag{1c}$$

$$\boldsymbol{I} = \begin{bmatrix}1 & 0\\0 & 1\end{bmatrix} \tag{1d}$$

$$\boldsymbol{R} = \begin{bmatrix}\cos(90°) & -\sin(90°)\\\sin(90°) & \cos(90°)\end{bmatrix} = \begin{bmatrix}0 & -1\\1 & 0\end{bmatrix} \tag{1e}$$

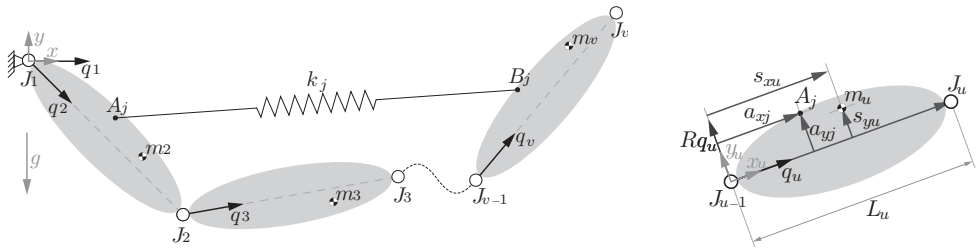

(a) (b)

Figure 1: (a) Schematic representation of a serial linkage in a state defined by unit vectors $\boldsymbol{q}$. (b) Parameterization of locations on link u in the Cartesian form.

Global coordinates of all point on the links are described as a linear combination of the state vectors and constant parameter values. Joint locations are described first. As said, fixed world joint $\boldsymbol{J}_1$ is located in the global origin. The distal joint $\boldsymbol{J}_u$ of a link u is always located on the local x_u-axis at distance L_u from the local origin (Figure 1b). Vector components of joint locations are set up in equation 2.

$$\boldsymbol{J}_1 = \begin{bmatrix}0\\0\end{bmatrix} \tag{2a}$$

$$\boldsymbol{J}_u = L_2\boldsymbol{I}\boldsymbol{q}_2 + L_3\boldsymbol{I}\boldsymbol{q}_3 + \cdots + L_u\boldsymbol{I}\boldsymbol{q}_u = \sum_{i=2}^{u} L_i\boldsymbol{I}\boldsymbol{q}_i = \boldsymbol{J}_{u-1} + L_u\boldsymbol{I}\boldsymbol{q}_u \tag{2b}$$

Spring attachment point locations for a spring j between link u to link v are $\boldsymbol{A}_j$ and $\boldsymbol{B}_j$ respectively. These locations are a linear combination of the proximal joint component $\boldsymbol{J}_{u-1}$, the local x_u component ($a_{xj}\boldsymbol{I}\boldsymbol{q}_u$) and the local y_u component ($a_{yj}\boldsymbol{R}\boldsymbol{q}_u$) (Eq. 3). A schematic representation containing these components is given in figure 1b.

$$\boldsymbol{A}_j = \boldsymbol{J}_{u-1} + (a_{xj}\boldsymbol{I} + a_{yj}\boldsymbol{R})\,\boldsymbol{q}_u \tag{3a}$$

$$\boldsymbol{B}_j = \boldsymbol{J}_{v-1} + (b_{xj}\boldsymbol{I} + b_{yj}\boldsymbol{R})\,\boldsymbol{q}_v \tag{3b}$$

Similarly the COM location of link u is set up (Eq. 4).

$$\boldsymbol{S}_u = \boldsymbol{J}_{u-1} + (s_{xu}\boldsymbol{I} + s_{yu}\boldsymbol{R})\boldsymbol{q}_u \tag{4}$$

2.2.2. Step 2: Energy equations and generalized form

This step is to write energy equations in the generalized form, separating the states $\boldsymbol{Q}$ and the parameters in the stiffness matrix $\boldsymbol{K}$.

$$U = \frac{1}{2}\boldsymbol{Q}^T\boldsymbol{K}\boldsymbol{Q} \tag{5}$$

Spring energy is expressed in this form first. The vector describing spring length and orientation for spring j, going from link u to link v, is $\boldsymbol{B}_j - \boldsymbol{A}_j$. This is as a function of the states, because the locations of points $\boldsymbol{B}_j$ and $\boldsymbol{A}_j$ are state dependent as well. The expression for this spring vector is derived in equation 6. An expression is obtained where

constants are separated for each state (Eq. 6e). The components $\boldsymbol{C}$ holding these constant parameters are shown in matrix form (Eq. 7).

$$\boldsymbol{B}_j - \boldsymbol{A}_j = \boldsymbol{J}_{v-1} - \boldsymbol{J}_{u-1} - (a_{xj}\boldsymbol{I} + a_{yj}\boldsymbol{R})\,\boldsymbol{q}_u + (b_{xj}\boldsymbol{I} + b_{yj}\boldsymbol{R})\,\boldsymbol{q}_v \tag{6a}$$

$$\boldsymbol{J}_{v-1} - \boldsymbol{J}_{u-1} = \boldsymbol{J}_u + \boldsymbol{J}_{u+1} + \cdots + \boldsymbol{J}_{v-1} = \sum_{n=u}^{v-1} L_n \boldsymbol{I}\boldsymbol{q}_n \tag{6b}$$

$$\boldsymbol{B}_j - \boldsymbol{A}_j = -(a_{xj}\boldsymbol{I} + a_{yj}\boldsymbol{R})\,\boldsymbol{q}_u + \sum_{n=u}^{v-1} L_n \boldsymbol{I}\boldsymbol{q}_n + (b_{xj}\boldsymbol{I} + b_{yj}\boldsymbol{R})\,\boldsymbol{q}_v \tag{6c}$$

$$= \underbrace{((L_u - a_{xj})\boldsymbol{I} - a_{yj}\boldsymbol{R})}_{\boldsymbol{C}_u}\boldsymbol{q}_u + \underbrace{\sum_{n=u+1}^{v-1} L_n \boldsymbol{I}}_{\boldsymbol{C}_{u+1}+\cdots+\boldsymbol{C}_{v-1}}\boldsymbol{q}_n + \underbrace{(b_{xj}\boldsymbol{I} + b_{yj}\boldsymbol{R})}_{\boldsymbol{C}_v}\boldsymbol{q}_v \tag{6d}$$

$$= \sum_{n=1}^{v} \boldsymbol{C}_n \boldsymbol{q}_n \tag{6e}$$

$$\boldsymbol{C}_u = \begin{bmatrix} L_u - a_{xj} & a_{yj} \\ -a_{yj} & L_u - a_{xj} \end{bmatrix} \tag{7a}$$

$$\boldsymbol{C}_i = \begin{bmatrix} L_i & 0 \\ 0 & L_i \end{bmatrix} \quad \text{, for } i = u+1, \cdots, v-1 \tag{7b}$$

$$\boldsymbol{C}_v = \begin{bmatrix} b_{xj} & -b_{yj} \\ b_{yj} & b_{xj} \end{bmatrix} \tag{7c}$$

$$\boldsymbol{C}_i = \begin{bmatrix} 0 & 0 \\ 0 & 0 \end{bmatrix} \quad \text{, for : } \begin{cases} i = 1, \cdots, u-1 \\ i = v+1, \cdots, n \end{cases} \tag{7d}$$

Knowing the spring length as a function of the states its potential energy can be calculated. The equation is set up for a ZFLS j with stiffness k_j (Eq. 8a) and rewritten in the generalized form (Eq. 8d). In this form the states ($\boldsymbol{Q}$) are separated from the parameters in the stiffness matrix of the spring ($\boldsymbol{K}_{s,j}$).

$$U_{s,j} = \frac{1}{2} k_j (\boldsymbol{B}_j - \boldsymbol{A}_j)^2 \tag{8a}$$

$$= \frac{1}{2} k_j \left(\sum_{u=1}^{n} \boldsymbol{C}_u \boldsymbol{q}_u \right)^2 \tag{8b}$$

$$= \frac{1}{2} k_j \begin{bmatrix} \boldsymbol{q}_1 \\ \vdots \\ \boldsymbol{q}_n \end{bmatrix}^T \begin{bmatrix} \boldsymbol{C}_1^T\boldsymbol{C}_1 & \cdots & \boldsymbol{C}_1^T\boldsymbol{C}_n \\ \vdots & \ddots & \vdots \\ \boldsymbol{C}_n^T\boldsymbol{C}_1 & \cdots & \boldsymbol{C}_n^T\boldsymbol{C}_n \end{bmatrix} \begin{bmatrix} \boldsymbol{q}_1 \\ \vdots \\ \boldsymbol{q}_n \end{bmatrix} \tag{8c}$$

$$= \frac{1}{2} \boldsymbol{Q}^T \boldsymbol{K}_{s,j} \boldsymbol{Q} \tag{8d}$$

$$\boldsymbol{K}_{s,j} = k_j \begin{bmatrix} \boldsymbol{C}_1^T\boldsymbol{C}_1 & \cdots & \boldsymbol{C}_1^T\boldsymbol{C}_n \\ \vdots & \ddots & \vdots \\ \boldsymbol{C}_n^T\boldsymbol{C}_1 & \cdots & \boldsymbol{C}_n^T\boldsymbol{C}_n \end{bmatrix} \tag{8e}$$

Next the gravitational energy is expressed in the generalized form of equation 5. The height of the masses is found in the second element of vector $\boldsymbol{S}_u$, containing the global COM y-coordinate of link u. The value for height is extracted by vector product: *height*= $\begin{bmatrix} 0 & 1 \end{bmatrix} \boldsymbol{S}_u$. This product is not jet expressed as in the generalized form because $\boldsymbol{S}_u$ does not contain multiplications of states. By using state $\boldsymbol{q}_1$, which is located on the fixed world, it is known that $(\boldsymbol{R}\boldsymbol{q}_1)^T = \begin{bmatrix} 0 & 1 \end{bmatrix}$, describing the gravitational field direction. Therefore the height of a mass is expressed as in the generalized form by product: *height*= $(\boldsymbol{R}\boldsymbol{q}_1)^T \boldsymbol{S}_u$. Based on this term the energy equations are first written for the mass of a single link u (Eq. 9) followed by a summed relation containing the masses of all links (Eq. 10). For this form the constant components $\boldsymbol{D}_u$ that fill the stiffness matrix are described (Eq. 11), followed by the generalized form of the energy equation (Eq. 12).

$$
\begin{aligned}
U_{m_u} &= m_u g(\boldsymbol{R}\boldsymbol{q}_1)^T \boldsymbol{S}_u && \text{(9a)}\\
U_{m_u} &= m_u g \boldsymbol{q}_1^T \boldsymbol{R}^T \boldsymbol{S}_u && \text{(9b)}\\
U_{m_u} &= m_u g \boldsymbol{q}_1^T \boldsymbol{R}^T \left[\boldsymbol{J}_{u-1} + (s_{xu}\boldsymbol{I} + s_{yu}\boldsymbol{R})\boldsymbol{q}_u\right] && \text{(9c)}\\
U_{m_u} &= m_u g \boldsymbol{q}_1^T \boldsymbol{R}^T \left[\sum_{i=1}^{u-1}(L_i \boldsymbol{q}_i) + (s_{xu}\boldsymbol{I} + s_{yu}\boldsymbol{R})\boldsymbol{q}_u\right] && \text{(9d)}
\end{aligned}
$$

Effect of combined mass of all links, for a linkage with n links (and thus $n-1$ moving links) is given (Eq. 10).

$$
\begin{aligned}
U_{\Sigma m} &= \sum_{u=2}^{n} U_{m_u} && \text{(10a)}\\
&= \boldsymbol{q}_1^T \sum_{u=2}^{n} \left(\boldsymbol{R}^T m_u g \left[\sum_{i=1}^{u-1}(L_i \boldsymbol{q}_i) + (s_{xu}\boldsymbol{I} + s_{yu}\boldsymbol{R})\boldsymbol{q}_u\right]\right) && \text{(10b)}\\
&= \boldsymbol{q}_1^T \sum_{u=2}^{n} \left(\underbrace{\boldsymbol{R}^T \left[\left(\sum_{i=u+1}^{n} m_i\right) g L_u \boldsymbol{I} + m_u g (s_{xu}\boldsymbol{I} + s_{yu}\boldsymbol{R})\right]}_{\boldsymbol{D}_u} \boldsymbol{q}_u \right) && \text{(10c)}
\end{aligned}
$$

The components $\boldsymbol{D}_u$ are directly obtained form equation 10c and are rewritten in matrix form (Eq. 11).

$$
\begin{aligned}
\boldsymbol{D}_u &= \boldsymbol{R}^T \left[\left(\sum_{i=u+1}^{n} m_i\right) g L_u \boldsymbol{I} + m_u g (s_{xu}\boldsymbol{I} + s_{yu}\boldsymbol{R})\right] && \text{(11a)}\\
&= \begin{bmatrix} m_u g s_{yu} & m_u g s_{xu} + \left(\sum_{i=u+1}^{n} m_i\right) g L_u \\ -m_u g s_{xu} - \left(\sum_{i=u+1}^{n} m_i\right) g L_u & m_u g s_{yu} \end{bmatrix} && \text{(11b)}
\end{aligned}
$$

The generalized form $U_{\Sigma m}$ is obtained as states and parameters are separated.

$$
\begin{aligned}
U_{\Sigma m} &= \frac{1}{2}\boldsymbol{Q}^T \boldsymbol{K}_m \boldsymbol{Q} && \text{(12a)}\\
\boldsymbol{K}_m &= \begin{bmatrix} \boldsymbol{O} & \boldsymbol{D}_2 & \cdots & \boldsymbol{D}_n \\ \boldsymbol{D}_2^T & \boldsymbol{O} & \cdots & \boldsymbol{O} \\ \vdots & \vdots & \ddots & \vdots \\ \boldsymbol{D}_n^T & \boldsymbol{O} & \cdots & \boldsymbol{O} \end{bmatrix} && \text{(12b)}
\end{aligned}
$$

When analyzing a new system it is possible to quickly set up the stiffness matrices without having to go through all derivations performed in this step. It is advised to directly substitute the component matrices for the springs $\boldsymbol{C}_u$(Eq. 7a-7d) and the mass components $\boldsymbol{D}_u$ (Eq.11). By substituting these component matrices in equation 8e and 12b the stiffness matrix $\boldsymbol{K}_{s,j}$ and $\boldsymbol{K}_m$ are obtained.

2.2.3. Step 3: Total stiffness matrix

The combined energy U_t, containing all spring and mass terms is obtained by combining the spring and mass stiffness matrices (Eq. 13).

$$
\begin{aligned}
U_t &= \frac{1}{2}\boldsymbol{Q}^T \boldsymbol{K}_t \boldsymbol{Q} && \text{(13a)}\\
\boldsymbol{K}_t &= \left(\sum_{i=1}^{n_{springs}} \boldsymbol{K}_{s,i}\right) + \boldsymbol{K}_m && \text{(13b)}
\end{aligned}
$$

2.2.4. Step 4: Constraint equations

In a balanced system, any state can be changed freely with respect to any other state without changing the overall potential energy level. For this to be the case, the effective stiffness between any two different states should be equal to zero. The effective stiffness terms for these relative rotations are found on the off-diagonal part of the stiffness matrix $\boldsymbol{K}_t$ [14]. As a result, all off-diagonal parts of the $\boldsymbol{K}_t$ matrix are constrained to be equal to zero for balance [13].

The number of constraint equations depends on the size of the $\boldsymbol{K}_t$ matrix, which in turn depends on the number of links n. The matrices are symmetrical, thus all relations are found in the upper triangular part (Eq. 8e, 12b). Additionally, all relations in one of these triangular parts occur twice, once in each even and uneven row. Thus only every other row has to be examined to obtain all relations. Altogether the amount of constraint equations for an n-link system is equal to $n(n-1)$ [14].

2.2.5. Step 5: Obtain balance by solving constraint equations

The next step is solving the obtained constraint equations. In general, the minimal amount of variables to be calculated is equal to the number of equations. For example, for a three link planar system the number of constraint equations is equal to six and as a result at least six parameters should be left free while solving such a system. The remaining parameters can be selected to have constant values.

3. Application and behavior

In this section two illustrative examples of balanced linkages are presented. The behavior of the balanced systems is analyzed. to gain a better understanding of how different parameters can be changed while maintaining the desired balance. Increased insight in the inner workings of the system will allow for a more efficient design process and a better overview of possible solutions. Found relations for varying parameters while maintaining balance are provided and visualized. The system studied in both examples has two moving links (Figure 2a). It is balanced using two different spring configurations. In example 1 the spring configuration of figure 2b is used, having two bi-articular springs. In example 2 the configuration of figure 2c is used, having a mono- and bi-articular springs. The steps described in the methods section provide guidance in both examples.

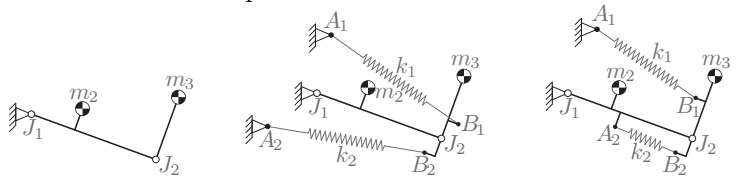

(a) (b) (c)

Figure 2: (a) Unbalanced linkage. (b) Spring configuration of example 1. (c) Spring configuration of example 2.

3.1. Example 1

Two bi-articular springs are used to balance the system both connecting the fixed world to link 3 (Figure 2b). In the first step the system locations in figure 2b are expressed in xy-coordinates as in figure 1b. The actual location vectors (Eq. 2,3,4) are not shown as their creation is not required for continuing in this method, nevertheless they are useful for instance to plot the system. In the second step the component matrices for the two springs $\boldsymbol{C}_1$ and $\boldsymbol{C}_2$ (Eq. 14a,14b) and the mass terms $\boldsymbol{D}$ (Eq. 14c) are constructed based on equations 7 and 11. By substituting these component matrices in equations 8e and 12b the spring matrices $\boldsymbol{K}_{s1}, \boldsymbol{K}_{s2}$ and mass stiffness matrix $\boldsymbol{K}_m$ are obtained (Eq. 15). The third step is to construct the total stiffness matrix by combining the spring and mass matrices (Eq. 15). In the fourth step the constraint equations are obtained from the $\boldsymbol{K}_t$ matrix (Eq. 16). The constraint equations to be satisfied for balance are the off-diagonal parts of the $\boldsymbol{K}_t$ matrix set equal to zero. Here only terms in odd rows (1 and 3) are considered as the even rows hold exactly the same relations.

$$\boldsymbol{C}_{1,1} = \begin{bmatrix} -a_{x1} & a_{y1} \\ -a_{y1} & -a_{x1} \end{bmatrix}; \quad \boldsymbol{C}_{1,2} = \begin{bmatrix} L_2 & 0 \\ 0 & L_2 \end{bmatrix}; \quad \boldsymbol{C}_{1,3} = \begin{bmatrix} b_{x1} & -b_{y1} \\ b_{y1} & b_{x1} \end{bmatrix} \tag{14a}$$

$$\boldsymbol{C}_{2,1} = \begin{bmatrix} -a_{x2} & a_{y2} \\ -a_{y2} & -a_{x2} \end{bmatrix}; \quad \boldsymbol{C}_{2,2} = \begin{bmatrix} L_2 & 0 \\ 0 & L_2 \end{bmatrix}; \quad \boldsymbol{C}_{2,3} = \begin{bmatrix} b_{x2} & -b_{y2} \\ b_{y2} & b_{x2} \end{bmatrix} \tag{14b}$$

$$\boldsymbol{D}_1 = \begin{bmatrix} 0 & 0 \\ 0 & 0 \end{bmatrix}; \quad \boldsymbol{D}_2 = \begin{bmatrix} m_2 g s_{y2} & m_3 g L_2 + m_2 g s_{x2} \\ -m_3 g L_2 - m_2 g s_{x2} & m_2 g s_{y2} \end{bmatrix}; \quad \boldsymbol{D}_3 = \begin{bmatrix} m_3 g s_{y3} & m_3 g s_{x3} \\ -m_3 g s_{x3} & m_3 g s_{y3} \end{bmatrix} \tag{14c}$$

$$\boldsymbol{K}_{si} = \frac{1}{2}k_i \begin{bmatrix} \boldsymbol{C}_{i,1}^T\boldsymbol{C}_{i,1} & \boldsymbol{C}_{i,1}^T\boldsymbol{C}_{i,2} & \boldsymbol{C}_{i,1}^T\boldsymbol{C}_{i,3} \\ & \boldsymbol{C}_{i,2}^T\boldsymbol{C}_{i,2} & \boldsymbol{C}_{i,2}^T\boldsymbol{C}_{i,3} \\ \text{sym} & & \boldsymbol{C}_{i,3}^T\boldsymbol{C}_{i,3} \end{bmatrix} \quad \boldsymbol{K}_m = \begin{bmatrix} \boldsymbol{O} & \boldsymbol{D}_2 & \boldsymbol{D}_3 \\ & \boldsymbol{O} & \boldsymbol{O} \\ \text{sym} & & \boldsymbol{O} \end{bmatrix} \quad \boldsymbol{K}_t = \boldsymbol{K}_{s1} + \boldsymbol{K}_{s2} + \boldsymbol{K}_m \tag{15}$$

$$\boldsymbol{K}_t(1,3) = 0 = -k_1 a_{x1} L_2 - k_2 a_{x2} L_2 + m_2 g s_{y2} \tag{16a}$$
$$\boldsymbol{K}_t(1,4) = 0 = -k_1 a_{y1} L_2 - k_2 a_{y2} L_2 + m_2 g s_{x2} + m_3 g L_2 \tag{16b}$$
$$\boldsymbol{K}_t(1,5) = 0 = -k_1(a_{x1}b_{x1} + a_{y1}b_{y1}) - k_2(a_{x2}b_{x2} + a_{y2}b_{y2}) + m_3 g s_{y3} \tag{16c}$$
$$\boldsymbol{K}_t(1,6) = 0 = k_1(a_{x1}b_{y1} - a_{y1}b_{x1}) + k_2(a_{x2}b_{y2} - a_{y2}b_{x2}) + m_3 g s_{x3} \tag{16d}$$
$$\boldsymbol{K}_t(3,5) = 0 = k_1 b_{x1} L_2 + k_2 b_{x2} L_2 \tag{16e}$$
$$\boldsymbol{K}_t(3,6) = 0 = -k_1 b_{y1} L_2 - k_2 b_{y2} L_2 \tag{16f}$$

In the final step constraints are solved for four different cases, each showing different behavior (Figure 3). Between these cases some general properties of the system are kept the same, specifically spring stiffness, mass and link length values. In each case, the constraints are solved for parameters $a_{x1}, a_{y1}, a_{x2}, a_{y2}, b_{x1}$ and b_{y1}, describing spring attachment locations A_1, A_2 and B_1. Varied between cases are parameters b_{x2} and b_{y2}, describing the location of B_2, while keeping the distance between joint J_2 and B_2 equal. Furthermore s_{x2} and s_{y2} are varied, describing the location of the COM of link 2, while keeping the distances from joint J_1 to the COM the same. Summarized parameter values of balanced configurations are found in table 3e. Parameters on the first six rows (above the horizontal line) are calculated by solving the constraints, remaining parameter values (under the line) are chosen inputs.

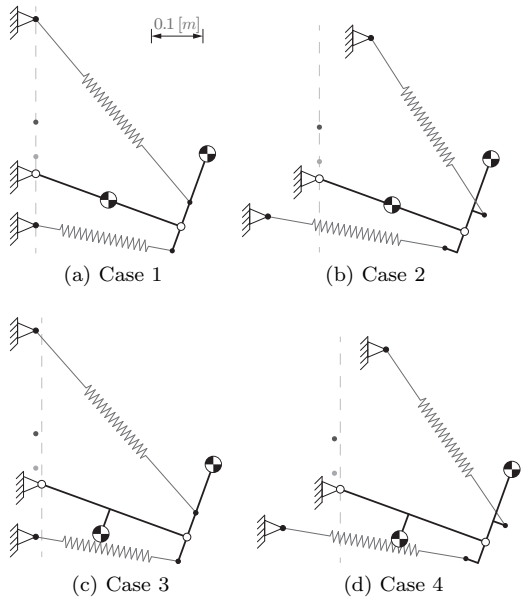

(a) Case 1 (b) Case 2

(c) Case 3 (d) Case 4

	Case 1	Case 2	Case 3	Case 4	Units
a_{x1}	0	0.1	-0.0114	0.0886	$[m]$
a_{y1}	0.3	0.2732	0.298	0.2712	$[m]$
a_{x2}	0	-0.1	-0.0114	-0.1114	$[m]$
a_{y2}	-0.1	-0.0732	-0.102	-0.0752	$[m]$
b_{x1}	0.05	0.0433	0.05	0.0433	$[m]$
b_{y1}	0	-0.025	0	-0.025	$[m]$
b_{x2}	-0.05	-0.0433	-0.05	0.0433	$[m]$
b_{y2}	0	0.025	0	0.025	$[m]$
k_1	147.15	147.15	147.15	147.15	$[\frac{N}{m}]$
k_2	147.15	147.15	147.15	147.15	$[\frac{N}{m}]$
m_2	2	2	2	2	$[kg]$
m_3	2	2	2	2	$[kg]$
L_2	0.3	0.3	0.3	0.3	$[m]$
s_{x2}	0.15	0.15	0.141	0.141	$[m]$
s_{y2}	0	0	-0.0513	-0.0513	$[m]$
s_{x3}	0.15	0.15	0.15	0.15	$[m]$
s_{y3}	0	0	0	0	$[m]$

(e)

Figure 3: In scale balanced solutions for example 1, the dark and light grey dots near the first joint represent points Z_1 and Z_2 (described later on in this example). (e) Parameter values for the different cases.

Case 1 presents the general balanced configuration of this example (Fig. 3a). Here, spring attachment points, COM locations and joints are aligned on each link. In case 2, spring attachment B_2 is rotated by an angle of $-30°$ about joint J_2 with respect to the aligned orientation (Figure 3b). Thus $b_{x2} = -0.05\cos(-30°) = -0.0433$ and $b_{y2} = -0.05\sin(-30°) = 0.025$ (Table 3e). When solved it is observed that all other attachments follow the applied rotation (Figure 3b). For case 3, the COM location of link 2 is rotated by an angle of $-20°$ around J_1 (Figure 3c). Thus the constraints are solved with $s_{x2} = 0.15\cos(-20°) = 0.141$ and $s_{y2} = 0.15\sin(-20°) = -0.0513$ as inputs (Table 3e). For this case it is observed that both fixed world spring attachments shift to the left and down. In the final case 4, both offsets of spring attachment B_2 and the COM of link 2 are applied to the system. As expected the solved configuration shows a combination of the behavior caused by the individual offsets of the previous cases (Figure 3d).

3.2. Behavior Example 1

The lower arm link, suspended to the fixed world by two springs, acts like a virtual ZFLS between its joint J and point Z_2 (Figure 4a-4j). This virtual ZFLS is used to balance the upper arm link to obtain the system of this example (Figure 4k-4l). Steps taken to obtain these results are visualized (Figure 4) and explained.

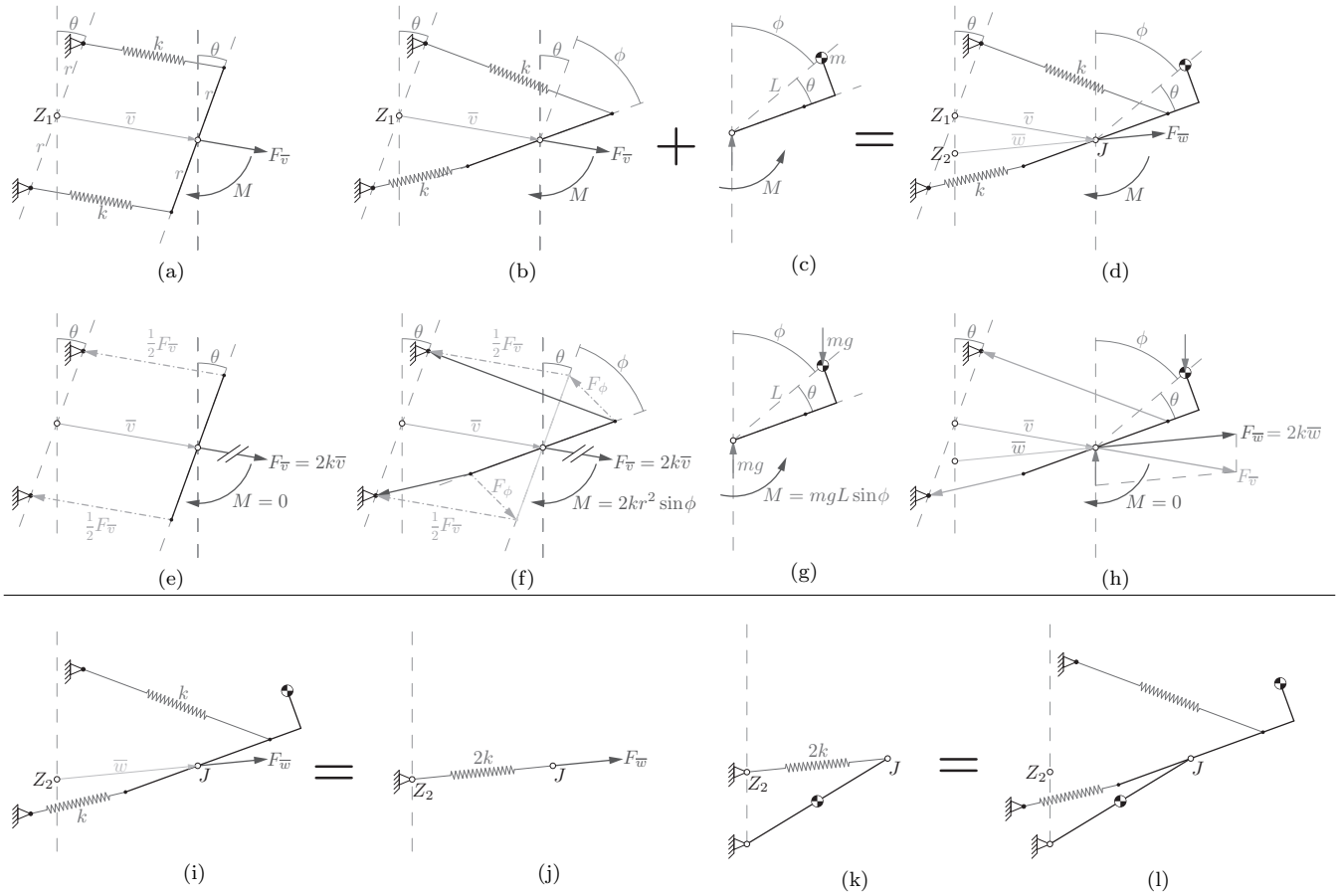

Figure 4: Behavioral analysis

Figure 4a shows a weightless link suspended to the fixed world by two ZFLSs. The link is positioned parallel to the fixed world spring attachments at constant angle θ, vector $\overline{v}$ describes its displacement. The force decomposition (Figure 4e) shows a reaction force equal to the sum of the two spring forces ($F_{\overline{v}} = 2k\overline{v}$). The moment $M = 0$ as the spring forces are equal and have opposite moment arms for any $\overline{v}$. In Figure 4b a rotation ϕ is applied to the link. In this state the springs have different lengths and thus unequal spring forces act on the link. Both spring forces are decomposed, each into two components (Figure 4f). The first force component ($\frac{1}{2}F_{\overline{v}}$) is dependent only on displacement $\overline{v}$ and the other (F_ϕ) depends solely on rotation ϕ. Components $\frac{1}{2}F_{\overline{v}}$ are equal to the spring forces in the unrotated case (Figure 4e-4f). Therefore they contribute to the reaction force ($F_{\overline{v}} = 2k\overline{v}$) but cause no moment ($M = 0$) as before. The angle dependent components (F_ϕ) act in opposite directions and have opposite moment arms with respect to the joint. As a result they have no influence on the reaction force but do contribute to moment M (eq. 17). It is key to observe that the reaction force depends solely on displacement of the link and the moment only on the rotation.

$$M \quad = \quad 2F_\phi \cdot r\cos(\frac{\phi}{2}) = 4kr^2\sin(\frac{\phi}{2})\cos(\frac{\phi}{2}) = 2kr^2\sin(\phi) \tag{17}$$

A mass is added to the link such that it is positioned above the joint when rotation ϕ is zero (Figure 4c). The force decomposition shows a reaction force in y-direction with magnitude mg and a moment ($M = mgL\sin\phi$) as a function of ϕ (Figure 4g). The moment functions of the spring system and the link with mass are both a function of $\sin\phi$, acting in opposite directions around the joint (Figure 4f-4g). When their magnitudes are selected equal ($2kr^2 = mgL$) the two can compensate for each other (Figure 4d). The force decomposition of the combined system shows this moment free behavior (Figure 4h). Furthermore the reaction force ($F_{\overline{w}} = 2k\overline{w}$) is composed of vertical gravity force mg and spring force $F_{\overline{v}}$ and is expressed as a function of displacement vector $\overline{w}$ (Figure 4h).

At joint J the combined system acts as a ZFLS as the only force experienced at this joint is a constant stiffness ($2k$) times a displacement ($\overline{w}$). Therefore the system is equivalent to a single ZFLS (Figure 4i,4j). A single (upper arm) link is balanced using a ZFLS (Figure 4k)[1]. Next, this ZFLS is replaced by the equivalent linkage from figure 4i (Figure 4l). The system of example 1 is obtained. Known techniques for rotating the spring of the single balanced link[1] are applied to complete the behavioral description (Figure 5).

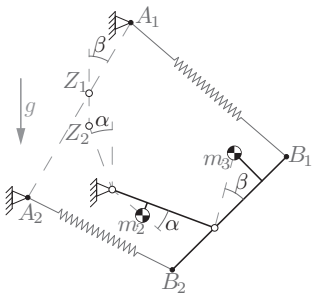

Figure 5: Illustrated behavior between the parameters of the linkage of example 1.

The obtained behavior illustrated in figure 5 shows at which orientations springs can be placed on the linkage. Relations between parameter magnitudes are described next. In general the magnitudes of stiffness and the lengths of certain moment arms are inversely related. For example, when reducing the stiffness in one of the springs by factor $\frac{1}{c}$ the respective distance from J_2 to B_1 (or B_2) is to be increased by factor c to keep the moment behavior on the outer link equal. Additionally, the changed stiffness value will affect the relative location of Z_1 ($F_{\overline{v}} = 0$) with respect to A_1 and A_2 while obeying $\frac{A_1 - Z_1}{A_2 - Z_1} = \frac{k_2}{k_1}$. At the same time, the distance from Z_1 to Z_2 will change as it is a function of the combined stiffness $(k_1 + k_2)$. The same is the case for the required position of Z_2 which also depends on this stiffness. Although the relations between parameter magnitudes are understood, it is observed that they are strongly related to each other. When a single parameter is changed, a lot of the other parameters will be affected to keep the system in balance.

In the orientation of figure 5 the stiffness values for both springs are positive. Yet it is possible to solve the stiffness matrix with negative stiffness values. These values occur when one of the two spring attachments of a spring cross a certain point. In the case of spring 1 this is when either A_1 or B_1 is located on the opposite side of Z_1 or J_2 respectively.

3.3. Example 2

Two springs are used to balance the system, one bi-articular ZFLS connecting the fixed world to link 3 and one mono-articular ZFLS that connects links 2 and 3 (Figure 2c). Constraint equations are set up similar to the first example, the steps are not shown for this example (steps 1 to 4). Next, these constraints are solved for four different cases (step 5) (Figure 6), each showing different behavior. Finally, the relations between parameters ensuring a balanced configuration are explained and illustrated.

Between these cases some general properties of the system remain the same. Specifically spring stiffness, mass and link length values. In each case the constraints are solved for parameters $a_{x1}, b_{x1}, b_{y1}, b_{x2}, b_{y2}$ and k_1. Varied inputs between cases are parameters a_{x2} and a_{y2}, describing the location of attachment A_2. Furthermore s_{y2} is varied, describing the location of the COM of link 2. Obtained parameter values of balanced configurations are summarized in table 6e.

In the first case all spring connections are aligned with the links (Figure 6a). In case 2, the second spring is rotated about the second joint(Figure 6b). In case 3, the COM of link 2 is relocated (Figure 6c). In the final case 4, the effects of case 2 and 3 are combined (Figure 6d).

3.4. Behavior in example 2

The four cases in example 2 are all statically balanced as they all fulfill the constraint equations. The unbalanced three link system is analyzed first in the orientation in which it has minimal gravitational energy (Figure 7a). In this position link 2 is oriented at angle α with respect to the vertical. Angle α is now determined by setting the moment M_{J_1} around J_1 to be equal to zero as it should be when in equilibrium (Eq.18). The system shown in figure 7b is equal to the linkage of figure 7a only with redrawn links that give room for springs to be drawn later on.

$$M_{J_1} = 0 = m_2 s_{y2} \cos(\alpha) - m_2 s_{x2} \sin(\alpha) - m_3 L_2 \sin(\alpha) \tag{18a}$$

$$(m_2 s_{x2} + m_3 L_2) \sin(\alpha) = m_2 s_{y2} \cos(\alpha) \tag{18b}$$

$$\frac{\sin(\alpha)}{\cos(\alpha)} = \tan(\alpha) = \frac{m_2 s_{y2}}{m_2 s_{x2} + m_3 L_2} \tag{18c}$$

$$\alpha = \tan^{-1}\left(\frac{m_2 s_{y2}}{m_2 s_{x2} + m_3 L_2}\right) \tag{18d}$$

Next, it is recognized that for balance a zero moment is required in all orientations. As this is already the case for the original system in the orientation of figure 7b neither of the added springs should apply a moment around any of

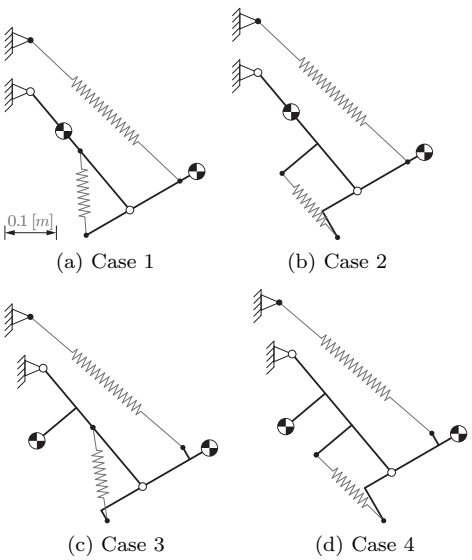

(a) Case 1 (b) Case 2

(c) Case 3 (d) Case 4

	Case 1	Case 2	Case 3	Case 4	Units
a_{x1}	0	0	-0.025	-0.025	$[m]$
b_{x1}	0.1125	0.1125	0.1059	0.1059	$[m]$
b_{y1}	0	0	0.0265	0.0265	$[m]$
b_{x2}	-0.0981	-0.0785	-0.0923	-0.06	$[m]$
b_{y2}	0	-0.0589	-0.0231	-0.0739	$[m]$
k_1	261.6	261.6	261.6	261.6	$[\frac{N}{m}]$
k_2	600	600	600	600	$[\frac{N}{m}]$
a_{y1}	0.1	0.1	0.1	0.1	$[m]$
a_{x2}	0.15	0.18	0.15	0.18	$[m]$
a_{y2}	0	-0.09	0	-0.09	$[m]$
m_2	2	2	2	2	$[kg]$
m_3	2	2	2	2	$[kg]$
L_2	0.3	0.3	0.3	0.3	$[m]$
s_{x2}	0.1	0.1	0.1	0.1	$[m]$
s_{y2}	0	0	-0.1	-0.1	$[m]$
s_{x3}	0.15	0.15	0.15	0.15	$[m]$
s_{y3}	0	0	0	0	$[m]$

(e)

Figure 6: In scale balanced solutions for example 2. (a) Case 1. (b) Case 2. (c) Case 3. (d) Case 4. (e) Parameter values for the different cases.

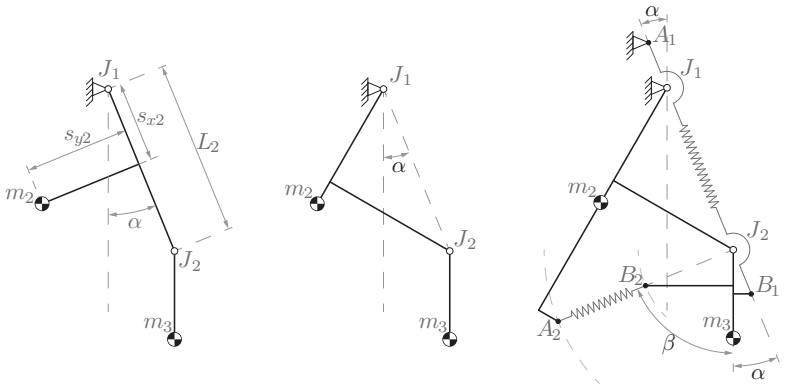

(a) (b) (c)

Figure 7: (a) and (b) Unbalanced linkage in equilibrium. (c) Relations between the location of spring attachment points required for a balanced system.

the joints to keep this moment free condition. Spring 1 is located between the fixed world point A_1 and link 3 at point A_3, and thus spawns both joints. As a result, spring connections A_1 and B_1 should be aligned with both joints J_1 and J_2, exactly at the previously determined angle α (Figure 7c). Spring 2 connects A_2 on link 2 and B_2 on link 3 and thus spawns only the second joint J_2. Therefore, in this orientation with minimal potential the two connection points of this spring are to be aligned with J_2 (Figure 7c).

Furthermore, as α is only dependent on parameters of the original linkage its value is unaffected by adjusting the other spring. For spring 2 the alignment of attachment A_2 depends on both angles α and β with respect to the local coordinate system of link 2. Attachment B_2 is dependent only on angle β with respect to the local coordinates of link 3. Therefore, by changing β spring 2 can be relocated anywhere on a ring shaped disk around J_2, as partially visualized by dotted lines in figure 7c.

The locations of the spring attachments are now described based on a single position of the linkage where the gravitational energy is at a minimum. This does not directly prove that the system is in balance in any pose as it is only clear that this one position is in equilibrium. However, the proof that the system can be balanced in any configuration is already given using the stiffness matrix approach. What the analysis of this single position does provide is insight in where the attachments can be placed and why they are constrained to lie on certain lines or positions. Additionally it can be reasoned that the system is capable of being balanced in all orientations as the energy behavior of all components is sinusoidal with respect to each rotation. These sinusoids have equal periods as these are equivalent to full rotations of a links, all having a minimum or maximum in the orientation of figure 7. The sinusoidal functions are either in phase or shifted by half a phase exactly and so can interfere with one another to cancel each other out.

The behavior described so far in this example is based on the orientations in which springs can be placed for the

selected spring configuration (Figure 7). However some additional interesting observations are made based on parameter magnitudes.

The first observation is that the location of spring attachment point B_1 (Figure 7c) is a unique point depending solely on parameters of the original linkage, i.e. it is fixed independently of all other spring related parameters. Using the `solve` function in MATLAB the constraint equations are solved for parameters b_{x1} and b_{x2}. These parameters describe the location of B_1, expressed as a function of the other parameters (Eq.19). The obtained equations consist solely of parameters describing link length, mass or COM location.

$$b_{x1} = \frac{L_2^2 m_3^2 s_{x3} + L_2 m_2 m_3 (s_{x2} s_{x3} + s_{y2} s_{y3})}{(L_2 m_3 + m_2 s_{x2})^2 + m_2^2 s_{y2}^2} \tag{19a}$$

$$b_{y1} = \frac{L_2^2 m_3^2 s_{y3} + L_2 m_2 m_3 (s_{x2} s_{y3} - s_{x3} s_{y2})}{(L_2 m_3 + m_2 s_{x2})^2 + m_2^2 s_{y2}^2} \tag{19b}$$

For the spring attachment A_1 an additional constraint is found. It is found that the distance from joint J_1 to this point A_1 is inversely related to its spring stiffness k_1. This is by solving the constraint equations (Eq.16) for the parameters a_{x1} and a_{y1} which describe the location of A_1 (Eq.20a and 20b). Furthermore, the relation for α can again be extracted from these constraints by looking at the relative magnitudes of a_{x1} and a_{y1} (Eq.20c).

$$a_{x1} = \frac{m_2 g s_{y2}}{L_2} \frac{1}{k_1} \tag{20a}$$

$$a_{y1} = \frac{m_2 g s_{x2} + m_3 g L_2}{L_2} \frac{1}{k_1} \tag{20b}$$

$$\alpha = \tan^{-1}\left(\frac{a_{x1}}{a_{y1}}\right) = \tan^{-1}\left(\frac{m_2 s_{y2}}{m_2 s_{x2} + m_3 L_2}\right) \tag{20c}$$

For spring 2, an additional constraint is found as well, this is next to angle β which describes the springs orientation. When all other parameters are fixed, the product of its stiffness k_2, distance from J_2 to A_2 and distance from J_2 to B_2 is constant ($k_2 \cdot |A_2 - J_2| \cdot |B_2 - J_2| = \text{constant}$). In other words, the two described lengths and the stiffness of this spring can be varied freely within these bounds without affecting any other parameter. This relation is affected by the location of A_1 and k_1, however it is unpractical to take these into account in the same relation and much more convenient to fix these parameters before altering either A_2, B_2 or k_2.

4. Discussion

Behavior found in the examples of this paper shows a number of simultaneous rotations of COM locations and/or spring connection points that can be performed without affecting the balance of the system (Figures 5 and 7). One could argue to use a polar coordinate system to describe this behavior as it is rotational. However, the centers of rotation for these simultaneous rotations can either be on the first joint, the second joint or a seemingly arbitrary point on one of the links. As the location of the center point is inconsistent it cannot be ensured that this point is always positioned on the origin of the local coordinate system. Furthermore, describing a rotation using polar coordinates about a point other than the origin is, according to the authors, unnecessarily complicated compared to describing such a rotation as a sum of vector components in a Cartesian coordinate system. For this reason an xy-coordinate system is recommended when altering a system having planar offsets. Other benefits of using a Cartesian system is that the resulting constraint equations will be free of sinusoidal term, and describing coordinates on a link using xy-components is more intuitive compared to using an angle and magnitude.

The graphical representation of the behavior in example 1 provides a building block for creating complex balanced linkages. The building block is the linkage provided in figure 4i, which is is equivalent to a ZFLS. Any ZFLS in a balanced system can be replaced by this building block, resulting in a balanced linkage of higher order. In this manner complex multi-articulated linkages can be constructed, based solely on this equivalence. Additionally the minimal number of springs required to balance a n-link linkage can be established. When starting with a single balanced link (Figure 4k) the ZFLS is replaced to obtain a two link two spring system (Figure 4l), effectively adding one spring and one link. Replacing a spring can be repeated many times to obtain a n-moving link system balanced by n-ZFLSs.

5. Conclusion

In this work the implementation of the stiffness matrix approach is altered such that states and link locations are expressed in the same coordinate system. The first goal was to implement Cartesian coordinates and comparing it to

the use of polar coordinates in the stiffness matrix approach. The Cartesian coordinates were successfully implemented and in comparison they were found to be more intuitive in use, provide simpler constraint equations and be more convenient for altering parameters of balanced systems. The second goal was to gain more insight in the relations between parameters while the third goal was to illustrate these behavioral relations in two examples. These two goals were achieved simultaneously as in the examples two basic systems (both having two moving links) were analyzed. Relations were found between orientation, positioning and magnitude of springs and masses. These are described and illustrated providing a visual overview of the design space. Obtained relations provide knowledge in the possibilities to vary spring system parameters while maintaining static balance.

Acknowledgments

This research is part of the project 'Flextension', sponsored by Technology Foundation STW, project 11832.

References

[1] J. L. Herder, Energy-free systems; theory, conception and design of statically balanced spring mechanisms, Ph.d. thesis, Delft University of Technology, iSBN 90-370-0192-0 (2001).

[2] S. K. Agrawal, A. Fattah, Gravity-balancing of spatial robotic manipulators, Mechanism and machine theory 39 (12) (2004) 1331–1344.

[3] A. H. Stienen, E. E. Hekman, G. B. Prange, M. J. Jannink, F. C. van der Helm, H. van der Kooij, Freebal: design of a dedicated weight-support system for upper-extremity rehabilitation, Journal of Medical Devices 3 (4) (2009) 041009.

[4] M. Carricato, C. Gosselin, A statically balanced gough/stewart-type platform: conception, design, and simulation, Journal of Mechanisms and Robotics 1 (3) (2009) 031005.

[5] K. Kobayashi, Comparison between spring balancer and gravity balancer in inertia force and performance, Journal of Mechanical Design 123 (4) (2001) 549–555.

[6] G. Endo, H. Yamada, A. Yajima, M. Ogata, S. Hirose, A passive weight compensation mechanism with a non-circular pulley and a spring, in: Robotics and Automation (ICRA), 2010 IEEE International Conference on, IEEE, 2010, pp. 3843–3848.

[7] C.-W. Hou, C.-C. Lan, Functional joint mechanisms with constant-torque outputs, Mechanism and Machine Theory 62 (2013) 166–181.

[8] R. Sapper, Lamp with an articulated support, uS Patent 3,790,773 (Feb. 5 1974).

[9] J. Wang, C. M. Gosselin, Static balancing of spatial three-degree-of-freedom parallel mechanisms, Mechanism and Machine Theory 34 (3) (1999) 437–452.

[10] H. Hilpert, Weight balancing of precision mechanical instruments, Journal of Mechanisms 3 (4) (1968) 289 – 302.

[11] S. K. Banala, S. K. Agrawal, A. Fattah, V. Krishnamoorthy, H. Wei-Li, J. Scholz, K. Rudolph, Gravity-balancing leg orthosis and its performance evaluation, Robotics, IEEE Transactions on 22 (6) (2006) 1228–1239.

[12] P.-Y. Lin, W.-B. Shieh, D.-Z. Chen, A theoretical study of weight-balanced mechanisms for design of spring assistive mobile arm support (mas), Mechanism and Machine Theory 61 (2013) 156–167.

[13] P.-Y. Lin, W.-B. Shieh, D.-Z. Chen, A stiffness matrix approach for the design of statically balanced planar articulated manipulators, Mechanism and Machine Theory 45 (12) (2010) 1877–1891.

[14] P.-Y. Lin, W.-B. Shieh, D.-Z. Chen, Design of statically balanced planar articulated manipulators with spring suspension, Robotics, IEEE Transactions on 28 (1) (2012) 12–21.

[15] Y.-Y. Lee, D.-Z. Chen, Determination of spring installation configuration on statically balanced planar articulated manipulators, Mechanism and Machine Theory 74 (2014) 319–336.

[16] S. R. Deepak, G. Ananthasuresh, Perfect static balance of linkages by addition of springs but not auxiliary bodies, Journal of Mechanisms and Robotics 4 (2) (2012) 021014.

2

PAPER 2

2.1. A CLOSE TO BODY, STATICALLY BALANCED MOBILE ARM SUPPORT BASED ON A NOVEL SPRING SYSTEM

This second paper is focused on designing a mobile arm support based on a spring system balancing a human arm for patients of Duchenne muscular dystrophy. Multiple steps are made to make this possible. Consisting of providing adjustability rules, allowing for balancing an arm with unknown mass. Furthermore, new techniques for slitting up springs, to create hollow spring structures, allowing for spring behavior in otherwise unreachable locations. The obtained design is evaluated in an experiment.

A close to body, statically balanced mobile arm support based on a novel spring system

M. P. Lustig[a], A. G. Dunning[a,b], J. L. Herder[b]

Delft University of Technology, Faculty of Mechanical, Maritime and Materials Engineering, Delft, The Netherlands

[a] *Department of Biomechanical Engineering,*
[b] *Department of Precision and Microsystems Engineering*

Abstract

Muscle weakness can hinder a person to lift his arms. For regaining arm related tasks, no adequate solution exists. State of the art arm supports do not fit the human in a fulfilling manner and limit the users range of motion. The goal of this work is to implement a novel spring system design in a mobile arm support, using two bi-articular zero-free-length springs, to statically balance the arm. Advantages of this system are that no parallelogram linkage is required, a natural range of motion is allowed and that the location of all spring attachment points are variable. Three sub-goals are set to achieve the main goal. The first is creating a simple system description. Two simple design equations are set up to describe balance conditions and adjustment rules are provided. The second sub-goal is to provide new technology to fit the system around the human body. New techniques are introduced for subdividing springs, allowing for the creation of 3D hollow spring structures. At low elevation angles a close fit to the body is observed, at higher elevations larger gaps are present. The final sub-goal is to perform an experimental evaluation on the prototype. Two output forces, at wrist and elbow, are measured in the four DOF system. At small elevations the desired balancing force is observed, at larger elevations differences are found. Possible causes are the loss of ZFLS behavior near the lower bound of the spring linearity region and inconsistent spring attachment locations. Solutions for future designs consist of avoiding the lower boundary of the linear ZFLS region and creating more consistent spring attachments. The main goal is fulfilled as the spring system shows great potential for application in an adjustable close-to-body mobile arm support.

Keywords: Mobile arm support, Duchenne muscular dystrophy, Static balance, Zero-free-length spring, Serial linkage

1. Introduction

Duchenne muscular dystrophy (DMD), is a genetic neuromuscular disorder, linked to the x-chromosome [1]. It occurs in roughly 1 out of every 3500 male births [2]. Patients with this disorder progressively lose muscle strength and have a life expectancy of 35 years [3]. Around the age of 14 they will lose the ability to walk and have insufficient strength to lift their arms [3]. This loss obstructs them in performing the most basic tasks of daily living. As a consequence, their quality of life is greatly reduced for over half of their life. Mobility can partially be regained by using a wheelchair. However, for arm related tasks, no adequate solution exists.

The state of the art of mobile arm supports consist of a variety of robotic and passive supporting solutions [4, 5]. In general, these solutions use a large volume and do not fit the human body in an elegant manner. Furthermore, most solutions constrain the natural range of motion of the human arm. They provide support, either only in a limited range of motion, or solely for the upper arm limb [4].

The most promising solutions make use of classical static balancing techniques to balance the arm [6, 7, 8]. In a statically balanced system, the gravitational force acting on a mass is compensated for, independent of its pose [9, 10]. A simple example of static balance is balancing a mass, using the upward lifting force of a helium balloon. This system can be moved to different positions and remain motionless, without the need for any external force or energy source. Most current arm support designs are based on classical balancing solutions for serial linkages, using mono-articular zero-free-length spring (ZFLS), where the spring force of a ZFLS is proportional to its length [6, 9]. These solutions require a parallelogram linkage alongside the upper arm, to provide a link with fixed orientation at the elbow joint [9]. Disadvantage of using parallelogram linkages are the restricted planar motion, the increased number of parts and added mass, inertia and volume of the linkage.

In recent literature, a method for designing statically balanced serial linkages, using multi-articular ZFLSs, was presented [11, 12]. Obtainable systems have the advantage of not requiring a parallelogram linkage. Therefore, a two-link system can be used, allowing spatial, out of plane rotations. Thus, these systems have the potential to balance the human arm in any natural pose. A spring configuration makes use of two ZFLSs to balance a two link system [13]. Here the first spring is a bi-articular ZFLS, between the fixed world and the lower arm. The second spring is a mono-articular ZFLS, connecting the upper and lower arm. In recent work this spring configuration was implemented in a mobile arm support [14]. Using this spring system, the arm is balanced while maintaining the natural range of motion of the human, a great improvement compared to current solutions. Nonetheless, a downside of this configuration is that the lower arm attachment point, for the spring connected to the fixed world, must be located on the combined COM of the arm limbs [15]. This un-adjustable point is located at an approximate distance of $0.1[m]$ from the elbow joint, in line with the arm. A shorter distance would allow for a closer fit around the human body.

A second new spring configuration, without auxiliary links, is examined in the present paper. This system is obtained using the same methods [11, 15]. It uses two bi-articular ZFLSs, both between the fixed world and the lower arm (Figure 1a). This configuration provides 4 degrees of freedom (DOFs) and allows for the natural range of motion of the human arm. Furthermore, all spring attachment point locations are adjustable, potentially allowing for a better fit to the human arm. Nevertheless, these attachment point locations can not be selected independent of each other. Specific relations between these locations and other parameters must be fulfilled for the system to be statically balanced [15].

As the state of the art mobile arm supports do not fit the human arm in a natural and inconspicuous manner, it is proposed to use the new spring system in a mobile arm support. The main goal of the presented paper is to implement this new spring configuration in a mobile arm support. Three sub-goals are set up to reach this goal. The first sub-goal is to describe the spring system in a novel way, providing adjustment rules required for balancing a system with unknown mass. The second is to provide new technology that makes it possible to fit the spring system around the human body. The final sub-goal is to perform an experimental evaluation of the created prototype.

In the method section of this paper, the system is first parameterized such that transparent design equations are obtained. These equations describe the conditions for static balance and contain rules for adjusting the spring system. Next, the springs are examined and techniques for subdividing springs are described. These techniques are used to create hollow spring structures fitting around the human arm. The experimental evaluation is elaborated and the findings are presented in the results section. The obtained results are discussed and the spring system is evaluated and compared to previous work. Finally, the overall conclusions are drawn.

2. Methods

2.1. Spring system

In the proposed spring system, two links are balanced using two ZFLSs. Both connect the lower arm link to the fixed world (Figure 1a). To ensure static balance, design equations are set up to be fulfilled. In current literature, on statically balancing serial linkages without auxiliary links, a general parameterization is used [11, 15]. The design equations in this general form are difficult to solve and interpret. In the present paper, the system is parameterized such that these equations can be written in an elegant form, providing insight in behavioral relations in the system. The used parameters for link and spring parameters are shown in figures 1a and 1b respectively. The corresponding design equations for static balance are given in equation 1. Proof that these equations describe all static balanced solutions and reasoning for defining the parameters as such, are elaborated hereafter. A comparison to the parameterization in literature is provided in the Discussion section.

$$m_1 g s_1 + m_2 g L = k d L \tag{1a}$$

$$m_2 g s_2 = k b c (1 - f) f \tag{1b}$$

Alongside parameters describing magnitudes for length, mass and stiffness, factor f is found in the design equations (Eq. 1). This factor describes the ratio between the spring stiffness of the upper and lower springs (Eq. 2).

$$f = \frac{k_1}{k_1 + k_2} = \frac{k_1}{k} = 1 - \frac{k_2}{k} \tag{2}$$

For a balanced system, this factor f is found between multiple system dimensions, other than this ratio between spring stiffness. To show where and why this factor is found, a force decomposition of the lower arm is set up (Figure 2a). Here the top and bottom spring forces are decomposed into two components each. The first being dependent solely

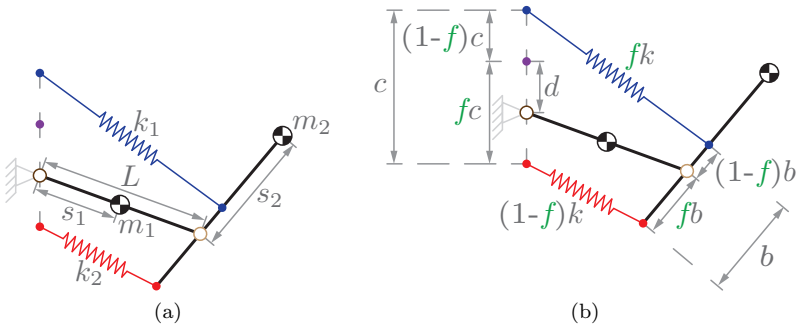

Figure 1: (a) Link parameters. (b) Spring parameters

on the elbow joint location, the second only on the lower arm orientation (Figure 2a). Therefore, the effect of spring force on the lower and upper arm can be examined separately.

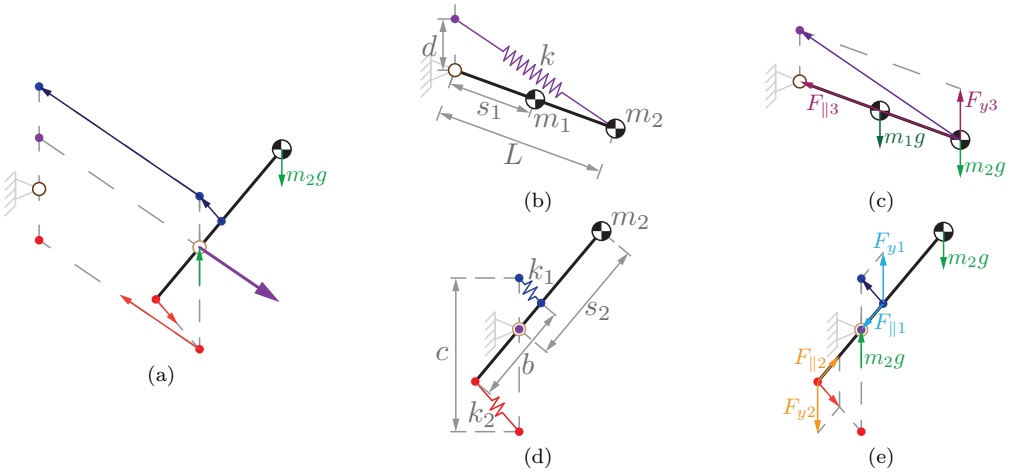

Figure 2: (a) Lower arm force decomposition. (b) Representation of effect springs on upper arm. (c) Decomposition of forces dependent on upper arm orientation. (d) Representation of effect springs on lower arm. (e) Decomposition of forces dependent on lower arm orientation.

The effect of the springs on the lower arm is depicted in figure 2d, its force decomposition is shown in figure 2e. For static balance, the resultant force at the elbow joint must be independent of the lower arm orientation. This is only the case when the force components aligned with the link, $F_{\parallel 1}$ and $F_{\parallel 2}$, have an equal magnitude and thus cancel each other out. These forces are a function of spring stiffness and the respective distance from joint to attachment (Eq. 3). It is found that these forces are equal only when the factor f is used to describe the ratio in distance b (Eq. 3c). Therefore b is parameterized using ratio f such that this requirement for balance is fulfilled consistently (Figure 1b). The moment around the elbow, created by vertical force components F_{y1} and F_{y2}, balances the weight of the lower arm.

$$F_{\parallel 1} = F_{\parallel 2} \tag{3a}$$
$$k_1 b_1 = k_2 b_2 \tag{3b}$$
$$fk(1-f)b = (1-f)kfb \tag{3c}$$

The force acting on the upper arm depends on the parallel force components of both springs (Figure 2a). Their magnitudes depend on the location of the elbow joint. The force is equal to zero when the elbow is located at distance d above the shoulder joint. The location of point d is determined by factor f, with respect to the distance between the fixed world attachment c (Figure 1b). When the elbow joint is moved from this force free point it behaves like a ZFLS with combined stiffness k. The effect of this virtual ZFLS on the upper arm is illustrated in figure 2b, the force decomposition is shown in figure 2c. The (purple) ZFLS, with stiffness k, can ensure static balance by providing a constant upward force (F_{y3}) at the elbow (Figure 2c).

The design equations (Eq. 1) each describe the balance relation for a different link. Upper arm balance is ensured by the first equation 1a, it only contains parameters affecting the upper arm (Figure 2b). Lower arm balance is described by the second equation 1b, it only holds parameters affecting the lower link (Figure 2d). In addition, the equations are

written such that the left sides contain the effects of mass and the right sides the effect of the springs. Therefore, rules for adjusting parameters to balance a different mass, either of the upper or the lower arm, are directly described in these design equations (Eq. 1). Thus increasing one of the spring parameters, on the right side (k, b, c, d), will result in an increase in the upward balancing force acting on one (or both) of the links, in a linear manner (Eq. 1).

These adjustment rules can be used to balance a system of which the exact mass is unknown, like a human arm. For an arbitrary arm, it is assumed the arm dimensions are known and two ZFLSs are used, having known spring stiffness values. Thus arm parameters L, s_1, and s_2 and spring parameters k and f are known constants. The springs are attached to the link, as in figure 1b, parameters are selected based on an estimate for the arm mass. However, the resulting system will, most likely, be unbalanced. For example, it is assumed the upper arm link is underbalanced and the lower arm link is overbalanced. To balance the upper arm a higher lifting force on this limb is required. Following equation 1a, parameter d must be increased until this link is balanced. For lower arm balance a lesser lifting force is required. Following equation 1b, either the magnitude of b, c or both can be reduced until a balanced state is obtained.

The simultaneous rotation α, of the spring attachment points, can be added to the system. This does not affect the 2D in-plane balance (Figure 3). For the fixed world attachments, the point of rotation is the (purple) point at a distance d above the shoulder joint. The lower arm attachments rotate about the elbow joint. Distances between attachments, b and c, as well as factor f still apply and follow the same design equations for static balance (Eq. 1). For 3D balance, angle α must be equal to zero [15]. At this angle, the system has a symmetry around the vertical axis through the shoulder joint. Therefore, it can rotate freely around this axis without changing spring length or COM height. Additionally, at $\alpha = 0$, the lower arm is balanced in every 3D pose. As at this angle, the system representing the lower arm behavior (Figure 2d), shows the same symmetry around the vertical axis. For any other α only motions in a single plane are balanced perfectly and the system has a tendency to fall out of this plane. In the present paper a system with $\alpha = 0$ is used to obtain the desired 3D static balance.

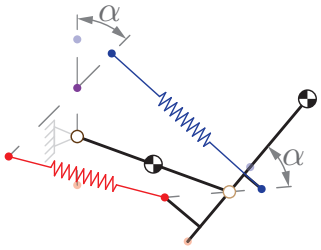

Figure 3: Rotation α does not affect 2D static balance behavior. 3D balance is afected by this rotation.

2.2. Springs

The springs used in the chosen spring-configuration have to be ZFLSs, thus having a reaction force proportional to the spring length. The springs used in this paper are elastic bands which approximate this desired behavior in a large deflection range. The material of these bands is synthetic natural rubber, also known as polyisoprene, the bands have an unloaded length of 88 [mm] (half of the perimeter length) and a cross sectional area of 26 [mm^2] (Figure 4a). Approximate ZFLS behavior is observed in the force deflection behavior, subsequent deflection cycles of the same spring are shown (Figure 4b). The ZFLS behavior is found in the elongation range within spring lengths of 150% upto 350%. Creep affects the force deflection behavior mainly in the first few elongations of these springs, the steady state behavior is observed after these effects took place. Consistent steady state behavior is observed for pre-strained springs for a duration of over a week.

2.3. Subdividing springs

ZFLSs can be subdivided such that a virtual ZFLS is created [9]. In this manner ZFLS behavior can be obtained in otherwise unreachable locations. A v-shape orientation of two ZFLSs, act as a single virtual ZFLS with the summed stiffness value (Figure 5a)[9, 16]. The location of the virtual attachment depends on the ratio in stiffness between the split up springs, represented by factor a (Figure 5a). As there is a point where all springs meet, the rigid link in this system can be in any orientation without affecting the ZFLS behavior of the virtual spring. A novel alternative way of subdividing springs is connecting two ZFLSs to two links (Figure 5b). When the two links are kept parallel to each other, a virtual ZFLS is created. The virtual attachment points are located in between the original attachments, at a location following ratio a between the spring stiffness values (Figure 5b). A rotation, between the two links, will introduce a moment in addition to the ZFLS behavior.

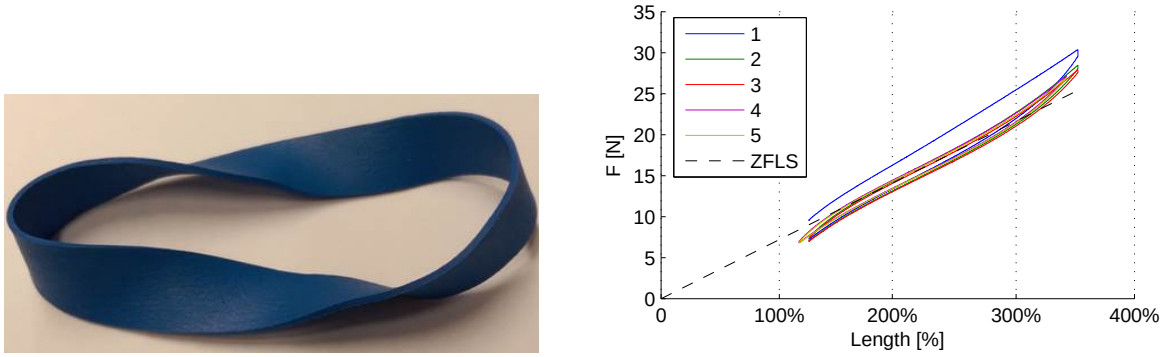

(a) (b)

Figure 4: (a) Rubber bands with approximate ZFLS behavior. (b) Force deflection curve of rubber band. Subsequent deflection cycles are labeled 1 to 5.

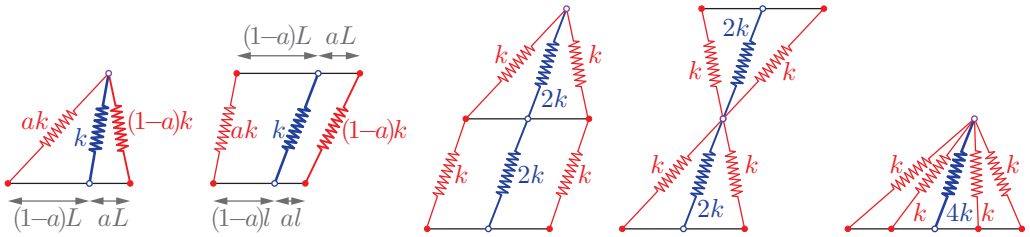

(a) (b) (c) (d) (e)

Figure 5: Subdivision schemes for ZFLSs, for creating equivalent virtual springs. (a) v-shaped configuration. (b) Parallel configuration. (c) Serial placements of two virtual springs, total stiffness value is k. (d) Serial x-shaped configuration, total stiffness value is k. (e) Parallel placement of two v-shaped configurations, summed stiffness value.

The virtual springs can be combined just like regular springs, they can be placed in series or in parallel to other (virtual) ZFLSs. Web like spring compositions can be created, acting as if a single ZFLS is used. The serial composition of v-shaped and parallel virtual springs (Figures 5a and 5b) is shown in figure 5c. ZFLS behavior is still present. Furthermore, the space directly in-between the virtual attachments becomes free. A second serial configuration, using two v-shaped virtual springs, is creating an x-shaped configuration (Figure 5d). Space is created near both virtual attachments. The orientations of the top and bottom links are free. A parallel combination is shown in figure 5e, here four springs act as a single virtual spring.

Subdividing ZFLSs is now extended to 3D. First, a cross section of a 2D spring subdividing scheme, perpendicular to the spring elongation direction, is shown in figure 6a. This new spring pair can be considered to be in a certain plane. This plane can be rotated around the line in which the original spring acts, while maintaining the original behavior. A 3D spring system is obtained by subdividing both spring in the new pair once more, each in a rotated plane (Figure 6b). A 3D subdivided spring system is obtained acting as the single original ZFLS. A hollow ZFLS is created where physical springs are located around the working line compared to all springs being directly on this line (Figure 6c). Such hollow springs allow for close to body spring systems.

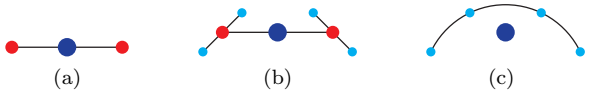

(a) (b) (c)

Figure 6: (a-c) Cross-section of 3D split up schemes, the blue dot represents the original spring, the two red dots and the four cyan dots are equivalent to orininal blue spring, stiffness is equivalent to surface area of dots.

2.4. Design around human body

The spring system (Figure 1) is now fitted on the human arm (Figure 7a). The top spring attachments are located above the shoulder joint and on the lower arm, in-between the elbow and wrist. The bottom spring is located underneath the shoulder joint, going to the lower arm at a location behind the elbow in line with this limb. In this set up, both springs will intersect the arm in many poses. Previously described techniques for splitting up springs are applied on this system, in order to prevent these conflicts and greatly increase the amount of allowable arm poses.

The top spring is examined first. How it intersects the human arm is examined in the pose of figure 7a. This pose represents an 'extreme' case for wheelchair bound applications, moving the arm back or down will result in hitting either the arm-support or backrest. Section A (Figure 7a) is the arm cross section in which the top spring acts. The cross section is illustrated in figure 7b. The green surfaces represent the upper and lower arm sections, the blue crosses are the desired spring attachment point locations. When a spring is placed directly in-between these points, both the upper and lower arm are clearly intersected by this spring (Figure 7c). The conflict at the lower arm can be resolved by using a v-shaped spring configuration, placing attachments on both sides of the lower arm, separated by a circular link fitted around the surface of the lower arm (Figure 7d). Nevertheless the upper arm is still intersected. A serial v-shape and parallel springs resolves this issue (Figure 7e). Here, an additional spatial circular arc is used to separate the springs at shoulder height. This arc connects the springs on both sides of the arm and runs in front of it, effectively creating a hollow spring structure. Additional spring split-up steps are added to further distribute the spring material, reducing the stiffness of individual elements (Figure 7f). Up to a final extend where a single thin sheath of spring material is used (Figure 7g). The embodiment of such a hollow spring structure is shown in figure 7h. The circular arc separating the springs is shown as well (Figure 8).

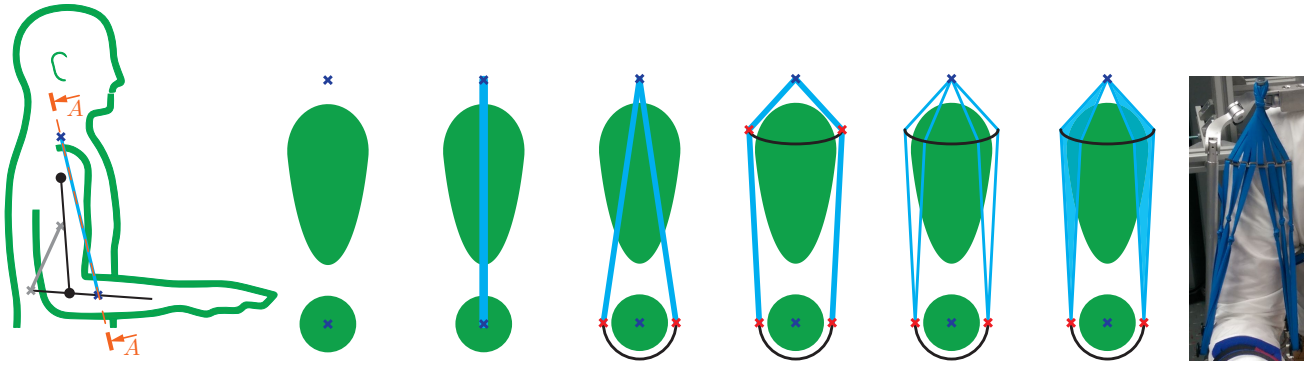

(a) (b) (c) (d) (e) (f) (g) (h)

Figure 7: (a) Definition of section A. (b-g) Subdivision schemes in section A. The two surfaces represent the cross sections of the human upper and lower arm. (h) Top spring embodiment.

Figure 8: Circular arc, for spring separation.

The lower spring is fitted around the human next. It connects the fixed world, underneath the shoulder, to the lower arm behind the elbow. The conflicts experienced by this spring are more difficult to capture in a single image. The different problem areas will be discussed separately. The (virtual) attachment on lower arm is located in the central line of the arm behind the elbow. When the lower arm is fully extended this virtual point is located inside the upper arm. To avoid this intersection the spring is separated to be on both sides of the arm. Once more, a circular link around the arm connects these points. The second critical area is at the fixed world attachment. Here the spring attachment should be located directly underneath the shoulder joint, directly in the users arm pit. A physical component at this exact point is undesirable, as it would inhibit the upper arm to be positioned vertically besides the body. Instead, a virtual spring is realized at this point, by splitting up this attachment to be on the chest (Q) and behind the shoulder (P) (Figures 9a, 9b and 9c). Thus both attachments of the lower spring are split up. Between these points an x-shaped spring system is used (Figure 9d), such a system provides a point around which the spring can rotate,at the center of the x, the location of this point (h) can be varied (Figure 9d).

An adjustable mobile arm support is obtained by combining the adjustment rules and the added variability of splitting up springs. A prototype based on the spring system of figure 1 is build, containing the described top and bottom springs (Figures 7e and 9d). The springs are suspended on a rigid linkage that runs alongside the body. This linkage has a pin joint aligned with the elbow and spherical joint behavior at the shoulder, with a virtual point of rotation aligned with the human shoulder joint. These joints allow for natural, three dimensional motions and provide the system with four degrees of freedom (3 at the shoulder, 1 at the elbow) [14]. The three fixed world spring attachments are fixated to a rigid frame. Pictures of the complete system in four different poses are provided (Figure 10).

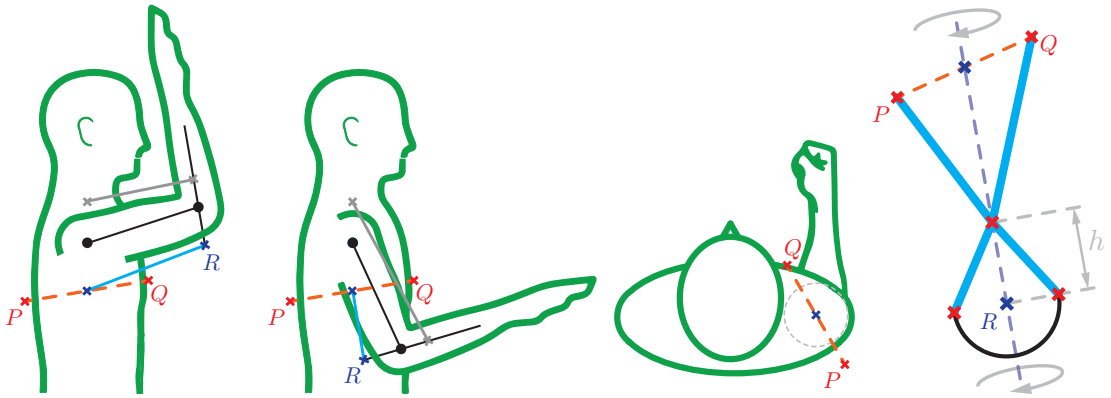

(a) (b) (c) (d)

Figure 9: (a-c) Different views of splitting up the bottom fixed world spring attachment point for better fit on the human. (d) x-shaped spring configuration, with split up fixed world attachments (top) and lower arm attachments (bottom).

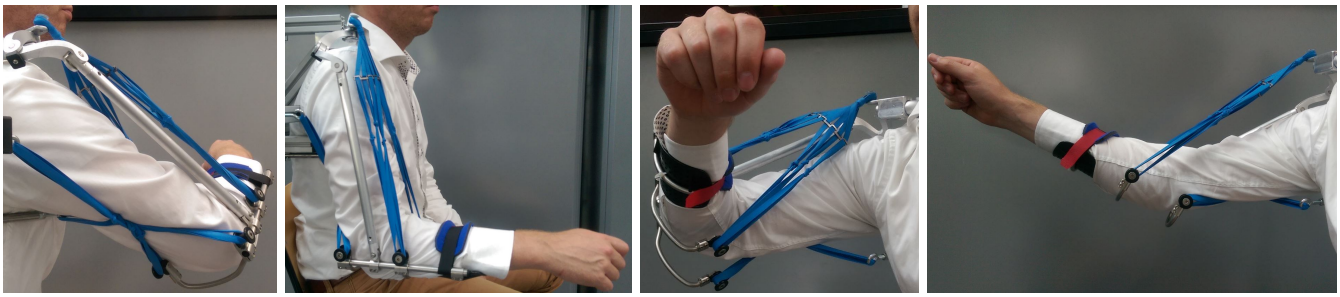

(a) (b) (c) (d)

Figure 10: (a-d) Spring system and supporting structure fitted around the human arm, positioned in multiple poses.

2.5. Experimental evaluation

An experimental evaluation is set up to assess the balancing quality of the prototype. A model is made for the set up, having a mass at the elbow (m_1) and wrist (m_2) (Figure 11a). The parameters of this model are listed in table 1. The values for masses m_1 and m_2 are calculated based on the other parameters, obeying the design equations (Eq. 1).

Parameter	*Value*	*Unit*
f	2/3	-
b	0.08	$[m]$
c	0.15	$[m]$
d	0.04	$[m]$
k	480	$[N/m]$
L_1	0.287	$[m]$
s_1	0.287	$[m]$
s_2	0.127	$[m]$
g	9.81	$[m/s^2]$
m_1	1.03	$[kg]$
m_2	0.93	$[kg]$

Table 1: Parameters of the experimental setup.

State	*Description*	*Angle*	*Description specific state value*
φ_1	Flexion Angle	45°	Partially Extended elbow.
		90°	Right angle elbow.
		120°	Flexed elbow.
φ_2	Orientation of Flexion Plane	0°	Type A. Arm in vertical plane.
		60°	Type B. Arm in front of chest.
φ_3	Elevation Angle	30°	Lowest elevation upper arm.
		50°	
		70°	
		90°	Horizontal upper arm.
		110°	Highest elevation upper arm.
φ_4	Orientation of Elevation Plane	45°	Abducted plane.
		90°	Forward plane.

Table 2: States at which measurements are performed.

The spring system statically balances the masses of the two limbs (Figure 11a). For the experiment the masses are removed, such that a system providing constant upward force remains. These upward forces are measured. The experimental setup uses a rigid structure to support the spring system (Figure 11c-11e). The upward force component is reduced by the weight of this structure. For the lower arm, the effect of this weight is insignificant. The mass of the lower arm structure is relatively low and its COM is located near the elbow joint. Thus, the force acting at the wrist is not affected significantly. The weight of the upper arm structure does affect the force output. The combined mass of the structure links, including attachment required for the measurement, is $m_s = 0.8[kg]$ and the combined COM

is located on the upper arm, at distance $s_s = 0.23[m]$ from the shoulder joint. Thus the upwards force which can be measured on the upper arm is reduced due to mass m_s.

The resulting system provides two upward output forces, one acting at the elbow F_{el}, the other force acts at the wrist F_{wr} (Figure 11b). Force F_{wr} is affected only by the weight of m_2 (Eq.4a). The force acting at the elbow (F_{el}) is affected by the weight of m_1 and the structure m_s (Eq.4b). The springs in the setup are split up, as described earlier (Figures 11c-11e). The fixed world attachments and the shoulder joint hinge point are connected to each other by a rigid frame construction. Furthermore, all forces are measured in the central axis of the arm construction. To this end, rods are added between the device and the attachment points of the force scales.

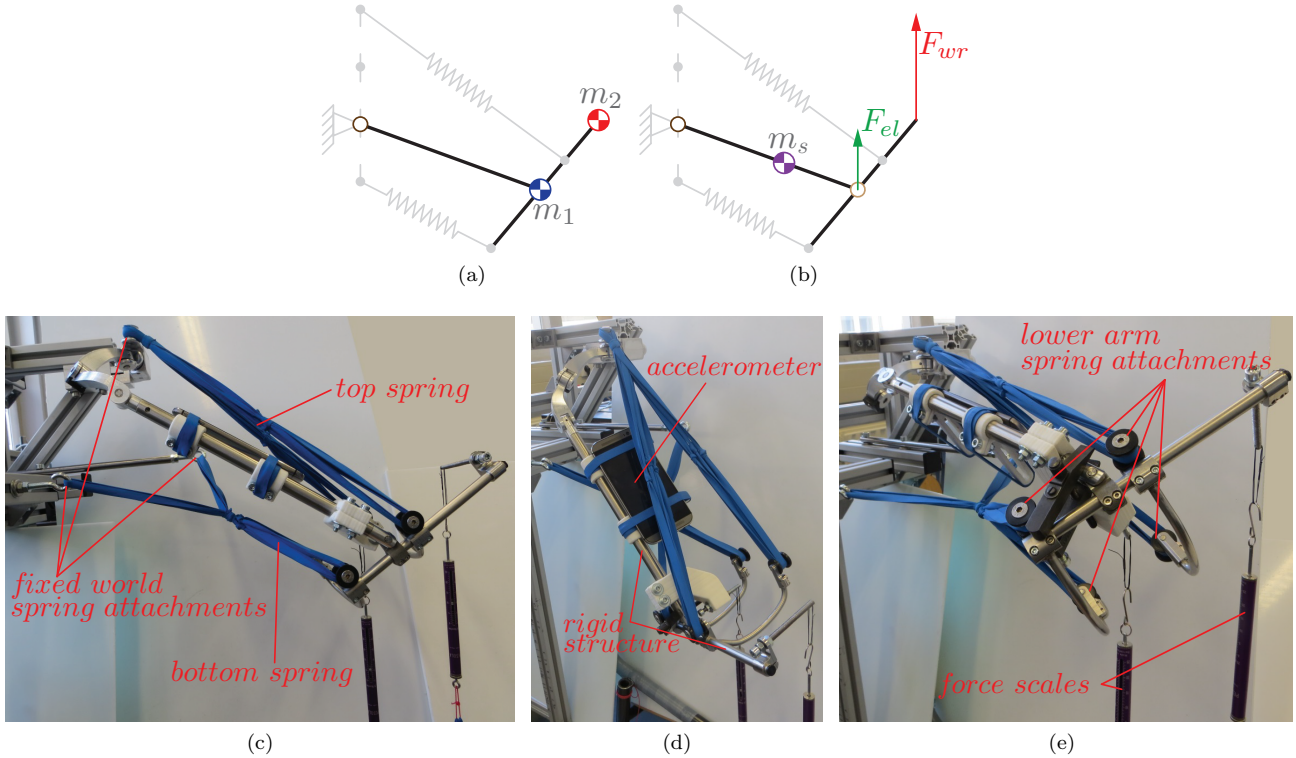

(a) (b) (c) (d) (e)

Figure 11: (a) Balanced model of experimental setup, mass m_1 is modeled to be at the elbow, mass m_2 is located at the wrist. (b) Masses m_1 and m_2 are removed from the system, what remains is structure mass m_s and two upward forces acting at the elbow and wrist (F_{el} and F_{wr} respectively). (c-e) Pictures of the experimental setup. Important components are indicated.

$$F_{wr} = m_2 g = 10.1[N] \tag{4a}$$

$$F_{el} = m_1 g - m_s g \frac{s_s}{L_1} = 2.83[N] \tag{4b}$$

Measurements are performed for different system states. The state of the system is defined by four DOFs, as described in literature [17]. It defines a flexion angle (φ_1), an elevation angle (φ_3) and the orientation of the flexion and elevation planes (φ_2 and φ_4 respectively)(Figure 12a). Measurements are performed for all possible combinations of states listed in table 2.

The theoretical force output of the system is known (Figure 11b). The experiment is set up to test the actual force output of the system, in multiple arm orientations. The difficulty, of measuring the studied system, is that there are four DOFs and two output forces. Because of this complexity, it is crucial to set up an experiment for which it is clear what the obtained measurements imply. Actions taken, to ensure clear measurements, consist of avoiding friction effects and measuring all forces in vertical direction.

For the used structure the friction in the elbow joint is found to be high. The effect of this friction component on the measured output are of the same order of magnitude as the desired output forces. As the goal is to measure the effect of the spring system, the experiment is designed to avoid the effects of the elbow friction component. This is obtained by mechanically constraining the elbow joint at a fixed angle (φ_1) during the measurements. Other states (φ_2, φ_3 and φ_4) are manually maneuvered to have specific values. The angles of these three states are measured by

using an accelerometer, to determine its orientation with respect to the gravitational acceleration field. This sensor is fixated to the upper arm (figure 12a), and the angles are positioned with 2° accuracy.

Two types of experiments are performed (Type A and B). The main difference is that for type A, a single vertical force is used to hold the system in place, while for type B, a second vertical force is required to determine all states. During a type A measurement, a single downwards force (F_A) is measured at the elbow joint (Figure 12b). Altering the location of the working line of this force, allows alterations of states φ_3 and φ_4. Remaining state φ_2 is left free, it will orient itself in its preferred upwards position, at $\varphi_2 = 0°$. For the type B measurement, an additional force is applied at the wrist. This force allows for altering state φ_2 to different values (Figure 12c).

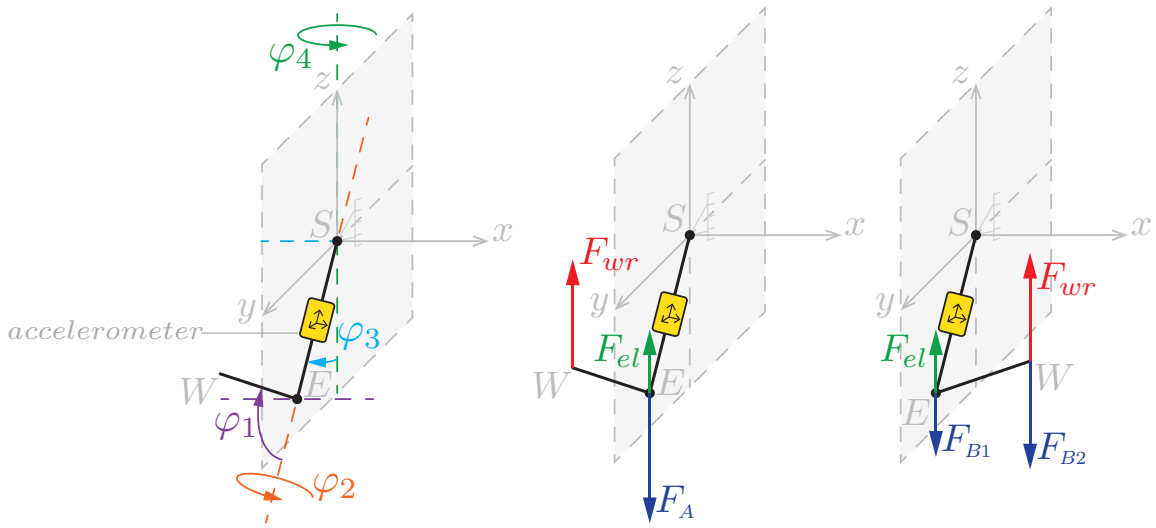

(a) (b) (c)

Figure 12: (a) Definition of state angles, the linkage represents the right human arm. Points S, E and W represent the shoulder, elbow and wrist respectively. (b) Forces acting during a type A measurement ($\varphi_2 = 0°$). (c) Forces acting during a type B measurement ($\varphi_2 = 60°$).

For type A, the ideal force measured at the elbow F_A is not constant, it is a function of the system states. This is because the ratio between moment arms, from shoulder to elbow and shoulder to wrist, is not constant either (Figure 12b). Therefore, the effect of the wrist force on the measured output varies for different arm poses. Equation 5a describes the ideal force, measured at the elbow, for a type A measurement. For a type B measurement, both ideal case forces (F_{B1} and F_{B2}) are constant (Eq. 5). Both forces directly counteract one of the two upward system forces (Figure 12c).

$$F_A = F_{el} + F_{wr}\left(\frac{L_1 \sin(\varphi_3) + s_2 \sin(\varphi_1 + \varphi_3)}{L_1 \sin(\varphi_3)}\right) \tag{5a}$$

$$F_{B1} = F_{el} \tag{5b}$$

$$F_{B2} = F_{wr} \tag{5c}$$

During a measurement states φ_1, φ_2 and φ_4 are kept constant while state φ_3, describing the elevation angle, is varied. Each measurement begins with an upwards arm position $\varphi_3 = 110°$, going in steps of $-20°$, to the downwards position $\varphi_3 = 30°$ and then back up again. This set is repeated twice, each measurement consists of four parts (D1, U1, D2, U2). At each step, the downwards force component(s) are measured using spring scales (Pesola, range: $0 - 25[N]$, resolution: $0.5[N]$).

3. Measurement results

Results are shown for flexion angle $\varphi_1 = 90°$ (Figure 13), for all variations of parameters φ_2, φ_3 and φ_4 as listed in table 2. Other results, for different flexion angles, are not shown, as they illustrate similar behavior. In these graphs the dotted line represents the ideal case measurement, obtained when the system behavior is ideal. For the type A measurements (Figures 13a and 13b) this ideal line follows equation 5a. For the type B measurements (Figures 13c and 13d), the ideal lines have a constant value (Eq. 5b and 5c).

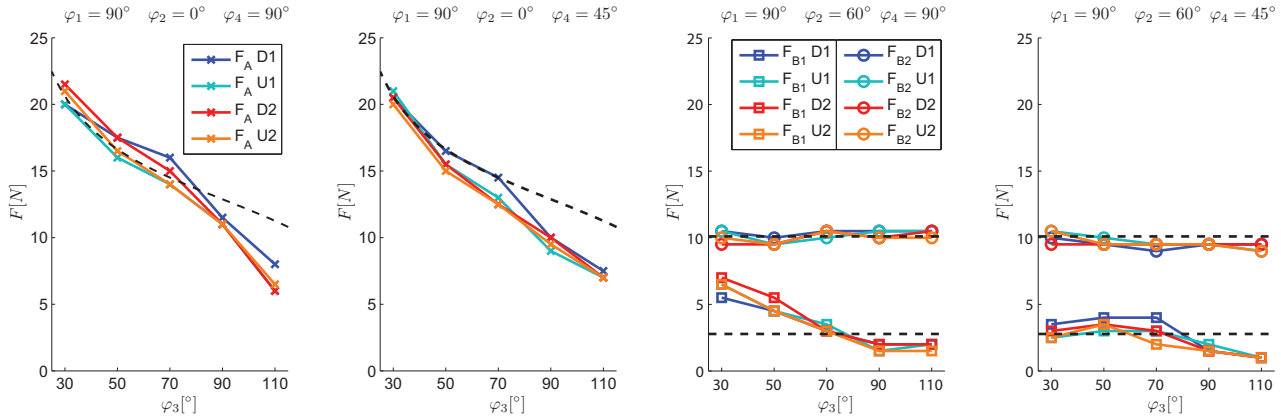

(a) (b) (c) (d)

Figure 13: Measurement results, each set consists of sequential downwards (D1), upwards (U1), downwards (D2) and upwards (U2) measurement. State values kept constant during a specific measurement are stated above each graph. (a-b) Type A measurements. (c-d) Type B measurements.

4. Discussion

4.1. Design equations

In literature on designing static balanced serial linkages, without auxiliary links, predefined parameterization is used. General parameters are implemented independent of the selected amount of links and spring configuration. The general parameters either describe link locations using polar coordinates and Cartesian coordinates for states [11]. Or by using Cartesian coordinates to describe locations as well as states [15]. These methods are extremely useful for creating new spring configurations, consisting of any amounts of links and springs. However, when a specific spring system is selected, custom parameters are recommended. Whit custom parameters, less and simpler design equations are obtained, providing more understanding of the described system. For example, for the spring system of the present work (Figure 1a), parameterizations from literature require six equations, on average containing 15 terms each [11]. While present parameters (Figure 1), only require two equations with an average of eight terms per equation (Eq. 1). Moreover, the effect of springs on different links is described in separate equations, providing useful adjustment rules. For creating custom parameters for larger linkages, it is advised to use factors between spring stiffness values as parameters and to describe virtual spring attachment locations, as in the present work.

4.2. Fit around human body

The fit of the spring system, around the human body, is evaluated for the prototype. In poses with low elevation angles a good fit is observed for both springs. The benefits of the 3D hollow spring structure become clear, as the spring arc of the top spring fits well around the upper arm in these poses (Figure 10b). For higher elevation angles larger gaps between the springs and the arm are observed (Figure 10d). As the upper arm and the spring are oriented as a parallelogram. Furthermore, at a pose with a high elevation and a large angle for the orientation of the flexion plane, the arc of the top spring is no longer aligned with the arm surface (Figure 10c). The reason is that this arc always has a parallel orientation with respect to the lower arm attachments of the top spring. In such a pose, the tip of the spring arc can touch the users arm and the spring system is oriented relatively far from the human body.

4.3. Measurements

The measurement results are analyzed. In some poses the balancing force approximates the ideal value. Others regions show an offset to this desired force. Possible sources of these errors are explained. Improvement are proposed for reducing these errors.

For type A measurements (Figures 13a and 13b), force F_A matches the ideal balancing force quite well at small elevation angles ($\varphi_3 \leq 70°$). For larger elevation angles ($\varphi_3 \geq 90°$), measured force F_A is clearly smaller than ideal, in all measurements. At these higher elevation, the top spring reaches its shortest lengths. Approximately down to 160% of the original unloaded spring length, near the boundary of the linearity region (Figure 4b). Furthermore, at these small elongations the output spring force is relatively low. Therefore, absolute errors in spring force have a relatively high impact on its force output. Altogether, this reduced force in the top spring decreases the upwards moment acting on the linkage, resulting in a lower upwards force measurement. To quantify this effect, the found absolute errors at $\varphi_3 = 110°$ is examined. The difference of about $5[N]$, between the ideal and measured force in this pose, corresponds to a force reduction in the top spring of approximately 20% of the ideal spring force. All in all, reduced force in the

top spring is a plausible cause for errors in this high elevation region of the measurements.

To analyze type B measurements, the design equations are used for identifying the source of errors. This is possible because the two measured upward forces (F_{B1} and F_{B2}) represent the upward force components, acting on the upper and lower arm limbs respectively. The design equations describe these same upwards components (left side of equations), as a function of spring parameters (right side of equations). Equation 1a describes the upper arm balance and can be linked to force F_{B1}, while equation 1b describes lower arm balance and is linked to measured force F_{B2}.

Force F_{B2}, acting at the wrist, is consistently measured near its ideal value, for all type B measurements (Figures 13c and 13d). Therefore, it is reasoned that spring parameters b, c and k do not significantly change for the type B measurements, as their product remains constant (Eq. 1b).

Measured force F_{B1}, acting on the upper arm, does deviate from the ideal value. In general, a relation is found between this elbow force and the elevation angle. At small elevation angles ($\varphi_3 \leq 50°$), a larger force than ideal is measured, at larger elevation angles ($\varphi_3 \geq 90°$), a smaller force is measured. Spring parameters affecting this force are d and k (Eq. 1a). Spring stiffness k is found to be relatively consistent (Figure 4b). Therefore, variations of parameter d are likely to contribute to the error in force F_{B1}. A possible source is found in the fixed world attachment of the top spring. Here, springs go around a cylinder shaped axis and are bound together by wrapping a piece of rubber around them, creating a knot. The effective location, from which the ZFLS behavior starts, changes for different orientations of the spring (Figure 14). For a small elevation angle (Figure 14a), the effective attachment point is found to be higher up, compared to larger elevation angles (Figure 14b). Height differences of approximately $0.012[m]$ are observed, for the effective location of the attachment. Other attachment points, have a different construction and do not shift as much. The height difference of the top attachment affects parameter d. The location described by d is located in between the top and bottom attachments, at factor f of the distance between these points (Figure 1b). Therefore, the resulting change in d is scaled by this same factor and is equal to $0.008[m]$. The resulting error in force F_{B1} is the product of this height error and k (Eq. 1a). Between the lowest and highest measured elevations, this corresponds to an error in force of $3.8[N]$. This force is in the same order of magnitude as observed in the measurements (Figures 13c and 13d).

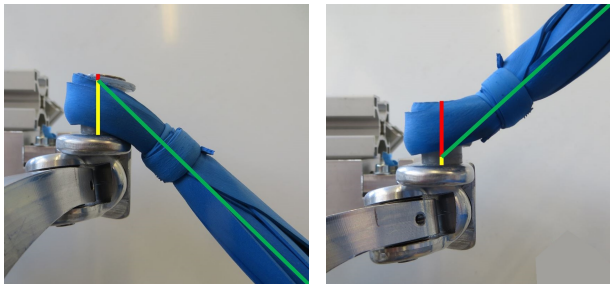

(a) (b)

Figure 14: Representation of varying location of fixed world attachment point of the top spring, dependent on the orientation of this spring. The green line represents the working line of the spring.

Finally, a difference is observed in the behavior of force F_{B1}, between variations in parameter φ_4, i.e. the difference between Figures 13c and 13d. When φ_4 is varied, the whole spring system rotates around the vertical axis. During this rotation, the height of the arm limbs and the effective length of the virtual springs remains the same. Nevertheless, there is a difference. Because, the fixed world attachment of the lower spring is split up to be in two locations (Figure 10). The orientation, with respect to these two locations, changes. When comparing the measurements, it is observed that, at low elevations ($\varphi_3 \leq 50°$), force F_{B1} is larger for $\varphi_4 = 90°$ than for $\varphi_4 = 45°$ (Figures 13c and 13d). As this bottom spring contains the only difference, a possible cause is found here. For $\varphi_4 = 90°$, at low elevations, the center knot location of this x-shaped spring is located close to the fixed world spring attachment on the chest. Part of the spring, from the center knot to this attachment, is too short to be in the linearity region in some poses. At the pose with lowest elevation ($\varphi_3 = 30°$ and $\varphi_4 = 90°$), a force reduction of 50% in this part of the spring, corresponds to the observed increase in F_{B1} of about $2.5[N]$. A hint of the same behavior is found in the type A measurements as well. At low elevation angles, the measured force at $\varphi_4 = 90°$ is slightly larger compared to the forces at $\varphi_4 = 45°$.

Different regions in the measurements are evaluated. The most likely cause of errors are provided for specific regions. By solving the causes of these errors, the balancing quality of the whole system can improve. A general improvement is to avoid the boundaries of the ZFLS linearity regions of the springs even more. Especially small elongations should be

avoided, as absolute force errors have a relatively high impact here. Improvements focused on the created prototype, consist of improving the spring attachment points to have more consistent locations. Furthermore, the measurements are now performed with fixed elbow joint (Type A measurements), because the friction in the elbow joint is large. This friction is to be reduced.

5. Conclusions

The main goal of this work is to implement a novel spring system, using two bi-articular ZFLSs, in a mobile arm support. Advantages of this spring system are that no parallelogram linkage is required and that all spring attachment locations are variable. Three sub-goals are set to achieve the main goal. The first, creating a simple description of the system, is realized. Conditions for static balance are described in two simple design equations, which are based on a graphical representation of the behavior. Adjustment rules are defined, for altering the balancing forces acting on the upper and lower arm limbs. These rules create the possibility to balance a system having unknown mass. The second sub-goal, providing technology to fit the system around the human, is fulfilled. A novel technique of subdividing ZFLSs is provided. 3D hollow spring structures are created based on combinations of subdivided spring elements. The resulting spring system closely fits the human body. At small elevation angles a nice fit is observed, at larger elevations a small gap appears. The final sub-goal, performing an experimental evaluation, is realized. Two output forces are measured, at the wrist and elbow, in a four DOF system. At smaller elevations the desired balancing force is observed. In poses with larger elevations differences are found. Possible causes consist of the loss of ZFLS behavior near the lower boundary of the spring linearity region and inconsistencies in spring attachment point locations. Solutions for improving the balancing quality consist of avoiding the lower boundary of the linear ZFLS region and creating spring attachments having more consistent locations. Finally, the main goal is fulfilled as the spring system shows great potential for application in an adjustable close-to-body mobile arm support.

6. References

[1] A. E. Emery, F. Muntoni, R. C. Quinlivan, Duchenne muscular dystrophy, OUP Oxford, 2015.

[2] A. E. Emery, Population frequencies of inherited neuromuscular diseasesa world survey, Neuromuscular disorders 1 (1) (1991) 19–29.

[3] M. Kohler, C. F. Clarenbach, C. Bahler, T. Brack, E. W. Russi, K. E. Bloch, Disability and survival in duchenne muscular dystrophy, Journal of Neurology, Neurosurgery & Psychiatry 80 (3) (2009) 320–325.

[4] A. G. Dunning, J. L. Herder, A review of assistive devices for arm balancing, in: Rehabilitation Robotics (ICORR), 2013 IEEE International Conference on, IEEE, 2013, pp. 1–6.

[5] R. Gopura, K. Kiguchi, D. Bandara, A brief review on upper extremity robotic exoskeleton systems, in: Industrial and Information Systems (ICIIS), 2011 6th IEEE International Conference on, IEEE, 2011, pp. 346–351.

[6] S. J. Housman, V. Le, T. Rahman, R. J. Sanchez, D. J. Reinkensmeyer, Arm-training with t-wrex after chronic stroke: preliminary results of a randomized controlled trial, in: Rehabilitation Robotics, 2007. ICORR 2007. IEEE 10th International Conference on, IEEE, 2007, pp. 562–568.

[7] G. Kramer, G. R. B. Römer, H. J. Stuyt, Design of a dynamic arm support (d as) for gravity compensation, in: Rehabilitation Robotics, 2007. ICORR 2007. IEEE 10th International Conference on, IEEE, 2007, pp. 1042–1048.

[8] T. Rahman, W. Sample, R. Seliktar, M. Alexander, M. Scavina, A body-powered functional upper limb orthosis, Journal of rehabilitation research and development 37 (6) (2000) 675–680.

[9] J. L. Herder, Energy-free systems; theory, conception and design of statically balanced spring mechanisms, Ph.d. thesis, Delft University of Technology, iSBN 90-370-0192-0 (2001).

[10] H. Hilpert, Weight balancing of precision mechanical instruments, Journal of Mechanisms 3 (4) (1968) 289 – 302.

[11] P.-Y. Lin, W.-B. Shieh, D.-Z. Chen, A stiffness matrix approach for the design of statically balanced planar articulated manipulators, Mechanism and Machine Theory 45 (12) (2010) 1877–1891.

[12] P.-Y. Lin, W.-B. Shieh, D.-Z. Chen, A theoretical study of weight-balanced mechanisms for design of spring assistive mobile arm support (mas), Mechanism and Machine Theory 61 (2013) 156–167.

[13] P.-Y. Lin, W.-B. Shieh, D.-Z. Chen, Design of statically balanced planar articulated manipulators with spring suspension, Robotics, IEEE Transactions on 28 (1) (2012) 12–21.

[14] P. N. Kooren, A. G. Dunning, M. M. H. P. Janssen, J. Lobo-Prat, B. F. J. M. Koopman, M. I. Paalman, I. J. M. de Groot, J. L. Herder, Design and validation of a-gear: a novel wearable dynamic arm support, submitted to Journal of Neuroengineering and Rehabilitation.

[15] M. P. Lustig, A. G. Dunning, J. L. Herder, Cartesian based stiffness matrix approach and graphical representation for designing statically balanced serial linkages, submitted to Mechanism and Machine Theory.

[16] B. M. Wisse, W. D. van Dorsser, R. Barents, J. Herder, Energy-free adjustment of gravity equilibrators using the virtual spring concept, in: Rehabilitation Robotics, 2007. ICORR 2007. IEEE 10th International Conference on, IEEE, 2007, pp. 742–750.

[17] L. F. Cardoso, S. Tomázio, J. L. Herder, Conceptual design of a passive arm orthosis, in: ASME 2002 International Design Engineering Technical Conferences and Computers and Information in Engineering Conference, American Society of Mechanical Engineers, 2002, pp. 747–756.

A

NEW PRINCIPLES

A.1. CONSTANT FORCE GENERATOR

Principle: Combine positive and negative stiffness spring to obtain constant force generator. This is the working principle of all ZFLS based static balanced systems.

Two springs are connected (Figure A.1). The green spring has a positive spring stiffness k. The red spring has a negative spring stiffness $-k$, of equal magnitudewith opposite sign. Both springs are zero free length springs.

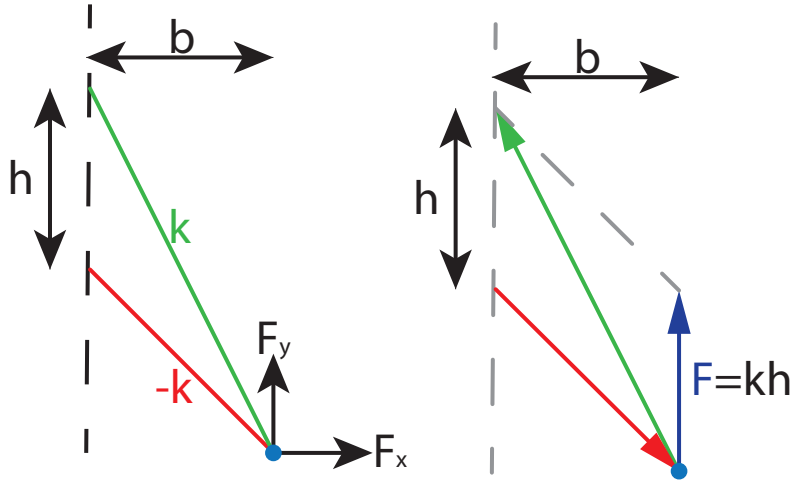

Figure A.1: Spring placement for a single balanced link.

The resulting forces acting on the blue dot in x and y components are:

$$F_x = b \cdot k - b \cdot k = 0 \tag{A.1}$$

$$F_y = (h+y)k - y \cdot k = h \cdot k = \text{constant} \tag{A.2}$$

A planar or spacial constant force generator is obtained. The only force acting on this blue dot is constant force F_y, it acts in line with the dotted line. This dotted line can be positioned in any orientation, in this manner the direction in which the constant force acts can be altered. Figure A.1 represents the underlying working principle of all statically balanced mechanism based on ZFLSs.

A.2. NEGATIVE STIFFNESS

Principle: Negative stiffness behavior is obtained by removing the positive stiffness component from a balanced linkage.

The obtained negative stiffness behavior is linear and acts as a ZFLS, between former attachment points of the removed spring. Thus, at a length of zero zero force acts on the springs output, from this point the spring will push outwards with an increasing force for increased elongations. Three examples of obtainable negative stiffness mechanisms are shown.

The advantages of obtainable systems are:
+ Perfectly linear negative stiffness ZFLS behavior.
+ Large displacement range with negative stiffness behavior obtainable.
+ Potential for high stiffness values.

Example 1:

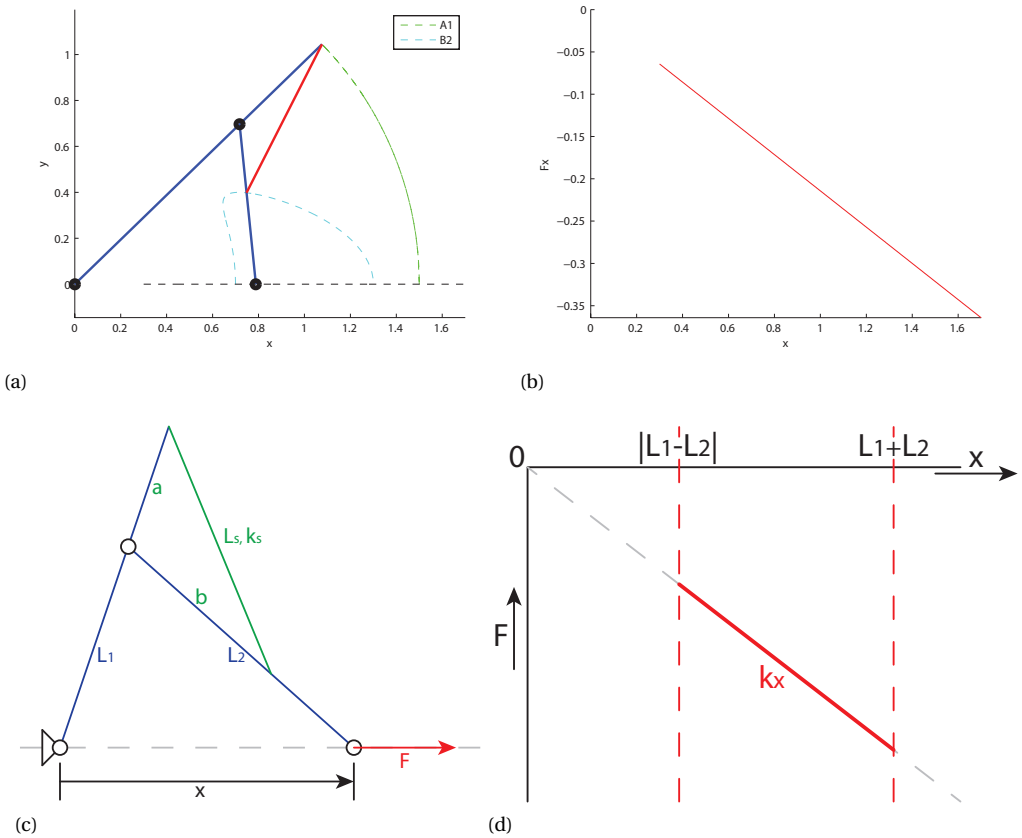

Figure A.2: (a-b) Matlab simulation of behavior. (c-d) Parameterized linkage, for determining magnitude of negative stiffness value and working range. At the dotted lines the system is oriented in a singular position.

Equations describing the magnitude of this negative stiffness value is provides:

$$0 = \overbrace{\frac{1}{2}k_s(a+b)^2 - \frac{1}{2}k_s(a-b)^2}^{E_{s,in}} + \overbrace{\frac{1}{2}k_x(L_1+L_2)^2 - \frac{1}{2}k_x(L_1-L_2)^2}^{E_{x,out}} \tag{A.3}$$

$$k_x = -\frac{(a+b)^2-(a-b)^2}{(L_1+L_2)^2-(L_1-L_2)^2}k_s \tag{A.4}$$

$$k_x = -\frac{ab}{L_1L_2}k_s \tag{A.5}$$

Example 2:

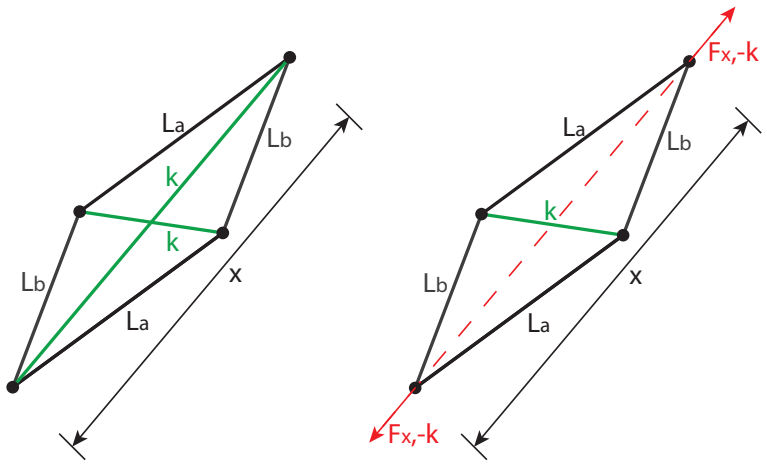

Figure A.3: [Left] Original balanced linkage. [Right] Negative stiffness linkage, obtained by removing a positive stiffness ZFLS.

Example 3:

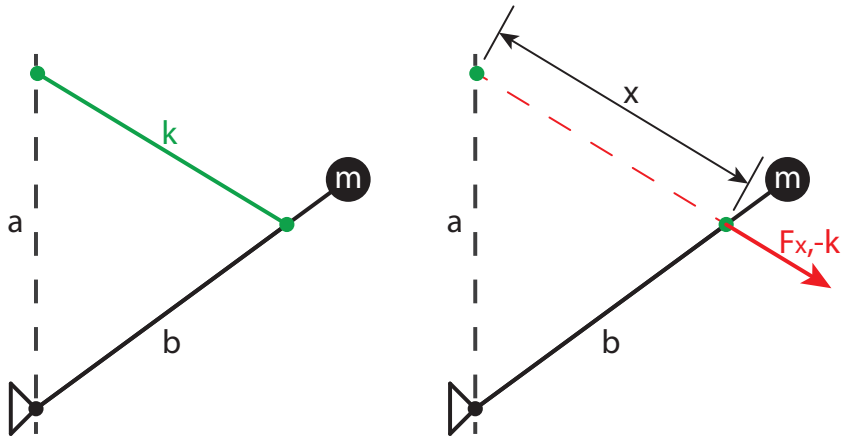

Figure A.4: [Left] Balanced linkage [Right] Negative stiffness linkage (Zero Length and linear).

$$k_{negative} = -k_{positive} = -\frac{mgL}{ab} \tag{A.6}$$

As a simple pendulum can be balanced using a +k ZFLS, it acts as a -k ZFLS between two possible attachment points. In other words, a pendulum can be examined in a line between a point on the fixed world and a point on the link, the force working in this line acts like a negative stiffness ZFLS between the two points.

A.3. LINKAGE ACTING AS A ZFLS

Principle: A balanced link, suspended to the fixed world by two ZFLSs, can act as a virtual ZFLS between a points on the link and a point on the fixed world.

A visualization is proveded of how a linkage with mass m, suspended by two ZFLS with stiffness k, acts like a virtual ZFLS with stiffness $2k$ (Figure A.5). The virtual ZFLS acts between the orange and purple points shown in figure A.5g. The orange point is positioned vertically below the center of the two fixed world spring attachments. This is due to the weight of the link, pulling this equilibrium position downwards.

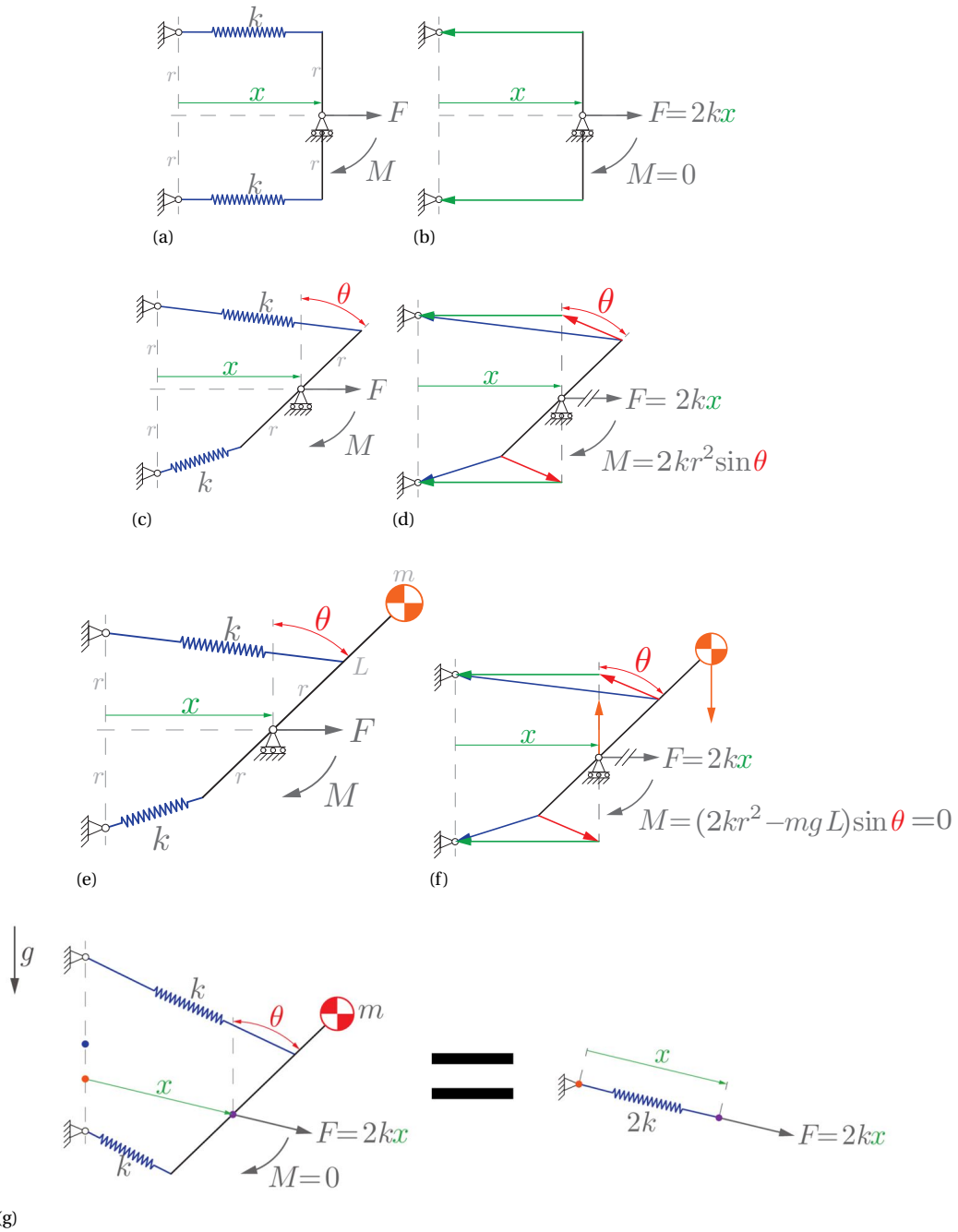

Figure A.5

A.4. CONSTRUCTING BALANCED SERIAL LINKAGE USING VIRTUAL ZFLS

Principle: Any ZFLS in a balanced linkage can be replaced by the virtual ZFLS linkage. Resulting in a higher order balanced system.

The ZFLS, in a clasical static balance solution of a single link, can be replaced by the virtual ZFLS. What is obtained in a statically balanced two link system without parallel beams (Figure A.6). This step can be repeated multiple times, any ZFLS can be replaced by 2 ZFLSs and a link, to create balance linkages consisting of many links.

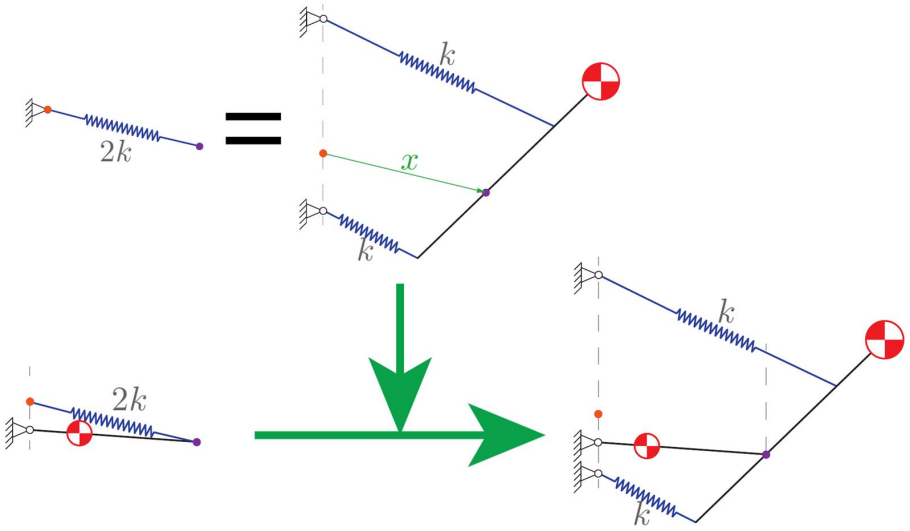

(a)

Figure A.6

A.5. FLOATING MECHANISMS

Principle: A floating multi-link system can be obtained by replacing a ZFLS, by the equivalent linkage, in a single link floating system.

A floating linkage is obtained when a single link is suspended by two ZFLS connected to the fixed world (Figure A.7a) [1]. As shown in the present work, this same linkage acts as a virtual ZFLS when moving the hinge point from the equilibrium position (Figure A.7b). Therefore this system can be used as a building block for replacing ZFLSs. The spring with stiffness k_3 (Figure A.7c) is replaced by the equivalent building block linkage (Figure A.7b). A serial linkage with a floating hinge point is obtained (Figure A.7d). Hence this two link linkage is suspended to the fixed world by three ZFLSs only, the joint floats freely. The major advantage of this system is that no mechanical shoulder joint is required.

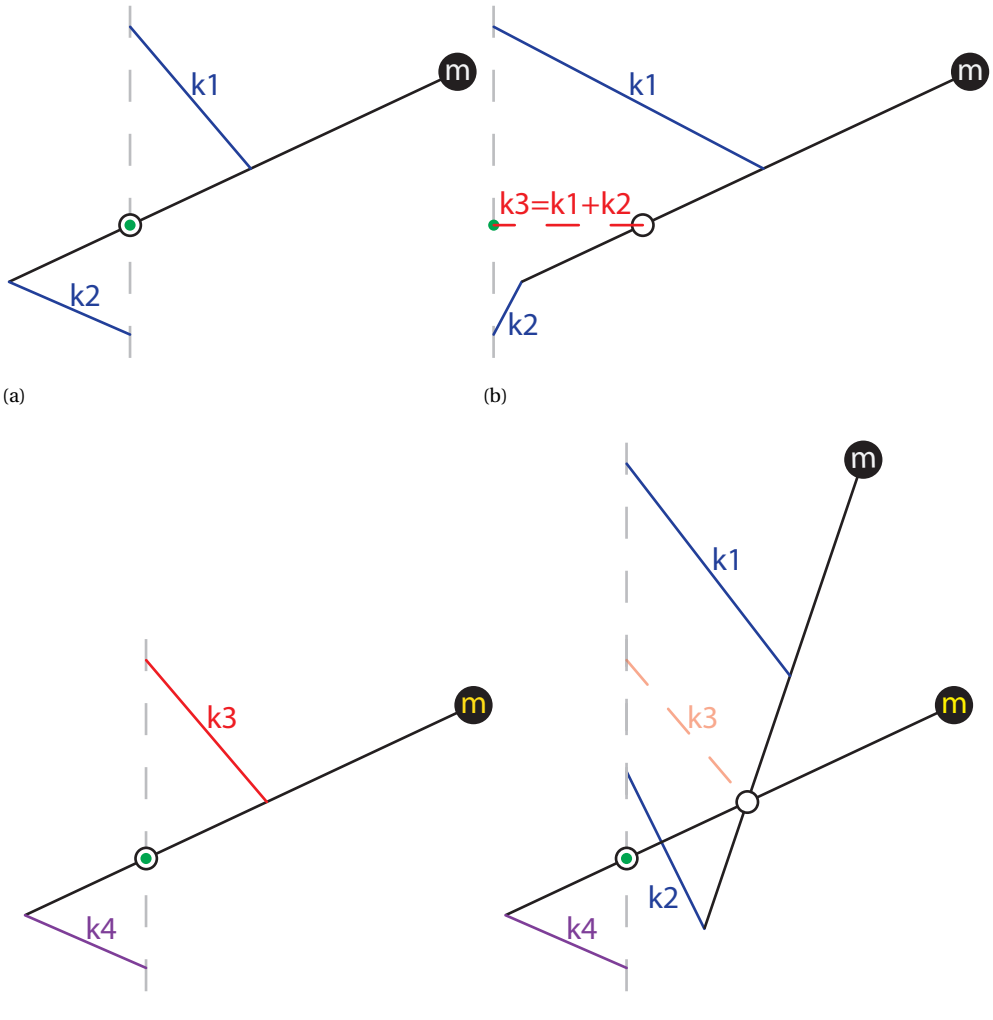

Figure A.7

A.5.1. FLOATING POINT LINKAGE FITTING AROUND ARM.

Five steps of obtaining the desired linkage are illustrated and a short explanation is added. The matlab code used to generate these steps is proveded in Apendix G.6. The parameter values used are provided in this code.

STEP 1: Initial moment balanced linkage, no floating point (Figure A.8a).
STEP 2: Moment balanced linkage + Force free point by adding 2 springs. One spring compensates vertical component other spring compensates force in line with upper arm link (Figure A.8b).
STEP 3: Split up spring in line with upper arm into two others (Figure A.8c).
STEP 4: Replace spring 4 and 5 by new spring 4 (Figure A.8d).
STEP 5: Variate values, points A2 on A3 (Figure A.8e).

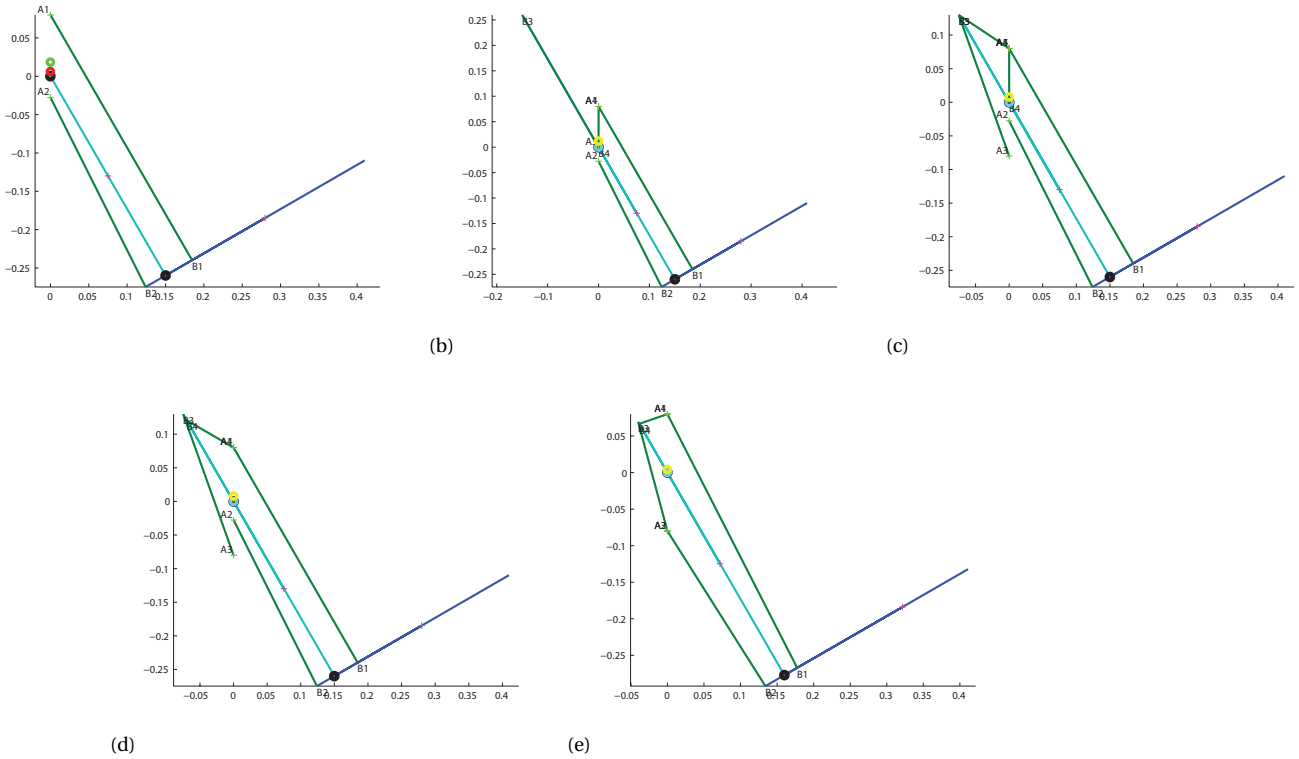

(a) (b) (c)

(d) (e)

Figure A.8

A.6. SUBDIVIDING SPRING

Principle: A ZFLS can be subdivided into multiple other ZFLSs such that the combined behavior remains equal. Possible applications are the creation of hollow spring structures.

ZFLSs can be subdivided such that a virtual ZFLS is created. In this manner ZFLS behavior can be obtained in otherwise unreachable locations. A v-shape orientation of two ZFLSs (red), act as a single virtual ZFLS (blue) with the summed stiffness value (Figure A.9a)[1, 2]. The location of the virtual attachment depends on the ratio in stiffness between the split up springs, represented by factor a (Figure A.9a). As there is a point where all springs meet, the rigid link in this system can be in any orientation without affecting the ZFLS behavior of the virtual spring. A second novel way of subdividing springs is connecting two ZFLSs to two links (Figure A.9b). When the two links are kept parallel to each other, a virtual ZFLS is created. The virtual attachment points are located in between the original attachments, at a location following ratio a between the spring stiffness values (Figure A.9b). A rotation, between the two links, will introduce a moment in addition to the ZFLS behavior.

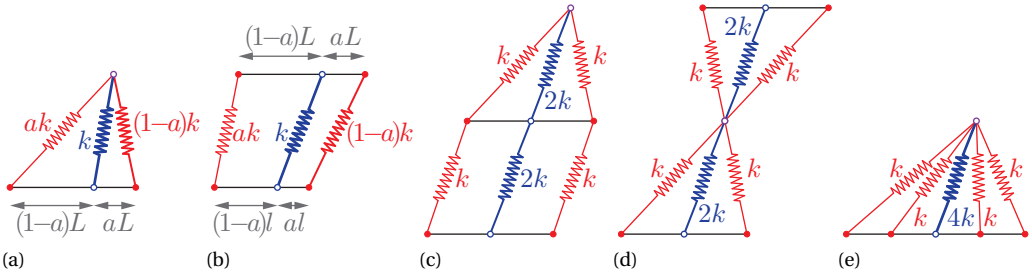

(a) (b) (c) (d) (e)

Figure A.9: Subdivision schemes for ZFLSs, for creating equivalent virtual springs. (a) v-shaped configuration. (b) Parallel configuration. (c) Serial placements of two virtual springs, total stiffness value is k. (d) Serial x-shaped configuration, total stiffness value is k. (e) Parallel placement of two v-shaped configurations, summed stiffness value.

The virtual springs can be combined just like regular springs, they can be placed in series or in parallel to other (virtual) ZFLSs. Web like spring compositions can be created, acting as if a single ZFLS is used. The serial composition of v-shaped and parallel virtual springs (Figures A.9a and A.9b) is shown in figure A.9c. ZFLS behavior is still present. Furthermore, the space directly in-between the virtual attachments becomes free. A second serial configuration, using two v-shaped virtual springs, is creating a x-shaped configuration (Figure A.9d). Here space is created near both virtual attachments. The orientations of the top and bottom links are free. A parallel combination is shown in figure A.9e, here four springs act as a single virtual spring.

The described subdivision schemes work in 3D as well. A slice of a spring subdivision scheme, perpendicular to the spring elongation direction, is shown in figure A.10a. The blue dot represents the original spring, the red dots represent the equivalent springs and have equal surface area. Each of the red dots can be subdivided in a similar manner, into the cyan dots, resulting in a spatial configuration (Figure A.10b). The spring represented by the four cyan dots are equivalent to the original blue dot spring. A hollow ZFLS is created where physical springs are located around the working line compared to all springs being directly on this line (Figure A.10c). Such hollow springs allow for close to body spring systems.

(a) (b) (c)

Figure A.10: (a-c) Cross-section of 3D subdivision schemes, the blue dot represents the original spring, the two red dots and the four cyan dots are equivalent to original blue spring, stiffness is equivalent to surface area of dots.

Note that the use of ZFLSs is essential. For non-ZFLSs subdivision schemes will have regions where the behavior differs from a spring with linear stiffness.

Pictures of subdivided springs are provided:

(a) (b) (c)

Figure A.11

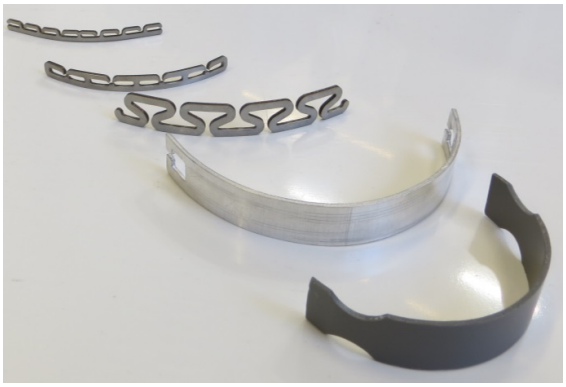

(a)

(b)

Figure A.12

A.7. DIFFERENT BEHAVIOR FROM DIFFERENT STATE PARAMETERS

Principle: The use of a system in line with a different state paramiterization has a major effect on the output behavior which can be obtained. From a single simple linkage, sinusoidal Moment-rotation behavior, constant force behavior or positive/negative ZFLS behavior can be obtained.

The energy equations for an equal system is compared for different parameterizations (Figure A.13a). Either ϕ, d or c1 is used to describe the state of the system. The system is examined for equal linkage parameters:

$$a_1 = a_2 = b_1 = b_2 = 1$$

$$k_1 = k_2 = \frac{1}{2}$$

It is clear that depending on the choice of the generalized coordinate the Energy-deflection behavior can be sinusoidal, linear or 2nd degree quadratic. This is for the coordinates respectively:
φ: Rotation between links.
d: Displacement of link A in direction of link B.
$c1$: Linear displacement of a point on link A with respect to point on link B (Spring Length).

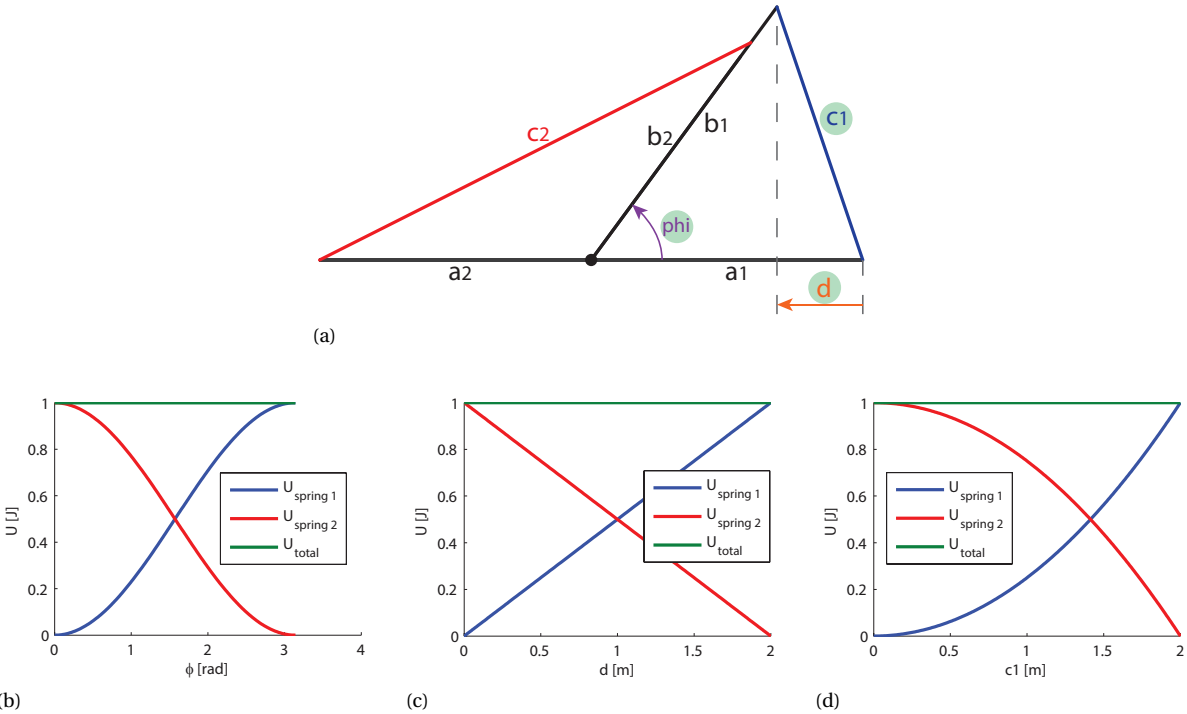

Figure A.13: [Top] Schematics of linkage. [Bottom] Energy graphs as a function of different generalized coordinates φ, d [3] and c_1 (marked by green dots).

The derivative of these energy functions with respect to the different generalized coordinates will result in moment (for φ) and force functions (for d and c_1).

When only one of the two springs is used, a mechanism with an output force is obtained:
φ: The moment between the two links, as a function of φ, will be sinusoidal.
d: A constant force is felt at the tip of the b link, in the direction of d. This is when the bottom A link is constrained to the fixed world.
c_1: Force behavior with a constant stiffness is obtained as a function of c_1, this can either be of positive or negative stiffness. The force acts between two points one on each link.

On this basic linkage a wide range of force deflection behavior can be obtained by selecting a different state parameterization as input.

B

STATIC BALANCING

B.1. STATIC BALANCE PRINCIPLE

Static balancing is the act of creating an equilibrium orientation independent of the system state. For example, for statically balancing a mass, located in a gravitational field, a constant upwards force is required to counteract the gravitational force. A simple solution is using a helium balloon to compensate for this downward force (Figure B.1). This balloon can be moved to any location and remain in equilibrium.

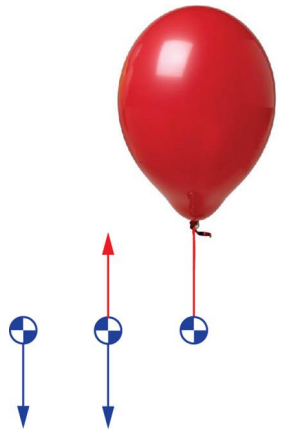

Figure B.1

B.2. STATIC BALANCE OF SINGLE LINK

Many solutions exist for statically balancing a single pendulum (Figure B.2a).

Possible solutions are:

(Figure B.2b) Regural spring (Non ZFLS) in combination with non-linear transmission [4].

(Figure B.2c) Compliant flexure element [5].

(Figure B.2d) Counter mass [1].

(Figure B.2e) ZFLS [1].

Except for the counter mass solution (Figure B.2d), all balancing solutions require a fixed world attachment point. This point is located at a set orientation with respect to the joint of the link. Nevertheless, the downside of this counter mass is the relatively large increase of system inertial and mass [6]. Furthermore, a link extending to the opposite side of the original COM at the opposite side of the joint has to be added.

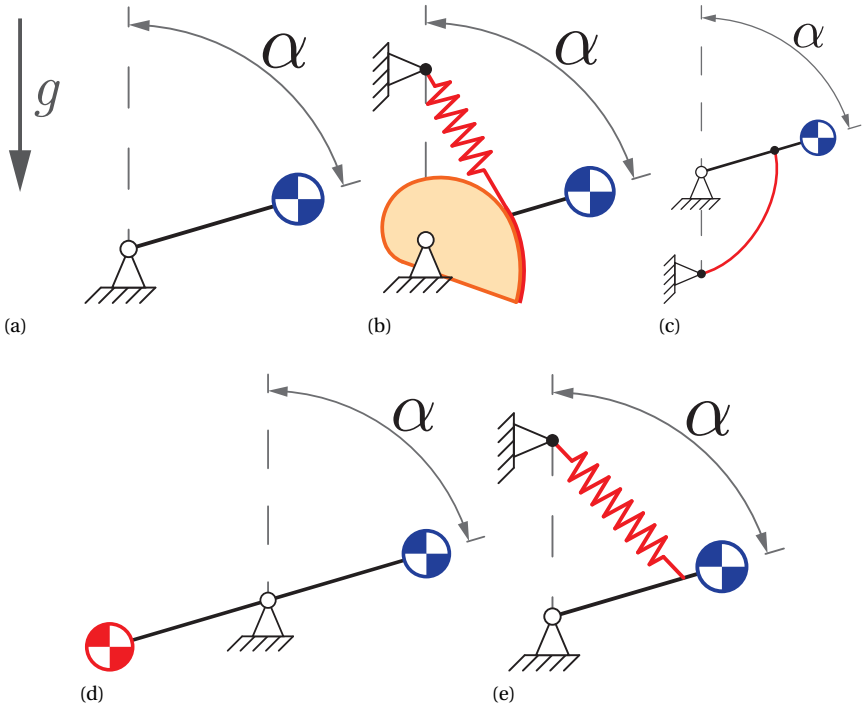

Figure B.2

B.3. STATIC BALANCE OF SERIAL 2 LINK SYSTEM

The system to be balanced is a planar two link system and has two DOFs (Figure B.3).

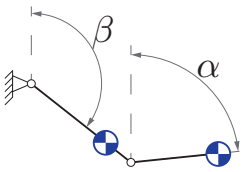

Figure B.3

B.3.1. CLASSICAL SOLUTIONS:

Classical solutions are based either on counter masses [7–9], or ZFLSs + parallel beams [1, 10, 11]. The downside of the counter mass solution becomes even greater here, as the lower arm counter mass is to be balanced by the upper arm counter mass as well [6]. The parallel beam construction of the spring based solution provides a fixed orientation with respect to the elbow joint. This is required for a single mono-articulate ZFLS to be able to balance the lower arm. Other solutions requiring such a fixed orientation can be used to balanced this linkage as well, as they can substitute the ZFLS in the parallel beam construction. Disadvantage of this parallel beam structure is the increased complexity and number of components and inertia and the inability to rotate the linkage out-of-plane.

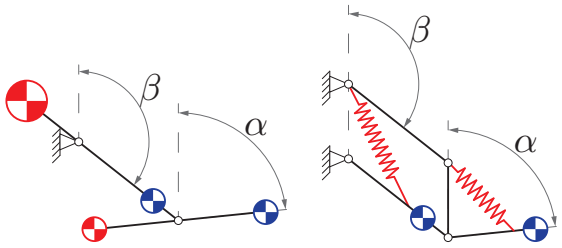

(a) (b)

Figure B.4

B.3.2. NEW SOLUTIONS, USING MULTI-ARTICULAR SPRINGS:

Recent literature presents new possibilities of balancing a serial linkage using multi-articulate ZFLS, without the need for a parallel beam construction [12]. The two solutions for balancing two links using two ZFLSs are shown (Figure B.5). The linkages are both examined as an example in Paper 1 of this report (Chapter 1).

In essence the linkage shown in figure B.5a can be seen as a combined positive and negative stiffness (Section A.1). Here the negative stiffness part is shown in figure A.2. The negative and positive springs come together at point C (Figure B.5a). As the upward force component acts exactly at this point the combined COM of the linkage must be located at this point as well for. Therefore, the location of point C is fixed on a location depending solely on the link mass and dimensions.

The balancing principle of the second linkage is explained in section A.4 and in more detail in paper 2 (Figure B.5b). For this linkage the location of all spring attachments is free. Nevertheless, there are relations between the locations of the attachment points that need to be fulfilled for balance.

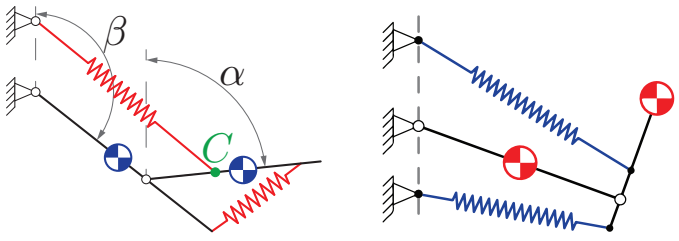

(a) (b)

Figure B.5

B.4. ENERGY

Another way of examining static balance is by examining the energy components. For example, when for the spring configuration of B.5a. The summed energy components for the mass of the two links and the energy in the two springs must be constant for all states. The sum of the three energy plots is constant (Figures B.6 B.7).

B.4.1. POTENTIAL ENERGY SERIAL LINKS MASS

The potential energy in upper and lower arm as a function of the arm state is shown B.6.

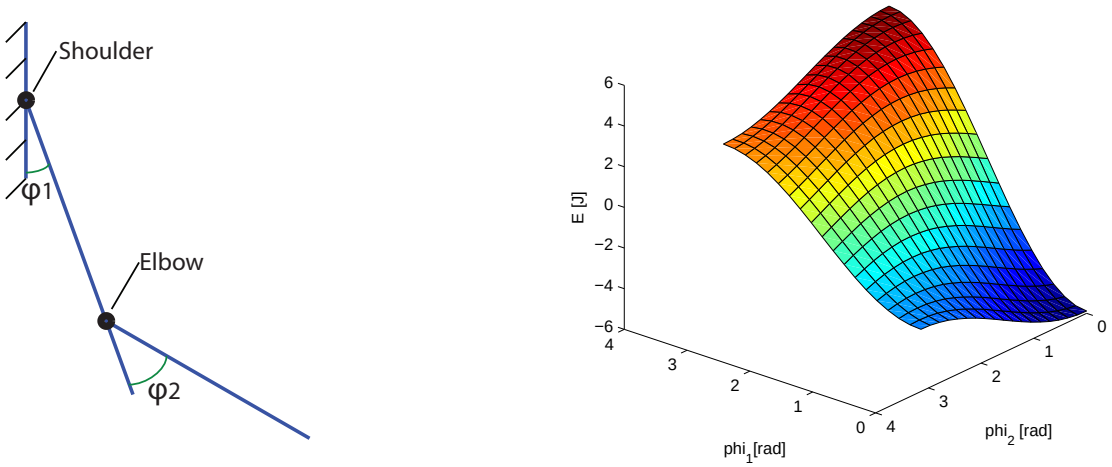

Figure B.6: [Left] System of arm. [Right] Potential mass energy against arm angles.

B.4.2. POTENTIAL ENERGY SERIAL LINKS SPRINGS

The energy components for the two springs are shown as well (Figure B.7).

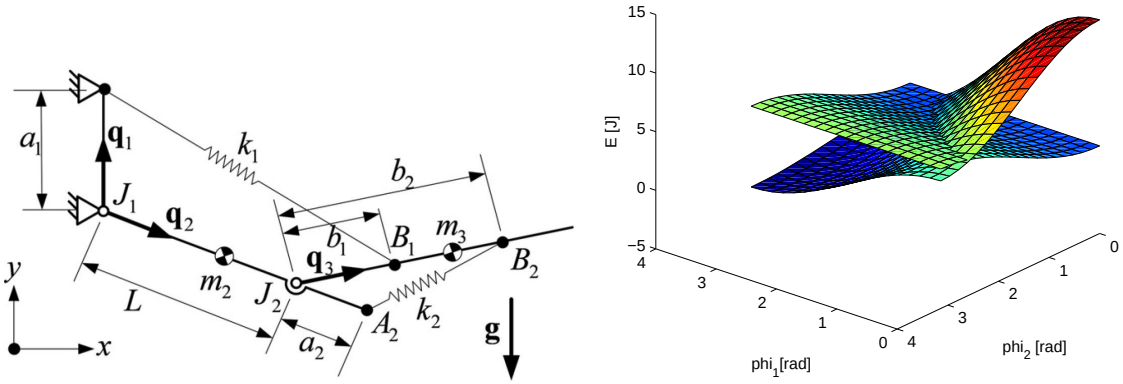

Figure B.7: [Left] Lin's system. [Right] Potential spring energy of the 2 springs against arm angles.

B.5. FORCES ACTING ON FIXED WORLD (SHOULDER)

The force balance at the (fixed) shoulder body is drawn in figure B.8. What remains at the shoulder is:

- Fm: Constant gravity force in y-direction.
- Ms: Varying rotational moment depending on state of arm. (Fmass * Δx com) (Figure B.9)

These forces are illustrated for a specific spring system. However these forces are always the same for any spring balanced system. This is because upwards forces required to lift the are equal for any spring system. The same goes for the moment arms at which these forces act.

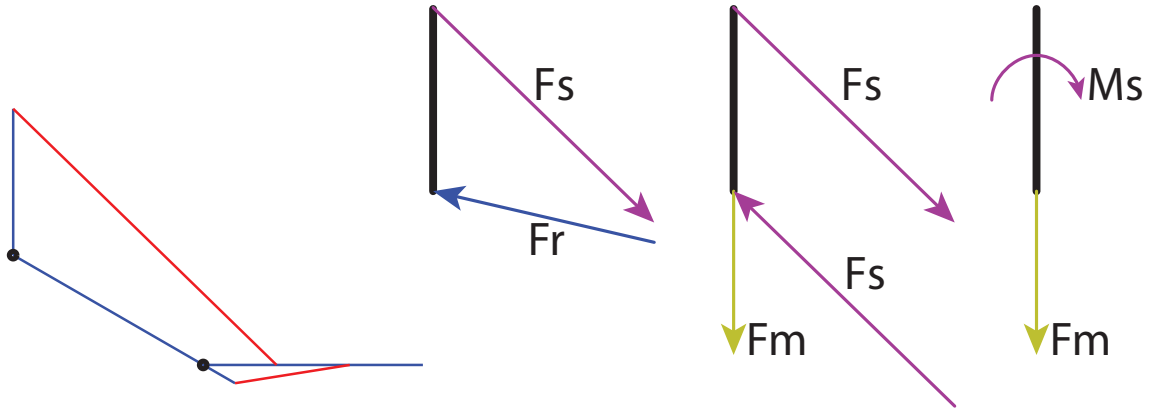

Figure B.8: [Left] Lin's system in analyzed position. [Right] Forces acting on shoulder bar.

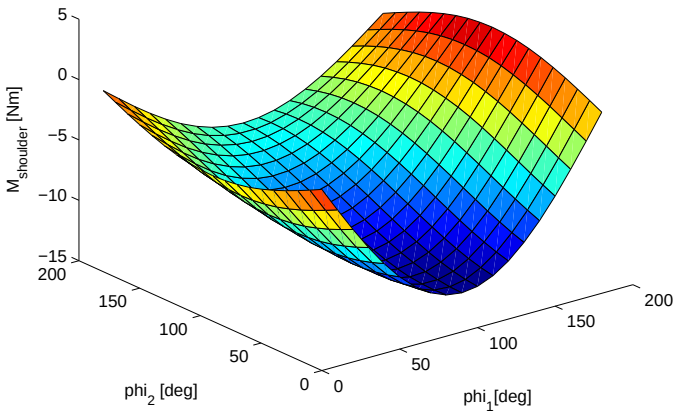

Figure B.9: [Moment acting on shoulder M_s as a function of the angles.

B.6. BALANCED CONFIGURATION WITH 3 LINKS AND 3 SPRINGS.

Statically balanced 3 link system, using 3 springs.

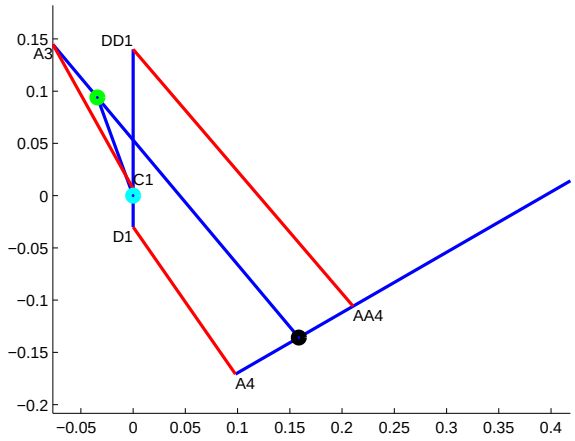

$$aa4 = 0.06$$
$$a4 = -0.07$$
$$dd1 = 0.14$$
$$d1 = -0.03$$
$$a3 = -0.0662$$
$$c1 = 0.0066$$
$$k13 = 2430$$
$$k14 = 247.3109$$
$$kk14 = 288.5294$$

Many parameters are calculated using the constraints, they are sensitive to change. In this case 4 parameters can be selected freely (I chose D1,A4,DD1,AA4) the other parameters are calculated (C1,A3,K13,K14,KK14). Only 5 parameters are calculated using the 6 constraints. This is possible because all spring connected to the lower arm (link 4) are connected to the fixed world (link 1). Therefore links 2 to 4 and 3 to 4 are spawned by the same two spring (k14 and kk14) resulting in two of the constraints having the same relation.

C

PROTOTYPES

C.1. SMALL SCALE PROTOTYPE

A small scale prototype is constructed to demonstrate the balancing quality of the selected spring configuration. The prototype makes use of spring steel coil springs. These springs are no ZFLSs. Known techniques for creating ZFLS behavior using a wire and pulley are used [1].

(a)

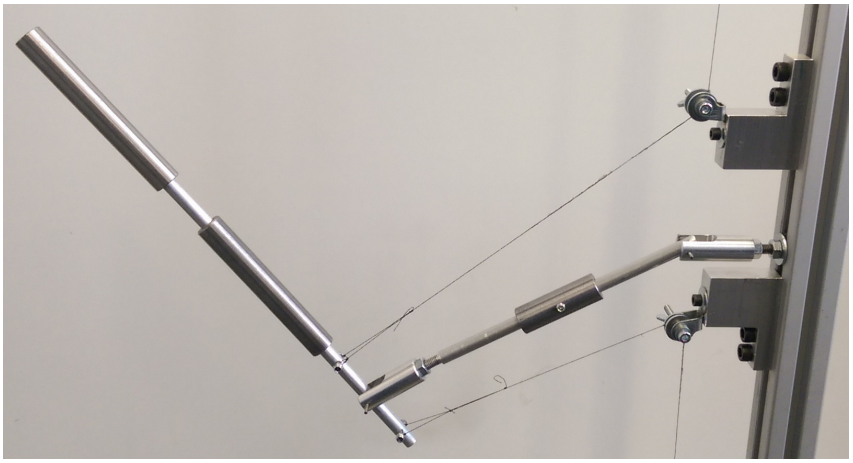

(b)

Figure C.1

C.2. FINAL PROTOTYPE

The final prototype consisted the spring system suspended on a rigid frame having 4 DOF (3 at the shoulder, 1 at the elbow). Pictures of the prototype are provided.

(a) (b) (c)

(d) (e)

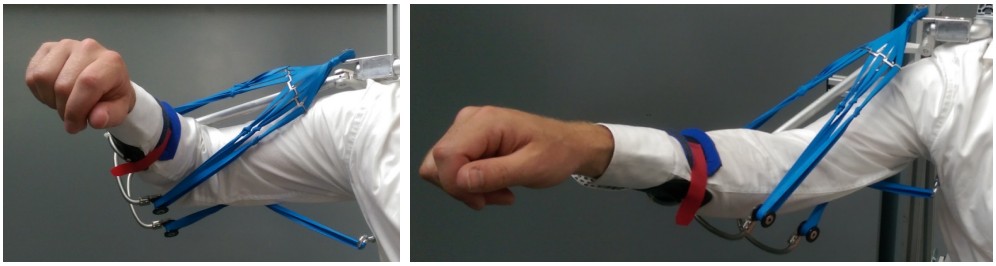

(f) (g)

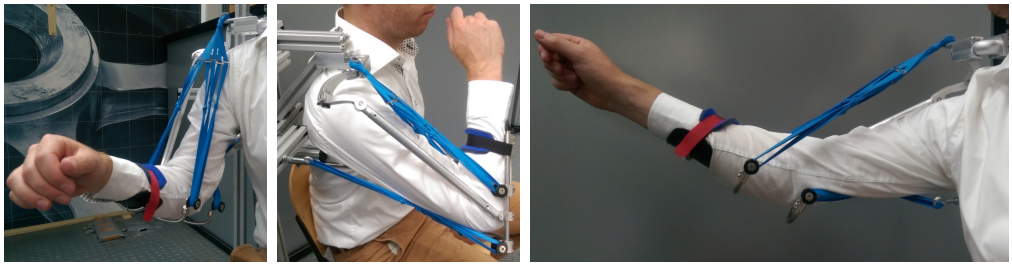

(h) (i) (j)

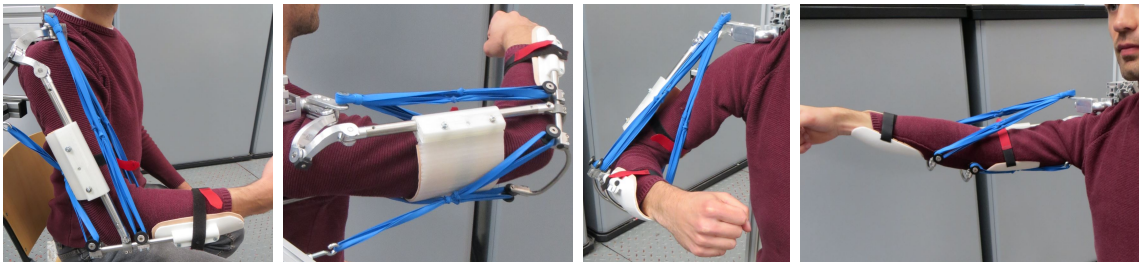

(k) (l) (m) (n)

Figure C.2

C.3. EXPERIMENTAL SETUP

Pictures for the experimental set up are shown here.

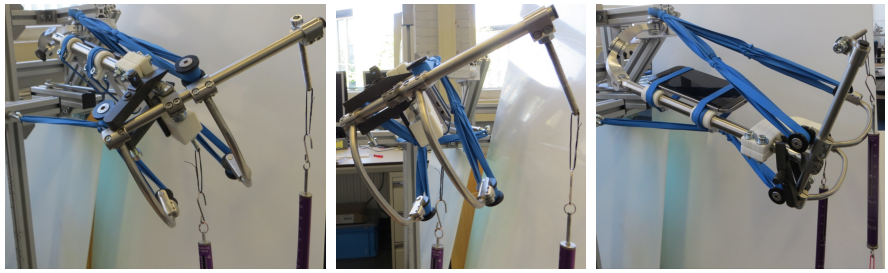

(a) (b) (c)

(d) (e) (f)

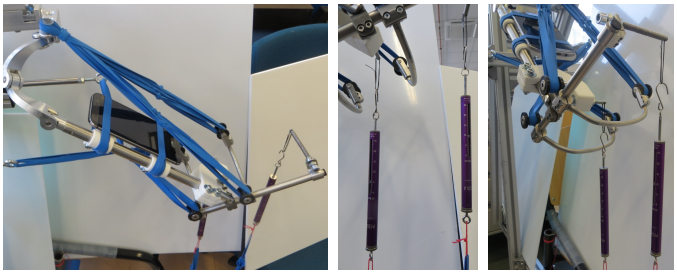

(g) (h) (i)

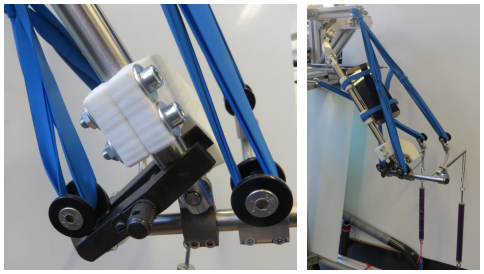

(j) (k)

Figure C.3

D

EXPERIMENTAL RESULTS

D.1. MEASUREMENTS PAPER 2: EXPERIMENTAL DATA

The measurement results of all tests are listed in tables (Figures D.1-D.3). Graphs of the data listed in these tables are made. The six graphs have the same respective positions as the tables. The dotted line in the graphs represents the ideal value for the measurements. The x-data in the graphs describe the elevation angle in degrees. The y-data represent the measured vertical force in Newtons.

The states used in these tables are different from the states described in paper 2. A description of what they represent is provided:

	Raw data	**FIXED ELBOW JOINT**
phi4	Plane:	P1 = upper arm moves in forward (sagittal) plane; P2 = upper arm moves in plane 45deg to right around vertical axis
phi2	Alpha:	a = elbow angle between upper and lower arm, is zero when hand at shoulder, 180 when fully extended
phi1	x:	x = arm rotation around horizontal component between shoulder and elbow
phi3	y:	y = downward rotation of arm, around horizontal line perpendicular to line of x
	e:	e = vertical force at elbow
	w:	w = vertical force at wrist
		D1 = downwards motion during measurements; U1 = upwards motion during measurements;
		negative angles are upwards zero angle is horizontal upper arm positive angles are downwards

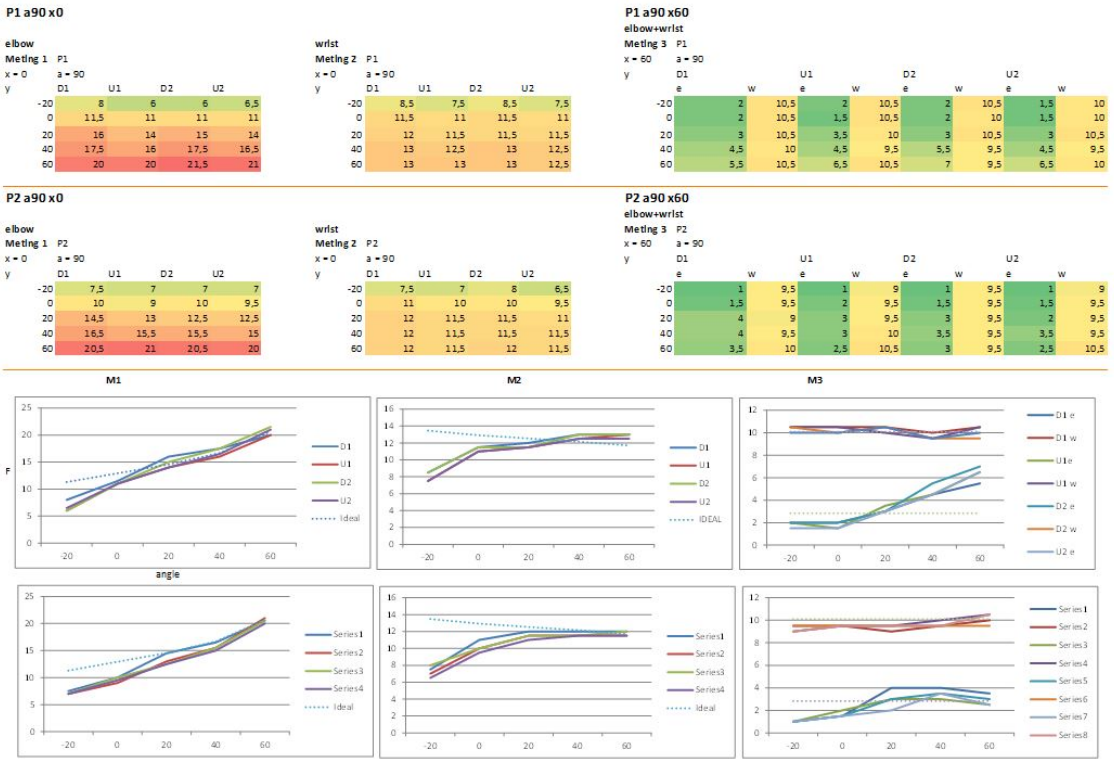

Figure D.1: Measurements at flexion of $\alpha = 90°$.

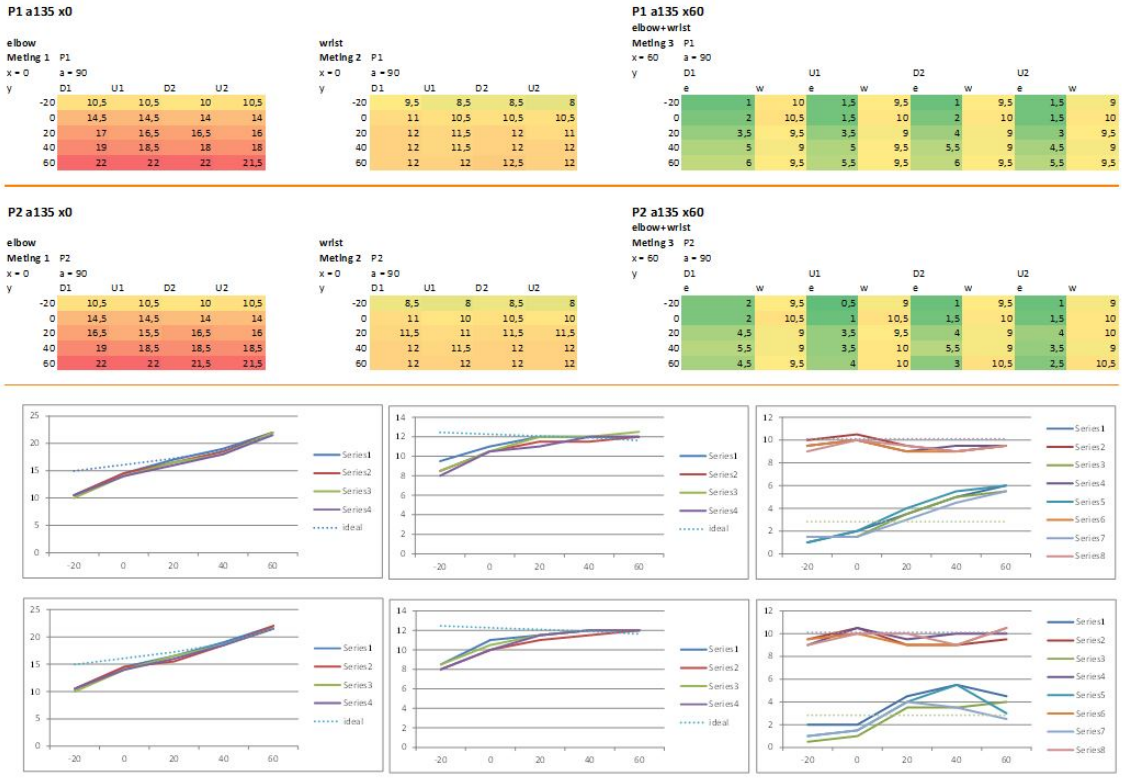

Figure D.2: (Measurements at flexion of $\alpha = 135°$.

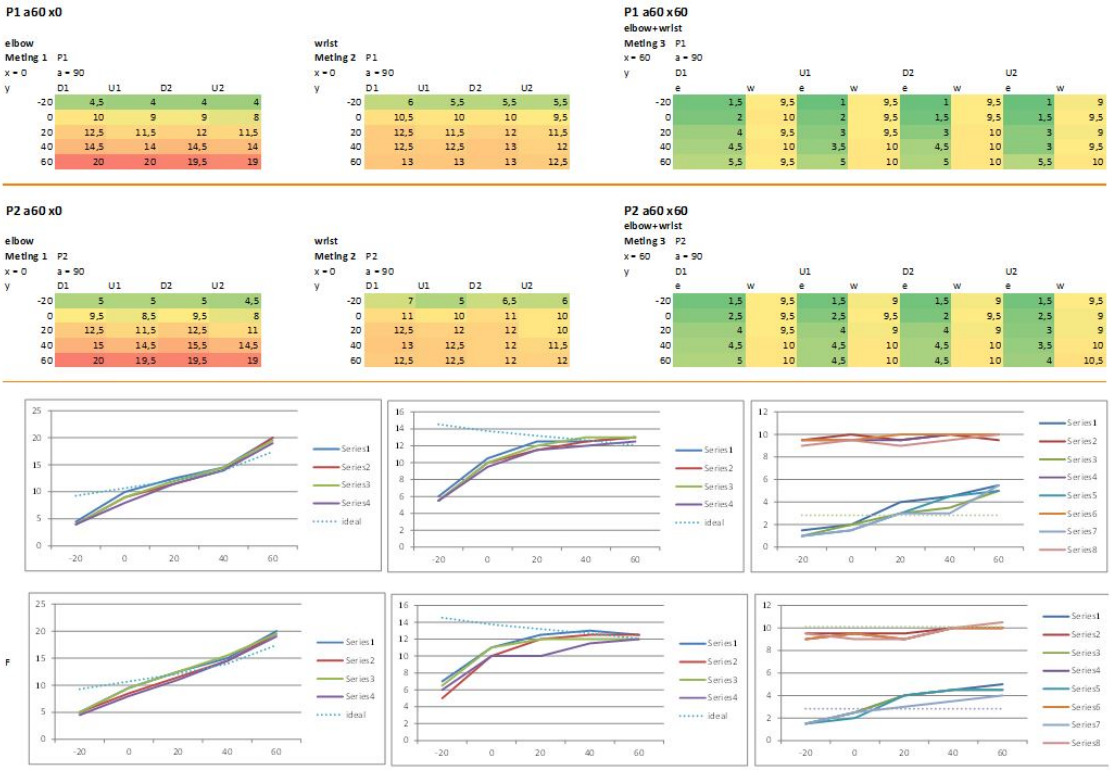

P1 a60 x0

elbow

Meting 1 P1

x = 0 a = 90

y	D1	U1	D2	U2
-20	4,5	4	4	4
0	10	9	9	8
20	12,5	11,5	12	11,5
40	14,5	14	14,5	14
60	20	20	19,5	19

wrist

Meting 2 P1

x = 0 a = 90

y	D1	U1	D2	U2
-20	6	5,5	5,5	5,5
0	10,5	10	10	9,5
20	12,5	11,5	12	11,5
40	12,5	12,5	13	12
60	13	13	13	12,5

P1 a60 x60

elbow+wrist

Meting 3 P1

x = 60 a = 90

y	D1		U1		D2		U2	
	e	w	e	w	e	w	e	w
-20	1,5	9,5	1	9,5	1	9,5	1	9
0	2	10	2	9,5	1,5	9,5	1,5	9,5
20	4	9,5	3	9,5	3	10	3	9
40	4,5	10	3,5	10	4,5	10	3	9,5
60	5,5	9,5	5	10	5	10	5,5	10

P2 a60 x0

elbow

Meting 1 P2

x = 0 a = 90

y	D1	U1	D2	U2
-20	5	5	5	4,5
0	9,5	8,5	9,5	8
20	12,5	11,5	12,5	11
40	15	14,5	15,5	14,5
60	20	19,5	19,5	19

wrist

Meting 2 P2

x = 0 a = 90

y	D1	U1	D2	U2
-20	7	5	6,5	6
0	11	10	11	10
20	12,5	12	12	10
40	13	12,5	12	11,5
60	12,5	12,5	12	12

P2 a60 x60

elbow+wrist

Meting 3 P2

x = 60 a = 90

y	D1		U1		D2		U2	
	e	w	e	w	e	w	e	w
-20	1,5	9,5	1,5	9	1,5	9	1,5	9,5
0	2,5	9,5	2,5	9,5	2	9,5	2,5	9
20	4	9,5	4	9	4	9	3	9
40	4,5	10	4,5	10	4,5	10	3,5	10
60	5	10	4,5	10	4,5	10	4	10,5

Figure D.3: Measurements at flexion of $\alpha = 60°$.

D.2. ELBOW JOINT FRICTION MEASUREMENT

Measurements of friction component in elbow joint of experimental setup. At fixed elevation angles the effect of friction on the elbow joint is examined. A single vertical force is measured at the wrist. During each downward motion a significantly higher force is required to initiate movement, compared to the upwards motions. Problems with this friction component should be overcome in future prototypes.

wrist
x=0 y=40

a	D1	U1	D2	U2
-60	13	7	13	7
-40	12,5	8	12,5	8
-20	12,5	8,5	12,5	8
0	12	8,5	12,5	8,5

wrist
x=0 y=60

a	D1	U1	D2	U2
-60	13	7	12,5	6
-40	12,5	7	12,5	7
-20	13	8	13	8
0	13	8,5	13	9
20	13	9	12,5	9

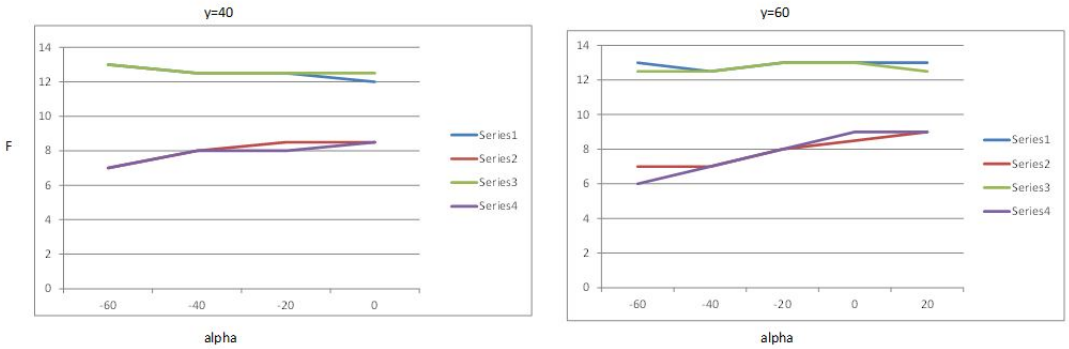

Figure D.4: Measurements at flexion of $\alpha = 60°$.

E

STIFFNESS MATRIX APPROACH

E.1. STIFFNESS MATRIX APPROACH USING POLAR COORDINATES

The stiffness matrix approach is explained here using a polar coordinate system as in current literature. This is in contrast to the new method of using Cartesian coordinates as in paper 1.

In this method a 2D linkage consisting of rigid links, pin joints, masses and zero free length springs is statically balanced. This balance is obtained by having the total potential energy of the linkage to be independent of its orientation.

The method can be described in five steps. The first step is to express all coordinates of joints, spring attachment points and center of mass locations as a function of the states and parameters. The second step is to set up potential energy equations for the different components in the linkage (springs and masses). The third step is to rewrite these equations in a generalized form, separating the variable states from the system parameters. The fourth step is to obtain constraint equations that allow balance when met. These are found from within the generalized form of the energy equation. The fifth and final step is to adjust the parameters such that the constraints are met, resulting in a balanced system.

Step 1: Coordinates
In the current papers on the stiffness matrix approach by Lin et al. [11–13] and Lee et al. [14] multiple different coordinate systems are used. All of which are based on polar coordinates. To explain the approach, a coordinate system similar to one of these systems is used [12].

The orientation of a single link u is described using a state unit vector $\boldsymbol{q}_u = \begin{bmatrix} q_{ux} & q_{uy} \end{bmatrix}^T$ pointing from the proximal joint (J_{u-1}) to the distal joint (J_u)[Figure E.2]. This is the case for each link. The combined state vector $\boldsymbol{Q}$ consists of the unit vectors of all n links. The first state vector $\boldsymbol{q}_1$ is attached to the fixed world and is therefore constant. It points upwards, parallel to, but with opposite direction as the gravitational vector. The other state vectors ($\boldsymbol{q}_2, \cdots \boldsymbol{q}, n$) are unit vectors that have variable directions.

$$\boldsymbol{Q} = \begin{bmatrix} \boldsymbol{q}_1 \\ \vdots \\ \boldsymbol{q}_n \end{bmatrix} \tag{E.1}$$

$$\boldsymbol{q}_1 = \begin{bmatrix} 0 \\ 1 \end{bmatrix} \tag{E.2}$$

The global coordinates of joints [$\boldsymbol{J}_u$], spring attachment points [$\boldsymbol{A}_j$, $\boldsymbol{B}_j$] and center of mass locations [$\boldsymbol{S}_u$] are described as a function of these states. Thus as a function of magnitudes, angles and the state vectors.

The parameter values of the linkage that are similar to Lin [13] are:

a_j = Magnitude from link origin to proximal attachment of spring j.
α_j = Angle between unit vector and vector from origin to proximal attachment of spring j.
b_j = Magnitude from link origin to distal attachment of spring j.
β_j = Angle between unit vector and vector from origin to distal attachment of spring j.
s_v = Magnitude from link origin to center of mass of link v.
σ_v = Angle between unit vector and vector from origin to enter of mass of link v.
r_v = Magnitude from proximal joint to distal joint on link v.
k_j = Spring stiffness of spring j.
m_v = Mass of link v.

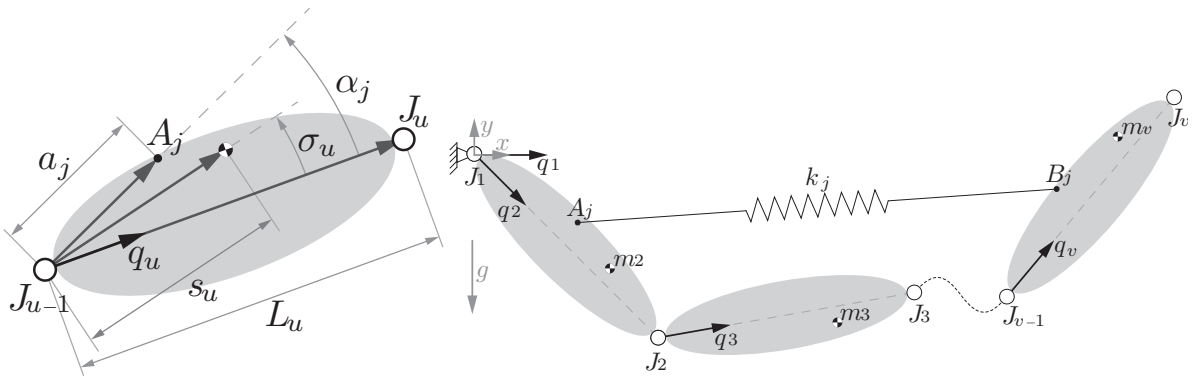

Figure E.1: ()

A schematic illustration of the states and parameters is shown in Figure ??.
Now the coordinates of all points are expressed using the parameters and states.

Joints:

$$\boldsymbol{J}_u = \sum_{i=1}^{u} L_i \boldsymbol{q}_i = \boldsymbol{J}_{u-1} + L_u \boldsymbol{q}_u \tag{E.3}$$

Spring attachments for a spring j. Going from $\boldsymbol{A}_j$, on link u, to $\boldsymbol{B}_j$, on link v:

$$\boldsymbol{A}_j = \boldsymbol{J}_{u-1} + a_j \boldsymbol{R}(\alpha_j)\boldsymbol{q}_u \tag{E.4}$$
$$\boldsymbol{B}_j = \boldsymbol{J}_{v-1} + b_j \boldsymbol{R}(\beta_j)\boldsymbol{q}_v \tag{E.5}$$

COM location on link u:

$$\boldsymbol{S}_u = \boldsymbol{J}_{u-1} + s_u \boldsymbol{R}(\sigma_u)\boldsymbol{q}_u \tag{E.6}$$

Step 2 and 3: Energy equations and generalized form
The goal is to write the energy equations in the following generalized form:

$$U = \frac{1}{2}\boldsymbol{Q}^T \boldsymbol{K} \boldsymbol{Q} \tag{E.7}$$

Spring:
The vector $\boldsymbol{B}_j - \boldsymbol{A}_j$ is the vector representing the orientation of spring j. Knowing this orientation the length of, and therefore the energy in, the spring are known as well. This is as a function of the states.

Vector of components spring j, from proximal link u to distal link v:

$$\boldsymbol{B}_j - \boldsymbol{A}_j = \boldsymbol{J}_{v-1} - \boldsymbol{J}_{u-1} - a_j \boldsymbol{R}(\alpha_j)\boldsymbol{q}_u + b_j \boldsymbol{R}(\beta_j)\boldsymbol{q}_v \tag{E.8}$$

$$\boldsymbol{J}_{v-1} - \boldsymbol{J}_{u-1} = \boldsymbol{J}_u + \boldsymbol{J}_{u+1} + \cdots + \boldsymbol{J}_{v-1} = \sum_{i=u}^{v-1} J_i = \sum_{i=u}^{v-1} L_i \boldsymbol{I}\boldsymbol{q}_i \tag{E.9}$$

$$\boldsymbol{B}_j - \boldsymbol{A}_j = \sum_{i=u}^{v-1} L_i \boldsymbol{I}\boldsymbol{q}_i - a_j \boldsymbol{R}(\alpha_j)\boldsymbol{q}_u + b_j \boldsymbol{R}(\beta_j)\boldsymbol{q}_v \tag{E.10}$$

$$\boldsymbol{B}_j - \boldsymbol{A}_j = \underbrace{(L_u \boldsymbol{I} - a_j \boldsymbol{R}(\alpha_j))}_{\boldsymbol{C}_u}\boldsymbol{q}_u + \underbrace{\sum_{i=u+1}^{v-1} L_i \boldsymbol{I}}_{\boldsymbol{C}_{u+1}+\cdots+\boldsymbol{C}_{v-1}}\boldsymbol{q}_i + \underbrace{b_j \boldsymbol{R}(\beta_j)}_{\boldsymbol{C}_v}\boldsymbol{q}_v = \sum_{i=u}^{v} \boldsymbol{C}_i \boldsymbol{q}_i \tag{E.11}$$

Potential energy in zero length spring j:

$$U_{s,j} = \frac{1}{2} k_j L_{s,j}^2 = \frac{1}{2} k_j (\boldsymbol{B}_j - \boldsymbol{A}_j)^2 \tag{E.12}$$

Generalized form U_s:

$$(\boldsymbol{B}_j - \boldsymbol{A}_j)^2 = \sum_{i=u}^{v}\sum_{i=i}^{v} \boldsymbol{q}_i^T \boldsymbol{C}_i^T \boldsymbol{C}_{ii} \boldsymbol{q}_{ii} \tag{E.13}$$

$$= \begin{bmatrix} \boldsymbol{q}_u \\ \vdots \\ \boldsymbol{q}_v \end{bmatrix}^T \begin{bmatrix} \boldsymbol{C}_u^T \boldsymbol{C}_u & \cdots & \boldsymbol{C}_u^T \boldsymbol{C}_v \\ & \ddots & \vdots \\ \boldsymbol{O} & & \boldsymbol{C}_v^T \boldsymbol{C}_v \end{bmatrix} \begin{bmatrix} \boldsymbol{q}_u \\ \vdots \\ \boldsymbol{q}_v \end{bmatrix} \tag{E.14}$$

$$U_{s,j} = \frac{1}{2} k_j \begin{bmatrix} \boldsymbol{q}_u \\ \vdots \\ \boldsymbol{q}_v \end{bmatrix}^T \begin{bmatrix} \boldsymbol{C}_u^T \boldsymbol{C}_u & \cdots & \boldsymbol{C}_u^T \boldsymbol{C}_v \\ & \ddots & \vdots \\ \boldsymbol{O} & & \boldsymbol{C}_v^T \boldsymbol{C}_v \end{bmatrix} \begin{bmatrix} \boldsymbol{q}_u \\ \vdots \\ \boldsymbol{q}_v \end{bmatrix} \tag{E.15}$$

$$= \frac{1}{2} \begin{bmatrix} \boldsymbol{q}_1 \\ \boldsymbol{q}_u \\ \vdots \\ \boldsymbol{q}_v \\ \boldsymbol{q}_n \end{bmatrix}^T \underbrace{k_j \begin{bmatrix} \boldsymbol{O} & & \cdots & & \boldsymbol{O} \\ & \boldsymbol{C}_u^T \boldsymbol{C}_u & \cdots & \boldsymbol{C}_u^T \boldsymbol{C}_v & \\ & & \ddots & \vdots & \vdots \\ & & & \boldsymbol{C}_v^T \boldsymbol{C}_v & \\ \boldsymbol{O} & & & & \boldsymbol{O} \end{bmatrix}}_{\boldsymbol{K}_{s,j}} \begin{bmatrix} \boldsymbol{q}_1 \\ \boldsymbol{q}_u \\ \vdots \\ \boldsymbol{q}_v \\ \boldsymbol{q}_n \end{bmatrix} \tag{E.16}$$

symetrical as in Lin necessary to get an actual stiffness matrix???? or alternatively having all information in top right diagonal part.

Mass:

The potential height energy of the different mass terms of the links is to be expressed in the same generalized form as well. In the equation of potential energy ($U = mgh$) the terms m and g are known constants. The height term h is expressed as a function of $\boldsymbol{q}_1 = \begin{bmatrix} 0 & 1 \end{bmatrix}^T$ and COM location $\boldsymbol{S} = \begin{bmatrix} s_x & s_y \end{bmatrix}^T$. The product of these terms is equal to the y-component of point $\boldsymbol{S}$ and thus to the height:

$$h = \boldsymbol{q}_1^T \boldsymbol{S} = \begin{bmatrix} 1 & 0 \end{bmatrix} \begin{bmatrix} s_x \\ s_y \end{bmatrix} = s_y \tag{E.17}$$

Effect of the mass of link u on potential energy:

$$U_{m_u} = m_u g \boldsymbol{q}_1^T \boldsymbol{S}_u \tag{E.18}$$

$$U_{m_u} = m_u g \boldsymbol{q}_1^T \left(\boldsymbol{J}_{u-1} + s_u \boldsymbol{R}(\sigma_u)\boldsymbol{q}_u \right) \tag{E.19}$$

$$U_{m_u} = m_u g \boldsymbol{q}_1^T \left(\sum_{i=1}^{u-1} L_i \boldsymbol{q}_i + s_u \boldsymbol{R}(\sigma_u)\boldsymbol{q}_u \right) \tag{E.20}$$

Effect of combined mass of all links, for a linkage with n links (and thus $n-1$ free links):

$$U_{\Sigma m} = \sum_{u=2}^{n} U_{m_u} \tag{E.21}$$

$$= \boldsymbol{q}_1^T \sum_{u=2}^{n} \left(m_u g \boldsymbol{q}_1^T \left[\sum_{i=1}^{u-1} L_i \boldsymbol{q}_i + s_u \boldsymbol{R}(\sigma_u) \boldsymbol{q}_u \right] \right) \tag{E.22}$$

$$= \boldsymbol{q}_1^T \sum_{u=2}^{n} \left(\underbrace{\left[\left(\sum_{i=u+1}^{n} m_i \right) g L_u \boldsymbol{I} + m_u g s_u \boldsymbol{R}(\sigma_u) \right]}_{\boldsymbol{D}_u} \boldsymbol{q}_u \right) \tag{E.23}$$

Generalized form U_m**:**

$$U_{\Sigma m} = \boldsymbol{Q}^T \underbrace{\begin{bmatrix} \boldsymbol{O} & \boldsymbol{D}_2 & \cdots & \boldsymbol{D}_n \\ & \boldsymbol{O} & \cdots & \boldsymbol{O} \\ & & \ddots & \vdots \\ \boldsymbol{O} & & & \boldsymbol{O} \end{bmatrix}}_{\boldsymbol{K}_m} \boldsymbol{Q} \tag{E.24}$$

Combined energy equation

$$U = \frac{1}{2} \boldsymbol{Q}^T \boldsymbol{K} \boldsymbol{Q} \tag{E.25}$$

$$\boldsymbol{K} = \left(\sum_{i=1}^{n_{springs}} \boldsymbol{K}_{s,i} \right) + \boldsymbol{K}_m \tag{E.26}$$

Step 4: Obtain constraint equations

Off-diagonal parts of K matrix are constraint equations. As these terms in the K matrix each are a measure of how the potential energy changes as a result of a relative rotation between two links. i.e.: K(2,3) indicates the stiffness of rotating link 2 relative to link 3. For a balanced system this stiffness is to be 0. This is the only stiffness for which a displacement does not cause a change in potential energy.

Step 5: Obtain balance by solving constraint equations

Solve equations for parameters. A number of parameter values can be selected freely. Others are solved for.

E.2. EXAMPLE CARTESIAN STIFFNESS MATRIX APPROACH

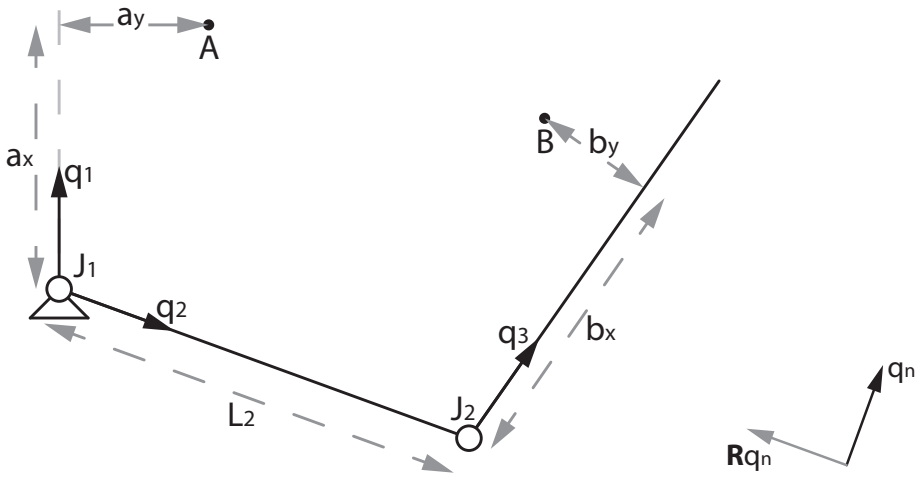

Figure E.2: [Left] Schematics of linkage with point A on link 1 (fixed world) and point B on link 3. [Right] q vector and 90° rotated vector.

$$\boldsymbol{I} = \begin{bmatrix} 1 & 0 \\ 0 & 1 \end{bmatrix} \tag{E.27}$$

$$\boldsymbol{R} = \begin{bmatrix} 0 & -1 \\ 1 & 0 \end{bmatrix} \tag{E.28}$$

$$\boldsymbol{q_n} = \begin{bmatrix} q_{nx} \\ q_{ny} \end{bmatrix} \tag{E.29}$$

$$\boldsymbol{A} = a_x \boldsymbol{I}\boldsymbol{q}_1 + a_y \boldsymbol{R}\boldsymbol{q}_1 = \begin{bmatrix} a_x & -a_y \\ a_y & a_x \end{bmatrix} \boldsymbol{q}_1 \tag{E.30}$$

$$\boldsymbol{J}_2 = L_2 \boldsymbol{I}\boldsymbol{q}_2 = \begin{bmatrix} L_2 & 0 \\ 0 & L_2 \end{bmatrix} \boldsymbol{q}_2 \tag{E.31}$$

$$\boldsymbol{B} = J_2 + b_x \boldsymbol{I}\boldsymbol{q}_3 + b_y \boldsymbol{R}\boldsymbol{q}_3 = \begin{bmatrix} L_2 & 0 \\ 0 & L_2 \end{bmatrix} \boldsymbol{q}_2 + \begin{bmatrix} b_x & -b_y \\ b_y & b_x \end{bmatrix} \boldsymbol{q}_3 \tag{E.32}$$

$$\boldsymbol{L}_{spring} = \boldsymbol{B} - \boldsymbol{A} = \underbrace{-\begin{bmatrix} a_x & -a_y \\ a_y & a_x \end{bmatrix}}_{\boldsymbol{C}_1} \boldsymbol{q}_1 + \underbrace{\begin{bmatrix} L_2 & 0 \\ 0 & L_2 \end{bmatrix}}_{\boldsymbol{C}_2} \boldsymbol{q}_2 + \underbrace{\begin{bmatrix} b_x & -b_y \\ b_y & b_x \end{bmatrix}}_{\boldsymbol{C}_3} \boldsymbol{q}_3 \tag{E.33}$$

$$= \boldsymbol{C}_1 \boldsymbol{q}_1 + \boldsymbol{C}_2 \boldsymbol{q}_2 + \boldsymbol{C}_3 \boldsymbol{q}_3 \tag{E.34}$$

$$\boldsymbol{L}^2_{spring} = \left(\boldsymbol{C}_1 \boldsymbol{q}_1 + \boldsymbol{C}_2 \boldsymbol{q}_2 + \boldsymbol{C}_3 \boldsymbol{q}_3\right)^2 \tag{E.35}$$

$$= \boldsymbol{q}_1^T \boldsymbol{C}_1^T \boldsymbol{C}_1 \boldsymbol{q}_1 + \boldsymbol{q}_1^T \boldsymbol{C}_1^T \boldsymbol{C}_2 \boldsymbol{q}_2 + \boldsymbol{q}_1^T \boldsymbol{C}_1^T \boldsymbol{C}_3 \boldsymbol{q}_3 + \ldots \tag{E.36}$$

$$\boldsymbol{q}_2^T \boldsymbol{C}_2^T \boldsymbol{C}_2 \boldsymbol{q}_2 + \boldsymbol{q}_2^T \boldsymbol{C}_2^T \boldsymbol{C}_3 \boldsymbol{q}_3 + \boldsymbol{q}_3^T \boldsymbol{C}_3^T \boldsymbol{C}_3 \boldsymbol{q}_3 \tag{E.37}$$

$$= \begin{bmatrix} \boldsymbol{q}_1 \\ \boldsymbol{q}_2 \\ \boldsymbol{q}_3 \end{bmatrix}^T \begin{bmatrix} \boldsymbol{C}_1^T \boldsymbol{C}_1 & \boldsymbol{C}_1^T \boldsymbol{C}_2 & \boldsymbol{C}_1^T \boldsymbol{C}_3 \\ 0 & \boldsymbol{C}_2^T \boldsymbol{C}_2 & \boldsymbol{C}_2^T \boldsymbol{C}_3 \\ 0 & 0 & \boldsymbol{C}_3^T \boldsymbol{C}_3 \end{bmatrix} \begin{bmatrix} \boldsymbol{q}_1 \\ \boldsymbol{q}_2 \\ \boldsymbol{q}_3 \end{bmatrix} \tag{E.38}$$

$$= \begin{bmatrix} \boldsymbol{q}_1 \\ \boldsymbol{q}_2 \\ \boldsymbol{q}_3 \end{bmatrix}^T \underbrace{\begin{bmatrix} \boldsymbol{D}_{11} & \boldsymbol{D}_{12} & \boldsymbol{D}_{13} \\ 0 & \boldsymbol{D}_{22} & \boldsymbol{D}_{23} \\ 0 & 0 & \boldsymbol{D}_{33} \end{bmatrix}}_{\boldsymbol{D}} \begin{bmatrix} \boldsymbol{q}_1 \\ \boldsymbol{q}_2 \\ \boldsymbol{q}_3 \end{bmatrix} \tag{E.39}$$

$$\boldsymbol{D}_{11} = \boldsymbol{C}_1^T\boldsymbol{C}_1 = \begin{bmatrix} -a_x & -a_y \\ a_y & -a_x \end{bmatrix}\begin{bmatrix} -a_x & a_y \\ -a_y & -a_x \end{bmatrix} = \begin{bmatrix} a_x^2+a_y^2 & 0 \\ 0 & a_x^2+a_y^2 \end{bmatrix} \tag{E.40}$$

$$\boldsymbol{D}_{12} = \boldsymbol{C}_1^T\boldsymbol{C}_2 = \begin{bmatrix} -a_x & -a_y \\ a_y & -a_x \end{bmatrix}\begin{bmatrix} L_2 & 0 \\ 0 & L_2 \end{bmatrix} = \begin{bmatrix} -a_xL_2 & -a_yL_2 \\ a_yL_2 & -a_xL_2 \end{bmatrix} \tag{E.41}$$

$$\boldsymbol{D}_{13} = \boldsymbol{C}_1^T\boldsymbol{C}_3 = \begin{bmatrix} -a_x & -a_y \\ a_y & -a_x \end{bmatrix}\begin{bmatrix} b_x & -b_y \\ b_y & b_x \end{bmatrix} = \begin{bmatrix} -a_xb_x-a_yb_y & a_xb_y-a_yb_x \\ a_xb_y-a_yb_x & -a_xb_x-a_yb_y \end{bmatrix} \tag{E.42}$$

$$\boldsymbol{D}_{22} = \boldsymbol{C}_2^T\boldsymbol{C}_2 = \begin{bmatrix} L_2 & 0 \\ 0 & L_2 \end{bmatrix}\begin{bmatrix} L_2 & 0 \\ 0 & L_2 \end{bmatrix} = \begin{bmatrix} L_2^2 & 0 \\ 0 & L_2^2 \end{bmatrix} \tag{E.43}$$

$$\boldsymbol{D}_{23} = \boldsymbol{C}_2^T\boldsymbol{C}_3 = \begin{bmatrix} L_2 & 0 \\ 0 & L_2 \end{bmatrix}\begin{bmatrix} b_x & -b_y \\ b_y & b_x \end{bmatrix} = \begin{bmatrix} b_xL_2 & -b_yL_2 \\ b_yL_2 & b_xL_2 \end{bmatrix} \tag{E.44}$$

$$\boldsymbol{D}_{33} = \boldsymbol{C}_3^T\boldsymbol{C}_3 = \begin{bmatrix} b_x & b_y \\ -b_y & b_x \end{bmatrix}\begin{bmatrix} b_x & -b_y \\ b_y & b_x \end{bmatrix} = \begin{bmatrix} b_x^2+b_y^2 & 0 \\ 0 & b_x^2+b_y^2 \end{bmatrix} \tag{E.45}$$

$$\boldsymbol{D} = \begin{bmatrix} \begin{bmatrix} a_x^2+a_y^2 & 0 \\ 0 & a_x^2+a_y^2 \end{bmatrix} & \begin{bmatrix} -a_xL_2 & -a_yL_2 \\ a_yL_2 & -a_xL_2 \end{bmatrix} & \begin{bmatrix} -a_xb_x-a_yb_y & a_xb_y-a_yb_x \\ a_xb_y-a_yb_x & -a_xb_x-a_yb_y \end{bmatrix} \\ 0 & \begin{bmatrix} L_2^2 & 0 \\ 0 & L_2^2 \end{bmatrix} & \begin{bmatrix} b_xL_2 & -b_yL_2 \\ b_yL_2 & b_xL_2 \end{bmatrix} \\ 0 & 0 & \begin{bmatrix} b_x^2+b_y^2 & 0 \\ 0 & b_x^2+b_y^2 \end{bmatrix} \end{bmatrix} \tag{E.46}$$

$$U_{spring} = \frac{1}{2}k\boldsymbol{Q}^T\boldsymbol{D}\boldsymbol{Q} \tag{E.47}$$

E.2.1. GENERAL FORM

For a spring k from link i to link j (proximal to distal, $i < j$), the D matrix can be expressed as:

$$\boldsymbol{A}_k = \boldsymbol{J}_{i-1} + a_{xk}\boldsymbol{I}\boldsymbol{q}_i + a_{yk}\boldsymbol{R}\boldsymbol{q}_i \tag{E.48}$$

$$= \boldsymbol{J}_{i-1} + \left(a_{xk}\boldsymbol{I} + a_{yk}\boldsymbol{R}\right)\boldsymbol{q}_i \tag{E.49}$$

$$\boldsymbol{B}_k = \boldsymbol{J}_{j-1} + b_{xk}\boldsymbol{I}\boldsymbol{q}_j + b_{yk}\boldsymbol{R}\boldsymbol{q}_j \tag{E.50}$$

$$= \boldsymbol{J}_{j-1} + \left(b_{xk}\boldsymbol{I} + b_{yk}\boldsymbol{R}\right)\boldsymbol{q}_j \tag{E.51}$$

$$\boldsymbol{B}_k - \boldsymbol{A}_k = \boldsymbol{J}_{j-1} - \boldsymbol{J}_{i-1} - \left(a_{xk}\boldsymbol{I} + a_{yk}\boldsymbol{R}\right)\boldsymbol{q}_i + \left(b_{xk}\boldsymbol{I} + b_{yk}\boldsymbol{R}\right)\boldsymbol{q}_j \tag{E.52}$$

$$\boldsymbol{J}_{j-1} - \boldsymbol{J}_{i-1} = \boldsymbol{J}_i + \boldsymbol{J}_{i+1} + \cdots + \boldsymbol{J}_{j-1} = \sum_{n=i}^{j-1} L_n\boldsymbol{I}\boldsymbol{q}_n \tag{E.53}$$

$$\boldsymbol{B}_k - \boldsymbol{A}_k = -\left(a_{xk}\boldsymbol{I} + a_{yk}\boldsymbol{R}\right)\boldsymbol{q}_i + \sum_{n=i}^{j-1} L_n\boldsymbol{I}\boldsymbol{q}_n + \left(b_{xk}\boldsymbol{I} + b_{yk}\boldsymbol{R}\right)\boldsymbol{q}_j \tag{E.54}$$

$$\boldsymbol{B}_k - \boldsymbol{A}_k = \underbrace{\left((L_i - a_{xk})\boldsymbol{I} - a_{yk}\boldsymbol{R}\right)}_{\boldsymbol{C}_i}\boldsymbol{q}_i + \underbrace{\sum_{n=i+1}^{j-1} L_n\boldsymbol{I}}_{\boldsymbol{C}_{i+1}+\cdots+\boldsymbol{C}_{j-1}}\boldsymbol{q}_n + \underbrace{\left(b_{xk}\boldsymbol{I} + b_{yk}\boldsymbol{R}\right)}_{\boldsymbol{C}_j}\boldsymbol{q}_j \tag{E.55}$$

$$= \sum_{n=1}^{j} \boldsymbol{C}_n\boldsymbol{q}_n \tag{E.56}$$

$$(\boldsymbol{B}_k - \boldsymbol{A}_k)^2 = \sum_{n=i}^{j}\sum_{m=n}^{j} \boldsymbol{q}_n^T\boldsymbol{C}_n^T\boldsymbol{C}_m\boldsymbol{q}_m \tag{E.57}$$

$$= \begin{bmatrix} \boldsymbol{q}_i \\ \vdots \\ \boldsymbol{q}_j \end{bmatrix}^T \begin{bmatrix} \boldsymbol{C}_i^T\boldsymbol{C}_i & \cdots & \boldsymbol{C}_i^T\boldsymbol{C}_j \\ & \ddots & \vdots \\ \boldsymbol{O} & & \boldsymbol{C}_j^T\boldsymbol{C}_j \end{bmatrix} \begin{bmatrix} \boldsymbol{q}_i \\ \vdots \\ \boldsymbol{q}_j \end{bmatrix} \tag{E.58}$$

$$U_k = \frac{1}{2}k_k(\boldsymbol{B}_k - \boldsymbol{A}_k)^2 \tag{E.59}$$

F

PAPER IFTOMM CONFERENCE

F.1. PARAMETER ANALYSIS FOR THE DEIGN OF STATICALLY BALANCED SERIAL LINKAGES USING A STIFFNESS MATRIX APPROACH WITH CARTESIAN COORDINATES

This paper contains almost the same contents as paper 1: *'Cartesian based stiffness matrix approach and graphical representation for designing statically balanced linkages'* (Chapter 1). It is submitted to and accepted by the 14th IFToMM World Congress in October 2015.

Parameter analysis for the design of statically balanced serial linkages using a stiffness matrix approach with Cartesian coordinates

M. P. Lustig*
Delft University of Technology
Delft, The Netherlands

A. G. Dunning†
Delft University of Technology
Delft, The Netherlands

J. L. Herder‡
Delft University of Technology
Delft, The Netherlands

Abstract—*A statically balanced system is in equilibrium in every pose. In classical balancing solutions for serial linkages, each DOF is balanced by an independent element (counter-mass or mono-articular spring). Disadvantages are increased mass and inertia for counter-mass, and auxiliary links for spring solutions. Recent literature presents a method for balancing serial linkages without auxiliary links; using multi-articular springs. This method obtains constraint equations from the stiffness matrix. Downsides are different coordinate systems for describing locations and states, and set criteria constraining attachments to fixed lines. In the presented paper this stiffness matrix approach is implemented using a consistent Cartesian system. Goal is comparing the use of this single coordinate system to the use of multiple, and obtaining increased insight in and providing a visualization of parameter relations. The Cartesian coordinates are implemented, providing a simple, intuitive method for designing statically balanced serial linkages. Obtained parameter relations are visualized in an example.*

Keywords: Static balance, Zero-free-length spring, Serial linkage

I. Introduction

A system which is in equilibrium in every motionless state is called statically balanced. For such systems the potential energy level remains constant in every pose [1]. This constant energy level greatly reduces operational effort as only dynamic effects remain to be overcome during motion. Many applications for static balancing exist due to these benefits [1], [2], [3], [4].

Different techniques exist to statically balance the rotation of a rigid pendulum. A simple option is adding a counter-mass [1], downside of which is the increased mass and inertia [5]. A second option is connecting a zero-free-length spring (ZFLS) between the link and fixed world [1]. For a ZFLS the spring force is proportional to its length. Other less common solutions use a non-circular cam [6] or compliant flexure elements [7]. These solutions are all designed to balance a single degree of freedom (DOF).

Solutions for balancing a serial linkage with multiple DOF make use of counter-mass or ZFLSs. In the first case a counter-mass is added to each link [8], [9], additional auxiliary links allow counter-mass relocation [10]. Inertia increase becomes a greater problem as added weights of distal counter-masses must be balanced as well. Classical ZFLS solutions require a parallel beam construction providing a link with fixed orientation at each joint [1], [11], [12]. Each link is balanced by a single ZFLS that spans the joint of the respective link, a mono-articular spring. The disadvantage of parallel beams are an increased complexity and added inertia. In these systems each DOF is balanced by an independent balancing element.

Recent literature presents two methods in which ZFLSs can span multiple joints to balance serial linkages without parallel beams. The first method is the stiffness matrix approach by Lin et al. [12], [13], [14], [15]. Energy equations are set up in a general form $U = \frac{1}{2}\boldsymbol{Q}^T\boldsymbol{K}\boldsymbol{Q}$, separating states $\boldsymbol{Q}$ and parameters in a stiffness matrix $\boldsymbol{K}$. Off-diagonal elements of $\boldsymbol{K}$ contain state dependent energy terms, constraining these terms equal to zero results in a statically balanced system [13]. The second method is an iterative method developed by Deepak and Ananthasuresh [16]. Balance is ensured link by link, in steps, starting at the most distal link. At each step, balance of a specific link is acquired by adding up to two ZFLSs between this link and fixed world. For each link only energy terms of the current and previous step links affect its constraint equations [16]. In these two methods each DOF is balanced by combined efforts of multiple ZFLSs.

Both methods can create statically balanced serial linkages and are based on an energy approach. Nevertheless multiple differences exist in ease of implementation and capabilities. The first is that in Lin's method all constraints are obtained at once for a chosen spring configuration, whereas in Deepak's method only a selection of the constraints is evaluated at once. If no straightforward solution is found, Deepak's method explains which spring(s) can be added for a solvable system, Lin's method does not directly. However, information on which links are unbalanced and thus require additional springs can be extracted from the stiffness matrix [15]. Another difference is that all springs are connected to the fixed world in Deepak's method while in Lin's method springs can be attached in between any two links, i.e. additional constraints are provided considering these springs. Finally, Deepak's method allows pla-

*M.P.Lustig@student.tudelft.nl
†A.G.Dunning@tudelft.nl
‡J.L.Herder@tudelft.nl

nar placement of spring attachments while in Lin's method criteria are set up constraining attachments to be located on fixed straight lines [15].

In the presented work the stiffness matrix approach is selected for calculating balanced linkages as it provides all constraints at once and allows additional spring placement options. The exact implementation however is altered. Current literature describes locations on links using polar coordinate systems, while states are described using unit vectors (xy-components). In the presented work Carthesian (xy-) coordinates are used describing link locations as well as the states.

Three goals are formulated in the presented paper. The first goal is to implement Cartesian coordinates in the stiffness matrix approach for balanced serial linkages to investigate its benefits over the combined use of polar coordinates for locations and xy-coordinates for states. The second goal is to gain more insight in the relations between different parameters of this method in the design space, for instance it will be investigated if placement of springs outside the vertical straight lines is allowed. The third goal is to visualize these behavioral relations in an example.

The structure of this paper is as follows. First, in 'Method' the Cartesian coordinate stiffness matrix approach is derived. Next, in 'Application and behavior' the example of a balanced linkages is presented of which the behavior is analyzed. Third, in 'Discussion' the use of Cartesian and polar coordinates are compared. Finishing with the obtained conclusions concerning the set goals.

II. Method

We propose the consistent use of Cartesian coordinates in the stiffness matrix approach for designing serial statically balanced linkages. This is in contrast to the use of polar coordinates for locations and Cartesian coordinates for states, as used in current literature on this method [12], [13], [14], [15]. In the presented paper the location of spring attachments, joints and COMs is described using (local) x- and y- coordinates on the respective links they are located on. In this section the assumptions are explained first, followed by the full derivation of the stiffness matrix approach using xy-coordinates.

A. Assumptions and limitations

The presented method is set up for planar linkages, the gravitational field acting in this plane has constant magnitude and direction. The links are connected to each other and/or the fixed world using revolute joints. All springs have linear ZFLS behavior and the mass of these springs is neglected. Mechanical limits of links/springs colliding with one another are not taken into account. The fixed world is assumed to be rigid and static.

B. Derivation of stiffness matrix

The stiffness matrix approach is derived in five steps. First all coordinate points are described as a function of the link states and parameter values. The second step is setting up potential energy equations for all spring and mass components and writing these equations in a generalized form. The third step is to combine the energy equations of the different components to obtain the total stiffness matrix. The fourth step is obtaining the constraint equations for balance from the stiffness matrix. The fifth and final step is focused on how to solve the obtained equations. The equations are set up for an n link system where the fixed world is link 1, as a result the system has $n-1$ moving links.

B.1 Step 1: Coordinate vectors

The state of link u is described by global unit vector $\boldsymbol{q}_u$ (Figure 1a). The fixed world vector $\boldsymbol{q}_1$ is constant, aligned with the global x-axis. For moving links ($u = 2 \cdots n$) vector $\boldsymbol{q}_u$ is aligned with the local x_u-axis. The origin of each local coordinate system is located at the proximal joint J_{u-1}. The y_u-axis are orientated perpendicular to the respective x_u-axis. A unit vector in this y_u direction is obtained by rotating the state vector $\boldsymbol{q}_u$ by 90° using rotation matrix $\boldsymbol{R}$. Combined state vector $\boldsymbol{Q}$ holds the states of all n-links.

$$\boldsymbol{q}_1 = \begin{bmatrix} 1 \\ 0 \end{bmatrix} \tag{1a}$$

$$\boldsymbol{q}_u = \begin{bmatrix} q_{xu} \\ q_{yu} \end{bmatrix} \tag{1b}$$

$$\boldsymbol{Q} = \begin{bmatrix} \boldsymbol{q}_1 \\ \vdots \\ \boldsymbol{q}_n \end{bmatrix} \tag{1c}$$

$$\boldsymbol{I} = \begin{bmatrix} 1 & 0 \\ 0 & 1 \end{bmatrix} \tag{1d}$$

$$\boldsymbol{R} = \begin{bmatrix} \cos(90^\circ) & -\sin(90^\circ) \\ \sin(90^\circ) & \cos(90^\circ) \end{bmatrix} = \begin{bmatrix} 0 & -1 \\ 1 & 0 \end{bmatrix} \tag{1e}$$

Global coordinates of all point on the links are described as a linear combination of the state vectors and constant parameter values. Joint locations are described first. As said, fixed world joint $\boldsymbol{J}_1$ is located in the global origin. The distal joint $\boldsymbol{J}_u$ of a link u is always located on the local x_u-axis at distance L_u from the local origin (Figure 1b). Vector components of joint locations are set up in equation 2.

$$\boldsymbol{J}_1 = \begin{bmatrix} 0 \\ 0 \end{bmatrix} \tag{2a}$$

$$\begin{aligned} \boldsymbol{J}_u &= L_2\boldsymbol{I}\boldsymbol{q}_2 + L_3\boldsymbol{I}\boldsymbol{q}_3 + \cdots + L_u\boldsymbol{I}\boldsymbol{q}_u \\ &= \sum_{i=2}^{u} L_i\boldsymbol{I}\boldsymbol{q}_i = \boldsymbol{J}_{u-1} + L_u\boldsymbol{I}\boldsymbol{q}_u \end{aligned} \tag{2b}$$

Spring attachment point locations for a spring j between link u to link v are $\boldsymbol{A}_j$ and $\boldsymbol{B}_j$ respectively. These locations are a linear combination of the proximal joint component

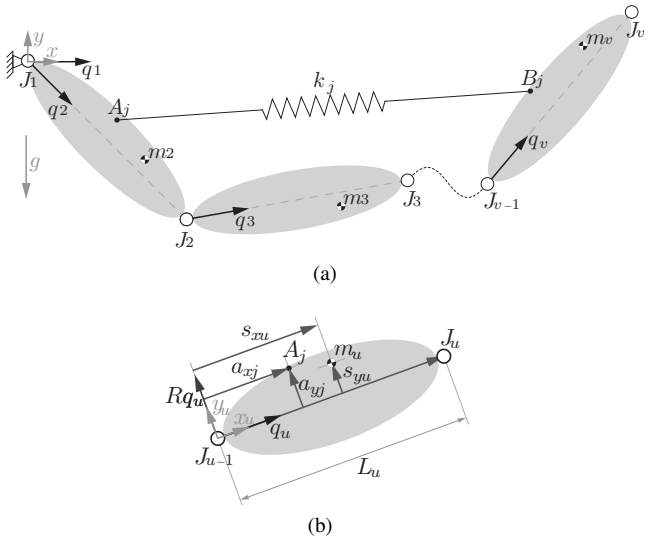

Fig. 1: (a) Schematic representation of a serial linkage in a state defined by unit vectors $\boldsymbol{q}$. (b) Parameterization of locations on link u in the Cartesian form.

$\boldsymbol{J}_{u-1}$, the local x_u component ($a_{xj}\boldsymbol{I}\boldsymbol{q}_u$) and the local y_u component ($a_{yj}\boldsymbol{R}\boldsymbol{q}_u$) (Eq. 3). A schematic representation containing these components is given in figure 1b.

$$\boldsymbol{A}_j = \boldsymbol{J}_{u-1} + (a_{xj}\boldsymbol{I} + a_{yj}\boldsymbol{R})\,\boldsymbol{q}_u \tag{3a}$$
$$\boldsymbol{B}_j = \boldsymbol{J}_{v-1} + (b_{xj}\boldsymbol{I} + b_{yj}\boldsymbol{R})\,\boldsymbol{q}_v \tag{3b}$$

Similarly the COM location of link u is set up (Eq. 4).

$$\boldsymbol{S}_u = \boldsymbol{J}_{u-1} + (s_{xu}\boldsymbol{I} + s_{yu}\boldsymbol{R})\boldsymbol{q}_u \tag{4}$$

B.2 Step 2: Energy equations and generalized form

This step is to write energy equations in the generalized form, separating the states $\boldsymbol{Q}$ and the parameters in the stiffness matrix $\boldsymbol{K}$.

$$U = \frac{1}{2}\boldsymbol{Q}^T\boldsymbol{K}\boldsymbol{Q} \tag{5}$$

Spring energy is expressed in this form first. The vector describing spring length and orientation for spring j, going from link u to link v, is $\boldsymbol{B}_j - \boldsymbol{A}_j$. This is as a function of the states, because the locations of points $\boldsymbol{B}_j$ and $\boldsymbol{A}_j$ are state dependent as well. The expression for this spring vector is derived in equation 6. An expression is obtained where constants are separated for each state (Eq. 6e). The components $\boldsymbol{C}$ holding these constant parameters are shown in matrix form (Eq. 7).

$$\begin{aligned}\boldsymbol{B}_j - \boldsymbol{A}_j =& \boldsymbol{J}_{v-1} - \boldsymbol{J}_{u-1} - (a_{xj}\boldsymbol{I} + a_{yj}\boldsymbol{R})\,\boldsymbol{q}_u \\ &+ (b_{xj}\boldsymbol{I} + b_{yj}\boldsymbol{R})\,\boldsymbol{q}_v\end{aligned} \tag{6a}$$

$$\begin{aligned}\boldsymbol{J}_{v-1} - \boldsymbol{J}_{u-1} =& \boldsymbol{J}_u + \boldsymbol{J}_{u+1} + \cdots + \boldsymbol{J}_{v-1} \\ =& \sum_{n=u}^{v-1} L_n\boldsymbol{I}\boldsymbol{q}_n\end{aligned} \tag{6b}$$

$$\begin{aligned}\boldsymbol{B}_j - \boldsymbol{A}_j =& -(a_{xj}\boldsymbol{I} + a_{yj}\boldsymbol{R})\,\boldsymbol{q}_u \\ &+ \sum_{n=u}^{v-1} L_n\boldsymbol{I}\boldsymbol{q}_n + (b_{xj}\boldsymbol{I} + b_{yj}\boldsymbol{R})\,\boldsymbol{q}_v\end{aligned} \tag{6c}$$

$$\begin{aligned}\boldsymbol{B}_j - \boldsymbol{A}_j =& \underbrace{((L_u - a_{xj})\boldsymbol{I} - a_{yj}\boldsymbol{R})}_{\boldsymbol{C}_u}\,\boldsymbol{q}_u \\ &+ \underbrace{\sum_{n=u+1}^{v-1} L_n\boldsymbol{I}}_{\boldsymbol{C}_{u+1}+\cdots+\boldsymbol{C}_{v-1}}\,\boldsymbol{q}_n + \underbrace{(b_{xj}\boldsymbol{I} + b_{yj}\boldsymbol{R})}_{\boldsymbol{C}_v}\,\boldsymbol{q}_v\end{aligned} \tag{6d}$$

$$\boldsymbol{B}_j - \boldsymbol{A}_j = \sum_{n=1}^{v} \boldsymbol{C}_n\boldsymbol{q}_n \tag{6e}$$

$$\boldsymbol{C}_u = \begin{bmatrix} L_u - a_{xj} & a_{yj} \\ -a_{yj} & L_u - a_{xj} \end{bmatrix} \tag{7a}$$

$$\boldsymbol{C}_i = \begin{bmatrix} L_i & 0 \\ 0 & L_i \end{bmatrix} \quad \text{, for } i = u+1, \cdots, v-1 \tag{7b}$$

$$\boldsymbol{C}_v = \begin{bmatrix} b_{xj} & -b_{yj} \\ b_{yj} & b_{xj} \end{bmatrix} \tag{7c}$$

$$\boldsymbol{C}_i = \begin{bmatrix} 0 & 0 \\ 0 & 0 \end{bmatrix} \quad \text{, for : } \begin{cases} i = 1, \cdots, u-1 \\ i = v+1, \cdots, n \end{cases} \tag{7d}$$

Knowing the spring length, as a function of the states, its potential energy can be calculated. The equation is set up for a ZFLS j with stiffness k_j (Eq. 8a) and rewritten in the generalized form (Eq. 8d). In this form the states ($\boldsymbol{Q}$) are separated from the parameters in the stiffness matrix of the spring ($\boldsymbol{K}_{s,j}$).

$$U_{s,j} = \frac{1}{2}k_j(\boldsymbol{B}_j - \boldsymbol{A}_j)^2 \tag{8a}$$
$$= \frac{1}{2}k_j\left(\sum_{u=1}^{n}\boldsymbol{C}_u\boldsymbol{q}_u\right)^2 \tag{8b}$$
$$= \frac{1}{2}k_j\begin{bmatrix}\boldsymbol{q}_1\\ \vdots\\ \boldsymbol{q}_n\end{bmatrix}^T\begin{bmatrix}\boldsymbol{C}_1^T\boldsymbol{C}_1 & \cdots & \boldsymbol{C}_1^T\boldsymbol{C}_n\\ \vdots & \ddots & \vdots\\ \boldsymbol{C}_n^T\boldsymbol{C}_1 & \cdots & \boldsymbol{C}_n^T\boldsymbol{C}_n\end{bmatrix}\begin{bmatrix}\boldsymbol{q}_1\\ \vdots\\ \boldsymbol{q}_n\end{bmatrix} \tag{8c}$$
$$= \frac{1}{2}\boldsymbol{Q}^T\boldsymbol{K}_{s,j}\boldsymbol{Q} \tag{8d}$$
$$\boldsymbol{K}_{s,j} = k_j\begin{bmatrix}\boldsymbol{C}_1^T\boldsymbol{C}_1 & \cdots & \boldsymbol{C}_1^T\boldsymbol{C}_n\\ \vdots & \ddots & \vdots\\ \boldsymbol{C}_n^T\boldsymbol{C}_1 & \cdots & \boldsymbol{C}_n^T\boldsymbol{C}_n\end{bmatrix} \tag{8e}$$

Next the gravitational energy is expressed in the generalized form of equation 5. The height of the masses is found in the second element of vector $\boldsymbol{S}_u$, containing the global COM y-coordinate of link u. The value for height is extracted by vector product: *height*$= \begin{bmatrix}0 & 1\end{bmatrix}\boldsymbol{S}_u$. This product is not jet expressed as in the generalized form because $\boldsymbol{S}_u$ does not contain multiplications of states. By using state $\boldsymbol{q}_1$, which is located on the fixed world, it is known that $(\boldsymbol{R}\boldsymbol{q}_1)^T = \begin{bmatrix}0 & 1\end{bmatrix}$, describing the gravitational field direction. Therefore the height of a mass is expressed as in the generalized form by product: *height*$= (\boldsymbol{R}\boldsymbol{q}_1)^T\boldsymbol{S}_u$. Based on this term the energy equations are first written for the mass of a single link u (Eq. 9) followed by a summed relation containing the masses of all links (Eq. 10). For this form the constant components $\boldsymbol{D}_u$ that fill the stiffness matrix are described (Eq. 11), followed by the generalized form of the energy equation (Eq. 12).

$$U_{m_u} = m_u g(\boldsymbol{R}\boldsymbol{q}_1)^T\boldsymbol{S}_u \tag{9a}$$
$$= m_u g\boldsymbol{q}_1^T\boldsymbol{R}^T\boldsymbol{S}_u \tag{9b}$$
$$= m_u g\boldsymbol{q}_1^T\boldsymbol{R}^T\left[\boldsymbol{J}_{u-1} + (s_{xu}\boldsymbol{I} + s_{yu}\boldsymbol{R})\boldsymbol{q}_u\right] \tag{9c}$$
$$= m_u g\boldsymbol{q}_1^T\boldsymbol{R}^T\left[\sum_{i=1}^{u-1}(L_i\boldsymbol{q}_i) + (s_{xu}\boldsymbol{I} + s_{yu}\boldsymbol{R})\boldsymbol{q}_u\right] \tag{9d}$$

Effect of combined mass of all links, for a linkage with n links (and thus $n-1$ moving links) is given (Eq. 10).

$$U_{\Sigma m} = \sum_{u=2}^{n}U_{m_u} \tag{10a}$$
$$= \boldsymbol{q}_1^T\sum_{u=2}^{n}\left(\boldsymbol{R}^T m_u g\left[\sum_{i=1}^{u-1}(L_i\boldsymbol{q}_i) + (s_{xu}\boldsymbol{I} + s_{yu}\boldsymbol{R})\boldsymbol{q}_u\right]\right) \tag{10b}$$
$$= \boldsymbol{q}_1^T\sum_{u=2}^{n}\left(\underbrace{\boldsymbol{R}^T\left[\left(\sum_{i=u+1}^{n}m_i\right)gL_u\boldsymbol{I} + m_u g(s_{xu}\boldsymbol{I} + s_{yu}\boldsymbol{R})\right]}_{\boldsymbol{D}_u}\boldsymbol{q}_u\right) \tag{10c}$$

$$\boldsymbol{D}_u = \boldsymbol{R}^T\left[\left(\sum_{i=u+1}^{n}m_i\right)gL_u\boldsymbol{I} + m_u g(s_{xu}\boldsymbol{I} + s_{yu}\boldsymbol{R})\right] \tag{11a}$$
$$= \begin{bmatrix} m_u g s_{yu} & m_u g s_{xu} + \left(\sum_{i=u+1}^{n}m_i\right)gL_u\\ -m_u g s_{xu} - \left(\sum_{i=u+1}^{n}m_i\right)gL_u & m_u g s_{yu}\end{bmatrix} \tag{11b}$$

The generalized form $U_{\Sigma m}$ is obtained as states and parameters are separated.

$$U_{\Sigma m} = \frac{1}{2}\boldsymbol{Q}^T\boldsymbol{K}_m\boldsymbol{Q} \tag{12a}$$
$$\boldsymbol{K}_m = \begin{bmatrix}\boldsymbol{O} & \boldsymbol{D}_2 & \cdots & \boldsymbol{D}_n\\ \boldsymbol{D}_2^T & \boldsymbol{O} & \cdots & \boldsymbol{O}\\ \vdots & \vdots & \ddots & \vdots\\ \boldsymbol{D}_n^T & \boldsymbol{O} & \cdots & \boldsymbol{O}\end{bmatrix} \tag{12b}$$

When analyzing a new system it is possible to quickly set up the stiffness matrices without having to go through all derivations performed in this step. It is advised to directly substitute the component matrices for the springs $\boldsymbol{C}_u$(Eq. 7a-7d) and the mass components $\boldsymbol{D}_u$ (Eq.11). By substituting these component matrices in equation 8e and 12b the stiffness matrix $\boldsymbol{K}_{s,j}$ and $\boldsymbol{K}_m$ are obtained.

B.3 Step 3: Total stiffness matrix

The combined energy U_t, containing all spring and mass terms is obtained by combining the spring and mass stiffness matrices (Eq. 13).

$$U_t = \frac{1}{2}\boldsymbol{Q}^T\boldsymbol{K}_t\boldsymbol{Q} \tag{13a}$$
$$\boldsymbol{K}_t = \left(\sum_{i=1}^{n_{springs}}\boldsymbol{K}_{s,i}\right) + \boldsymbol{K}_m \tag{13b}$$

B.4 Step 4: Constraint equations

In a balanced system, any state can be changed freely with respect to any other state without changing the overall potential energy level. For this to be the case, the effective stiffness between any two different states should be equal to zero. These represent all state dependent energy terms. The effective stiffness terms for these relative rotations are found on the off-diagonal part of the stiffness matrix $\boldsymbol{K}_t$ [14]. As a result, all off-diagonal parts of the $\boldsymbol{K}_t$ matrix are constrained to be equal to zero for balance [13].

The number of constraint equations depends on the size of the $\boldsymbol{K}_t$ matrix, which in turn depends on the number of links n. The matrices are symmetrical, thus all relations are found in the upper triangular part (Eq. 8e, 12b). Additionally, all relations in one of these triangular parts occur twice, once in each even and uneven row. Thus only every other row has to be examined to obtain all relations. Altogether the amount of constraint equations for an n-link system is equal to $n(n-1)$ [14].

B.5 Step 5: Obtain balance by solving constraint equations

The next step is solving the obtained constraint equations. In general, the minimal amount of variables to be calculated is equal to the number of equations. For example, for a three link planar system the number of constraint equations is equal to six and as a result at least six parameters should be left free while solving such a system. The remaining parameters can be selected to have constant values.

III. Application and behavior

In this section an illustrative example of a balanced linkage is presented. The behavior of the balanced system is analyzed to gain a better understanding of how different parameters can be changed while maintaining the desired balance. Increased insight in the inner workings of the system will allow for a more efficient design process and a better overview of possible solutions. Found relations for varying parameters while maintaining balance are provided and visualized. The system studied has two moving links (Figure 2a) and is positioned in a gravitational field acting in the $y-$direction with $g = 9.81m/s^2$.

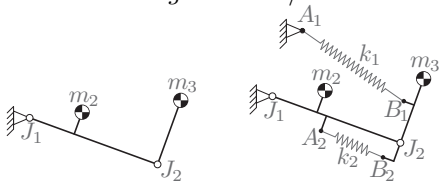

(a) (b)

Fig. 2: (a) Unbalanced linkage. (b) Spring configuration of example 1. (c) Spring configuration of example 2.

A. Example

Two springs are used to balance the system, one bi-articular ZFLS connecting the fixed world to link 3 and one mono-articular ZFLS that connects links 2 and 3 (Figure 2b). In the first step the system locations in figure 2b are expressed in xy-coordinates as in figure 1b. The actual location vectors (Eq. 2,3,4) are not shown as their creation is not required for continuing in this method, nevertheless they are useful for instance to plot the system. In the second step the component matrices for the two springs $\boldsymbol{C}_1$ and $\boldsymbol{C}_2$ (Eq. 14) and the mass terms $\boldsymbol{D}$ (Eq. 15) are constructed based on equations 7 and 11. By substituting these component matrices in equations 8e and 12b the spring matrices $\boldsymbol{K}_{s1}, \boldsymbol{K}_{s2}$ and mass stiffness matrix $\boldsymbol{K}_m$ are obtained (Eq. 16a,16b). The third step is to construct the total stiffness matrix by combining the spring and mass matrices (Eq. 16c). In the fourth step the constraint equations are obtained from the $\boldsymbol{K}_t$ matrix (Eq. 17). The constraint equations to be satisfied for balance are the off-diagonal parts of the $\boldsymbol{K}_t$ matrix set equal to zero. Here only terms in odd rows (1 and 3) are considered as the even rows contain the same relations.

$$\begin{aligned}
\boldsymbol{C}_{1,1} &= \begin{bmatrix} -a_{x1} & a_{y1} \\ -a_{y1} & -a_{x1} \end{bmatrix} & \boldsymbol{C}_{2,1} &= \begin{bmatrix} 0 & 0 \\ 0 & 0 \end{bmatrix} \\
\boldsymbol{C}_{1,2} &= \begin{bmatrix} L_2 & 0 \\ 0 & L_2 \end{bmatrix} & \boldsymbol{C}_{2,2} &= \begin{bmatrix} L_2 - a_{x2} & a_{y2} \\ -a_{y2} & L_2 - a_{x2} \end{bmatrix} \\
\boldsymbol{C}_{1,3} &= \begin{bmatrix} b_{x1} & -b_{y1} \\ b_{y1} & b_{x1} \end{bmatrix} & \boldsymbol{C}_{2,3} &= \begin{bmatrix} b_{x2} & -b_{y2} \\ b_{y2} & b_{x2} \end{bmatrix}
\end{aligned} \tag{14}$$

$$\begin{aligned}
\boldsymbol{D}_1 &= \begin{bmatrix} 0 & 0 \\ 0 & 0 \end{bmatrix} \\
\boldsymbol{D}_2 &= \begin{bmatrix} m_2 g s_{y2} & m_3 g L_2 + m_2 g s_{x2} \\ -m_3 g L_2 - m_2 g s_{x2} & m_2 g s_{y2} \end{bmatrix} \\
\boldsymbol{D}_3 &= \begin{bmatrix} m_3 g s_{y3} & m_3 g s_{x3} \\ -m_3 g s_{x3} & m_3 g s_{y3} \end{bmatrix}
\end{aligned} \tag{15}$$

$$\boldsymbol{K}_{si} = \frac{1}{2} k_i \begin{bmatrix} \boldsymbol{C}_{i,1}^T \boldsymbol{C}_{i,1} & \boldsymbol{C}_{i,1}^T \boldsymbol{C}_{i,2} & \boldsymbol{C}_{i,1}^T \boldsymbol{C}_{i,3} \\ & \boldsymbol{C}_{i,2}^T \boldsymbol{C}_{i,2} & \boldsymbol{C}_{i,2}^T \boldsymbol{C}_{i,3} \\ \text{sym} & & \boldsymbol{C}_{i,3}^T \boldsymbol{C}_{i,3} \end{bmatrix} \tag{16a}$$

$$\boldsymbol{K}_m = \begin{bmatrix} \boldsymbol{O} & \boldsymbol{D}_2 & \boldsymbol{D}_3 \\ & \boldsymbol{O} & \boldsymbol{O} \\ \text{sym} & & \boldsymbol{O} \end{bmatrix} \tag{16b}$$

$$\boldsymbol{K}_t = \boldsymbol{K}_{s1} + \boldsymbol{K}_{s2} + \boldsymbol{K}_m \tag{16c}$$

$$\begin{aligned}
\boldsymbol{K}_t(1,3) = 0 &= -k_1 a_{x1} L_2 + m_2 g s_{y2} \\
\boldsymbol{K}_t(1,4) = 0 &= -k_1 a_{y1} L_2 + m_2 g s_{x2} + m_3 g L_2 \\
\boldsymbol{K}_t(1,5) = 0 &= -k_1 (a_{x1} b_{x1} + a_{y1} b_{y1}) + m_3 g s_{y3} \\
\boldsymbol{K}_t(1,6) = 0 &= k_1 (a_{x1} b_{y1} - a_{y1} b_{x1}) + m_3 g s_{x3} \\
\boldsymbol{K}_t(3,5) = 0 &= k_1 b_{x1} L_2 - k_2 (a_{y2} b_{y2} - b_{x2} (L_2 - a_{x2})) \\
\boldsymbol{K}_t(3,6) = 0 &= -k_1 b_{y1} L_2 - k_2 (a_{y2} b_{x2} + b_{y2} (L_2 - a_{x2}))
\end{aligned} \tag{17}$$

In the final step the constraint equations are solved for four different cases, each showing different behavior (Figure 3). Between these cases some general properties of the system remain the same. Specifically spring stiffness, mass and link length values. In each case the constraints are solved for parameters $a_{x1}, b_{x1}, b_{y1}, b_{x2}, b_{y2}$ and k_1. Varied inputs between cases are parameters a_{x2} and a_{y2}, describing the location of attachment A_2. Furthermore s_{y2} is varied, describing the location of the COM of link 2. Obtained parameter values of balanced configurations are summarized in table 3e. Parameters on the first six rows (above the horizontal line) are calculated by solving the constraints, remaining parameter values (under the line) are chosen inputs.

In the first case all spring connections are aligned with the links (Figure 3a). In case 2, attachment A_2 of the second spring is rotated about the joint J_2, as a result attachment B_2 rotates with the same angle about J_2 as well (Figure 3b). In case 3, the COM of link 2 is relocated. Resulting in simultaneous rotations of attachments B_1 and B_2 (Figure 3c). In the final case 4, both offsets of A_2, as in case 2, and s_{y2}, as in case 3, are combined. The solved configuration shows a combination of the behavior caused by the individual offsets of the previous cases (Figure 3d).

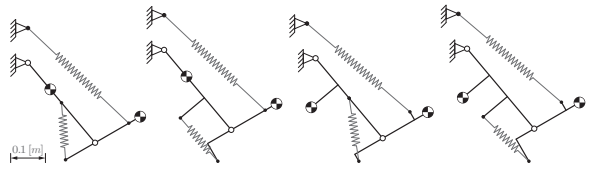

(a) Case 1 (b) Case 2 (c) Case 3 (d) Case 4

	Case 1	Case 2	Case 3	Case 4	Units
a_{x1}	0	0	-0.025	-0.025	$[m]$
b_{x1}	0.1125	0.1125	0.1059	0.1059	$[m]$
b_{y1}	0	0	0.0265	0.0265	$[m]$
b_{x2}	-0.0981	-0.0785	-0.0923	-0.06	$[m]$
b_{y2}	0	-0.0589	-0.0231	-0.0739	$[m]$
k_1	261.6	261.6	261.6	261.6	$[\frac{N}{m}]$
k_2	600	600	600	600	$[\frac{N}{m}]$
a_{y1}	0.1	0.1	0.1	0.1	$[m]$
a_{x2}	0.15	0.18	0.15	0.18	$[m]$
a_{y2}	0	-0.09	0	-0.09	$[m]$
m_2	2	2	2	2	$[kg]$
m_3	2	2	2	2	$[kg]$
L_2	0.3	0.3	0.3	0.3	$[m]$
s_{x2}	0.1	0.1	0.1	0.1	$[m]$
s_{y2}	0	0	-0.1	-0.1	$[m]$
s_{x3}	0.15	0.15	0.15	0.15	$[m]$
s_{y3}	0	0	0	0	$[m]$

(e)

Fig. 3: In scale balanced solutions for example 2. (a) Case 1. (b) Case 2. (c) Case 3. (d) Case 4. (e) Parameter values for the different cases.

B. Behavior in example

The four cases in example 2 are all statically balanced as they all fulfill the constraint equations. The unbalanced three link system is analyzed first in the orientation in which it has minimal gravitational energy (Figure 4a). In this position link 2 is oriented at angle α with respect to the vertical. Angle α is now determined by setting the moment M_{J_1} around J_1 to be equal to zero as it should be when in equilibrium (Eq.18). The system shown in figure 4b is equal to the linkage of figure 4a only with redrawn links that give room for springs to be drawn later on.

$$M_{J_1} = 0 = m_2 s_{y2}\cos(\alpha) - m_2 s_{x2}\sin(\alpha) - m_3 L_2 \sin(\alpha) \tag{18a}$$

$$(m_2 s_{x2} + m_3 L_2)\sin(\alpha) = m_2 s_{y2}\cos(\alpha) \tag{18b}$$

$$\frac{\sin(\alpha)}{\cos(\alpha)} = \tan(\alpha) = \frac{m_2 s_{y2}}{m_2 s_{x2} + m_3 L_2} \tag{18c}$$

$$\alpha = \tan^{-1}\left(\frac{m_2 s_{y2}}{m_2 s_{x2} + m_3 L_2}\right) \tag{18d}$$

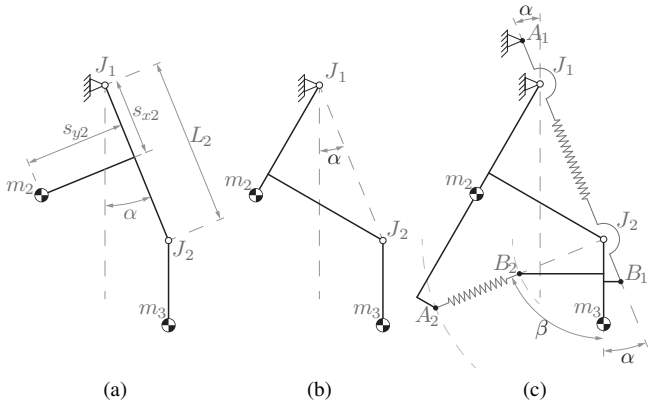

(a) (b) (c)

Fig. 4: (a) and (b) Unbalanced linkage in equilibrium. (c) Relations between the location of spring attachment points required for a balanced system.

Next, it is recognized that for balance a zero moment is required in all orientations. As this is already the case for the original system in the orientation of figure 4b neither of the added springs should apply a moment around any of the joints to keep this moment free condition. Spring 1 is located between the fixed world point A_1 and link 3 at point A_3, and thus spawns both joints. As a result, spring connections A_1 and B_1 should be aligned with both joints J_1 and J_2, exactly at the previously determined angle α (Figure 4c). Spring 2 connects A_2 on link 2 and B_2 on link 3 and thus spawns only the second joint J_2. Therefore, in this orientation with minimal potential the two connection points of this spring are to be aligned with J_2 (Figure 4c).

Furthermore, as α is only dependent on parameters of the original linkage its value is unaffected by adjusting the other spring. For spring 2 the alignment of attachment A_2

depends on both angles α and β with respect to the local coordinate system of link 2. Attachment B_2 is dependent only on angle β with respect to the local coordinates of links 3. Therefore, by changing β spring 2 can be relocated anywhere on a ring shaped disk around J_2, as partially visualized by dotted lines in figure 4c.

The locations of the spring attachments are now described based on a single position of the linkage where the gravitational energy is at a minimum. This does not directly prove that the system is in balance in any pose as it is only clear that this one position is in equilibrium. However, the proof that the system can be balanced in any configuration is already given using the stiffness matrix approach. What the analysis of this single position does provide is insight in where the attachments can be placed and why they are constrained to lie on certain lines or positions. Additionally it can be reasoned that the system is capable of being balanced in all orientations as the energy behavior of all components is sinusoidal with respect to each rotation. These sinusoids have equal periods as these are equivalent to full rotations of a links, all having a minimum or maximum in the orientation of figure 4. The sinusoidal functions are either in phase or shifted by half a phase exactly and so can interfere with one another to cancel each other out.

The behavior described so far in this example is based on the orientations in which springs can be placed for the selected spring configuration (Figure 4). However some additional interesting observations are made based on parameter magnitudes.

The first observation is that the location of spring attachment point B_1 (Figure 4c) is a unique point depending solely on parameters of the original linkage, i.e. it is fixed independently of all other spring related parameters. Using the `solve` function in MATLAB the constraint equations are solved for parameters b_{x1} and b_{x2}. These parameters describe the location of B_1, expressed as a function of the other parameters (Eq.19). The obtained equations consist solely of parameters describing link length, mass or COM location.

$$b_{x1} = \frac{L_2^2 m_3^2 s_{x3} + L_2 m_2 m_3 (s_{x2} s_{x3} + s_{y2} s_{y3})}{(L_2 m_3 + m_2 s_{x2})^2 + m_2^2 s_{y2}^2} \tag{19a}$$

$$b_{y1} = \frac{L_2^2 m_3^2 s_{y3} + L_2 m_2 m_3 (s_{x2} s_{y3} - s_{x3} s_{y2})}{(L_2 m_3 + m_2 s_{x2})^2 + m_2^2 s_{y2}^2} \tag{19b}$$

For the spring attachment A_1 an additional constraint is found. It is found that the distance from joint J_1 to this point A_1 is inversely related to its spring stiffness k_1. This is by solving the constraint equations (Eq.17) for the parameters a_{x1} and a_{y1} which describe the location of A_1 (Eq.20a and 20b). Furthermore, the relation for α can again be extracted from these constraints by looking at the relative magnitudes of a_{x1} and a_{y1} (Eq.20c).

$$a_{x1} = \frac{m_2 g s_{y2}}{L_2} \frac{1}{k_1} \tag{20a}$$

$$a_{y1} = \frac{m_2 g s_{x2} + m_3 g L_2}{L_2} \frac{1}{k_1} \tag{20b}$$

$$\alpha = \tan^{-1}\left(\frac{a_{x1}}{a_{y1}}\right) = \tan^{-1}\left(\frac{m_2 s_{y2}}{m_2 s_{x2} + m_3 L_2}\right) \tag{20c}$$

For spring 2, an additional constraint is found as well, this is next to angle β which describes the springs orientation. When all other parameters are fixed, the product of its stiffness k_2, distance from J_2 to A_2 and distance from J_2 to B_2 is constant ($k_2 \cdot |A_2 - J_2| \cdot |B_2 - J_2| = \text{constant}$). In other words, the two described lengths and the stiffness of this spring can be varied freely within these bounds without affecting any other parameter. This magnitude of the 'constant' value in this relation is affected by the location of A_1 and k_1, however it is unpractical to take these into account in the same relation and much more convenient to fix these parameters before altering either A_2, B_2 or k_2.

IV. Discussion

Constraint equations in polar form, for the system studied in the presented example, are set up in the work of Lin et al.[13]. In this form link locations are defined by a magnitude and an angle, representing the same relations as in equation 17. Behavior found in the presented example shows a number of simultaneous rotations of COM locations and/or spring connection points that can be performed without affecting the balance of the system (Figure 4). One could argue to use a polar coordinate system to describe this behavior as it is rotational. However, the centers of rotation for these simultaneous rotations can either be on the first joint, the second joint or a seemingly arbitrary point on one of the links. As the location of the center point is inconsistent it cannot be ensured that this point is always positioned on the origin of the local coordinate system from which the polar coordinates are defined. Furthermore, describing a rotation using polar coordinates about a point other than the origin is, according to the authors, unnecessarily complicated compared to describing such a rotation as a sum of vector components in a Cartesian coordinate system. For this reason an xy-coordinate system is recommended when altering a system having planar offsets. Other benefits of using a Cartesian system are that the resulting constraint equations will be free of sinusoidal term, and describing coordinates on a link using xy-components is more intuitive compared to using an angle and magnitude.

V. Conclusion

In this work the implementation of the stiffness matrix approach is altered such that states and link locations are expressed in the same coordinate system. The first goal was to implement Cartesian coordinates and comparing it to the use of polar coordinates in the stiffness matrix approach.

The Cartesian coordinates were successfully implemented and in comparison they were found to be more intuitive in use, provide simpler constraint equations and be more convenient for altering parameters of balanced systems. The second goal was to gain more insight in the relations between parameters while the third goal was to illustrate these behavioral relations in two examples. These two goals were achieved simultaneously as in the example a basic system (having two moving links) was analyzed. Relations were found between orientation, positioning and magnitude of springs and masses. These are described and illustrated providing a visual overview of the design space. Obtained relations provide knowledge in the possibilities to vary spring system parameters while maintaining static balance.

VI. Acknowledgments

This research is part of the project 'Flextension', sponsored by Technology Foundation STW, project 11832.

References

[1] J. L. Herder, Energy-free systems; theory, conception and design of statically balanced spring mechanisms, Ph.d. thesis, Delft University of Technology, iSBN 90-370-0192-0 (2001).

[2] S. K. Agrawal, A. Fattah, Gravity-balancing of spatial robotic manipulators, Mechanism and machine theory 39 (12) (2004) 1331–1344.

[3] A. H. Stienen, E. E. Hekman, G. B. Prange, M. J. Jannink, F. C. van der Helm, H. van der Kooij, Freebal: design of a dedicated weight-support system for upper-extremity rehabilitation, Journal of Medical Devices 3 (4) (2009) 041009.

[4] M. Carricato, C. Gosselin, A statically balanced gough/stewart-type platform: conception, design, and simulation, Journal of Mechanisms and Robotics 1 (3) (2009) 031005.

[5] K. Kobayashi, Comparison between spring balancer and gravity balancer in inertia force and performance, Journal of Mechanical Design 123 (4) (2001) 549–555.

[6] G. Endo, H. Yamada, A. Yajima, M. Ogata, S. Hirose, A passive weight compensation mechanism with a non-circular pulley and a spring, in: Robotics and Automation (ICRA), 2010 IEEE International Conference on, IEEE, 2010, pp. 3843–3848.

[7] C.-W. Hou, C.-C. Lan, Functional joint mechanisms with constant-torque outputs, Mechanism and Machine Theory 62 (2013) 166–181.

[8] R. Sapper, Lamp with an articulated support, uS Patent 3,790,773 (Feb. 5 1974).
URL https://www.google.com/patents/US3790773

[9] J. Wang, C. M. Gosselin, Static balancing of spatial three-degree-of-freedom parallel mechanisms, Mechanism and Machine Theory 34 (3) (1999) 437–452.

[10] H. Hilpert, Weight balancing of precision mechanical instruments, Journal of Mechanisms 3 (4) (1968) 289 – 302.

[11] S. K. Banala, S. K. Agrawal, A. Fattah, V. Krishnamoorthy, H. Wei-Li, J. Scholz, K. Rudolph, Gravity-balancing leg orthosis and its performance evaluation, Robotics, IEEE Transactions on 22 (6) (2006) 1228–1239.

[12] P.-Y. Lin, W.-B. Shieh, D.-Z. Chen, A theoretical study of weight-balanced mechanisms for design of spring assistive mobile arm support (mas), Mechanism and Machine Theory 61 (2013) 156–167.

[13] P.-Y. Lin, W.-B. Shieh, D.-Z. Chen, A stiffness matrix approach for the design of statically balanced planar articulated manipulators, Mechanism and Machine Theory 45 (12) (2010) 1877–1891.

[14] P.-Y. Lin, W.-B. Shieh, D.-Z. Chen, Design of statically balanced planar articulated manipulators with spring suspension, Robotics, IEEE Transactions on 28 (1) (2012) 12–21.

[15] Y.-Y. Lee, D.-Z. Chen, Determination of spring installation configuration on statically balanced planar articulated manipulators, Mechanism and Machine Theory 74 (2014) 319–336.

[16] S. R. Deepak, G. Ananthasuresh, Perfect static balance of linkages by addition of springs but not auxiliary bodies, Journal of Mechanisms and Robotics 4 (2) (2012) 021014.

G

MATLAB CODE

G.1. RUNFILE

This script creates design equations for a selected spring configuration and solves it for provided parameters. The result is plotted.

```
%% 2014-07-29 Maarten Lustig
% Solve constraint equations for multiple linkages, in xy coordinates
%%
%% %%%%%%%%%%%%%%%%%%%%%%%%% 2 links 2 springs fixed world %%%%%%%%%%%%%%%%%%%%%%%%%%
clearvars -except L8 %except a symbolic parameter, prevents symbolic toolbox to ...
    restart every run
% clear all
clc

springs = [1,3;1,3]; % select spring configuration. Add spring between links for ...
    example: 1,4;
Methode_xy_fun
% Constant parameters
m2 = 2; m3 = 2;
L2 = 0.3; L3 = 0.3;
sx2 = double(L2/2); sx3 = double(L3/2);
sy2 = 0; sy3 = 0;
g=9.81;
%
ay1 = 0.09
ay2= -0.06
ax1 = 0
ax2 = 0

% bx1 = 0.03
bx2 = -0.04
by1 = 0
by2 = 0


% k1 =   245.2500
% k2 =   245.2500


Methode_xy_evalsubs

plot_links_xy

eval(subs(Kt))
```

G.2. METHODE_XY_FUN.M

In this script the stiffness matrix is created for the input spring configuration. From this stiffness matrix design equations are extracted.

```
%% 2014-07-18 Maarten Lustig
% Make constraint equations for n-link system in xy coordinates
%%
% clear all;clc
% clearvars ¬except L8 %except a symbolic parameter, prevents symbolic toolbox to ...
    restart every run
clc
%% %%%%%%%%%%%%%%%%%%%%%%%%% INPUT %%%%%%%%%%%%%%%%%%%%%%%%%%
% springs = [1,2;2,3;1,4;1,4];%[0,1;0,2;0,2]; %0,4; 0,5;0,5];
% springs = [1,2;2,3;1,4;1,4];

n_links =  max(max(springs)); %including fixed world link
n_springs = length(springs(:,1));

%% %%%%%%%%%%%%%%%%%%%%%%%%% VARIABLES %%%%%%%%%%%%%%%%%%%%%%%%%%
syms L1 L2 L3 L4 L5 L6 L7 L8            % link lenght
syms ax1 ax2 ax3 ax4 ax5 ax6 ax7 ax8    % spring attachment proximal
syms ay1 ay2 ay3 ay4 ay5 ay6 ay7 ay8
syms bx1 bx2 bx3 bx4 bx5 bx6 bx7 bx8    % spring attachment distal
syms by1 by2 by3 by4 by5 by6 by7 by8
syms sx1 sx2 sx3 sx4 sx5 sx6 sx7 sx8    % distance joint to centre of mass
syms sy1 sy2 sy3 sy4 sy5 sy6 sy7 sy8
syms k1 k2 k3 k4 k5 k6 k7 k8            % spring constants
syms m1 m2 m3 m4 m5 m6 m7 m8            % mass of links
syms g                                  % gravitational constant

%% %%%%%%%%%%%%%%%%%%%%%%%%% CONSTANTS %%%%%%%%%%%%%%%%%%%%%%%%%%
%Identity matrix
I = [1,0;0,1];
% Rotation matrix 90 degrees
R = [0,-1;1,0];

%% %%%%%%%%%%%%%%%%%%%%%%%%% K-matrix springs %%%%%%%%%%%%%%%%%%%%%%%%%%
% For all springs
clear Cuv K
for j=1:n_springs
    clear Cuv
    u=springs(j,1);
    v=springs(j,2);
    n=n_links;
    %% Make C components for spring
    % Cu: proximal spring attatchment
    if u == 1
        Cuv(:,:,u) =  - eval(['ax' num2str(j)])*I - eval(['ay' num2str(j)])*R;
    else
        Cuv(:,:,u) = (eval(['L' num2str(u)]) - eval(['ax' num2str(j)]))*I - ...
            eval(['ay' num2str(j)])*R;
    end

    % Cu+1 Cv-1: links inbetween proximal and distal attatchment links
    for u = u+1:v-1
        Cuv(:,:,u) =  eval(['L' num2str(u)])*I;
    end

    %Cv: Distal spring attatchment
    Cuv(:,:,v) = ( eval(['bx' num2str(j)])*I + eval(['by' num2str(j)])*R );

    %C>v: Add zeros to make size of K consistent
    if n>v
        for u = v+1:n
            Cuv(:,:,u) = [0 0;0 0];
        end
    end

    % Fill Ks-matrix
```

```
64      for i_row = 1:n_links
65          for i_col = i_row:1:n_links
66              Ks(2*i_row-1:2*i_row,2*i_col-1:2*i_col,j) = ...
                    Cuv(:,:,i_row).'*Cuv(:,:,i_col) * eval(['k' num2str(j)]);
67          end
68      end
69      Cuv
70  end
71  Ks
72
73  %% %%%%%%%%%%%%%%%%%%%%%%%%% K-matrix mass %%%%%%%%%%%%%%%%%%%%%%%%%%%%
74  clear Du
75  for u = 2:n_links
76      clear m_temp m_sum
77
78      % Sum of all mass terms distal of joint Jn
79      if u == n_links
80          m_temp = 0;
81      else
82          for i = u+1:n_links
83              m_temp(i) = eval(['m' num2str(i)]);
84          end
85      end
86      m_sum = sum(m_temp);
87
88      %% D components
89      Du(:,:,u) = R'*(m_sum * g * eval(['L' num2str(u)]) * I + eval(['m' num2str(u)]) * ...
            g * ( eval(['sx' num2str(u)]) * I + eval(['sy' num2str(u)]) * R));
90
91  end
92
93  % Fill Km-matrix
94  for i_col = 1:u
95      Km(1:2,2*i_col-1:2*i_col) = Du(:,:,i_col);
96  end
97  Km(2*n,2*n)= 0;
98  Km
99
100 %% %%%%%%%%%%%%%%%%%%%%%%%%% K-matrix total %%%%%%%%%%%%%%%%%%%%%%%%%%%%
101
102 % Kt = sum of all Ks matrices and Km matrix
103 Kt = Km;
104 for i = 1 : n_springs
105     Kt = Kt + Ks(:,:,i);
106 end
107 Kt
108
109 %% %%%%%%%%%%%%%%%%%%%%%%%%% Constraint equations %%%%%%%%%%%%%%%%%%%%%%%%%%%%
110 % Non diagonal parts of Kt-matrix (only uneven rows)
111 CS = 0;
112 for i = 1:2:n_links*2-3
113     CS = [CS; Kt(i,i+2:n_links*2).'];
114 end
115
116 CS = CS(find(CS≠0))
117
118
119 %% %%%%%%%%%%%%%%%%%%%%%%%%% Constant parameter values %%%%%%%%%%%%%%%%%%%%%%%%%%%%
120
121 % if exist('defign_m_L','var')
122 % else
123 % % lengths of links
124 % L1 = 0.3; L2 = 0.3; L3 = 0.3; L4 = 0.3; L5 = 0.3;
125 %
126 % % mass
127 % m1 = 2; m2 = 2; m3 = 2; m4 = 2; m5 = 2;
128 %
129 % % gravity constant
130 % g = 9.81;
131 %
132 % % % distance from centre of mass to proximal joint
```

```
% % sx2 = double(L2/2);
% sx2 = double(2/2); sx3 = double(L3/2);  sx4 = double(L4/2); sx5 = double(L5/2);
% % sy2 = 0;
% sy2 = 0; sy3 = 0; sy4 = 0; sy5 = 0;
% end
%% Substitute constants
CSs = subs(CS)
variables = symvar(CSs)

%% %%%%%%%%%%%%%%%%%%%%%%%% Solve constraints for parameters %%%%%%%%%%%%%%%%%%%%%%%%%%%%

% y1 = solve(CSs==zeros(length(CSs),1))%,'k1,k2')
```

G.3. METHODE_XY_EVALSUBS.M

In this script the design equations are solved for provided input. Depending on the input different parameters can be the variable solved for.

```
%% SOLVE DESIGN EQUATIONS %%
%%%%%%%%%%%%%%%%%%%%%%%%%%%%%%%%%%%%%%%%%%%%%%%%%%%%%%%%%%%%%%%%%%%%%%%%%%%%%%%%%%%%

CSs0 = subs(CSs)
CSs0 = CSs0(find(CSs0≠0))

% CSs0 = [CSs0(1);CSs0(4)]
% assume(k1 ≥ 0)
y1 = solve(CSs0==zeros(length(CSs0),1))

% ax2 =eval( y1)

vars0 = subs(fieldnames(y1)).'


%% k
if ismember([k1],vars0)==1;    k1 = eval(subs(y1.k1(1)))
end
if ismember([k2],vars0)==1;    k2 = eval(subs(y1.k2(1)))
end
if ismember([k3],vars0)==1;    k3 = eval(subs(y1.k3(1)))
end
if ismember([k4],vars0)==1;    k4 = eval(subs(y1.k4(1)))
end

%% ax
if ismember([ax1],vars0)==1;    ax1 = eval(subs(y1.ax1(1)))
end
if ismember([ax2],vars0)==1;    ax2 = eval(subs(y1.ax2(1)))
end
if ismember([ax3],vars0)==1;    ax3 = eval(subs(y1.ax3(1)))
end
if ismember([ax4],vars0)==1;    ax4 = eval(subs(y1.ax4(1)))
end

%% ay
if ismember([ay1],vars0)==1;    ay1 = eval(subs(y1.ay1(1)))
end
if ismember([ay2],vars0)==1;    ay2 = eval(subs(y1.ay2(1)))
end
if ismember([ay3],vars0)==1;    ay3 = eval(subs(y1.ay3(1)))
end
if ismember([ay4],vars0)==1;    ay4 = eval(subs(y1.ay4(1)))
end

%% bx
if ismember([bx1],vars0)==1;    bx1 = eval(subs(y1.bx1(1)))
end
if ismember([bx2],vars0)==1;    bx2 = eval(subs(y1.bx2(1)))
end
if ismember([bx3],vars0)==1;    bx3 = eval(subs(y1.bx3(1)))
end
if ismember([bx4],vars0)==1;    bx4 = eval(subs(y1.bx4(1)))
end

%% by
if ismember([by1],vars0)==1;    by1 = eval(subs(y1.by1(1)))
end
if ismember([by2],vars0)==1;    by2 = eval(subs(y1.by2(1)))
end
if ismember([by3],vars0)==1;    by3 = eval(subs(y1.by3(1)))
end
if ismember([by4],vars0)==1;    by4 = eval(subs(y1.by4(1)))
end
```

```
66 %% L
67 if ismember([L2],vars0)==1;    L2 = eval(subs(y1.L2(1)))
68 end
69 if ismember([L3],vars0)==1;    L3 = eval(subs(y1.L3(1)))
70 end
71 if ismember([L4],vars0)==1;    L4 = eval(subs(y1.L4(1)))
72 end
73 if ismember([L5],vars0)==1;    L5 = eval(subs(y1.L5(1)))
74 end
75
76 %% sx
77 if ismember([sx2],vars0)==1;    sx2 = eval(subs(y1.sx2(1)))
78 end
79 if ismember([sx3],vars0)==1;    sx3 = eval(subs(y1.sx3(1)))
80 end
81 if ismember([sx4],vars0)==1;    sx4 = eval(subs(y1.sx4(1)))
82 end
83 if ismember([sx5],vars0)==1;    sx5 = eval(subs(y1.sx5(1)))
84 end
```

G.4. PLOT_LINKS_XY.M

The obtained balanced system is plotted in this script. Plots can be made for systems with any amount of links, in any selected spring configuration and for different set of parameter values.

```
%% 2014-07-21 Maarten Lustig
%Plot n-link system in xy coordinates
%% %%%%%%%%%%%%%%%%%%%%%%%%%% Plot line colors %%%%%%%%%%%%%%%%%%%%%%%%%%%%
ccl=lines(7);
cch=hsv(12);
cc=[ccl;cch(2:end,:)]; %colors eerst alle line colors dan hsv
clear ccl cch
%% %%%%%%%%%%%%%%%%%%%%%%%%%% State vectors %%%%%%%%%%%%%%%%%%%%%%%%%%%%%%
clear qn

%phi = [180 110 200 180 0]/180*pi;
phi = [180 30 120 180 0]/180*pi;


qn(:,1)= [1;0];
for i = 2 : n_links
    %states
    qn(:,i) = [sin(phi(i)); -cos(phi(i))];
end

%% %%%%%%%%%%%%%%%%%%%%%%%%%% Coordinate vectors %%%%%%%%%%%%%%%%%%%%%%%%%%%%
clear Sn Jn An Bn

% Joint coordinates
Jn = [0;0];
for i = 2:n_links
    Jn(:,i) = Jn(:,i-1) + eval(['L' num2str(i)]) * qn(:,i);
end

% Spring attatchment coordinates A and B
for i = 1 : n_springs
    spring_i = springs(i,:);
    %Proximal attatchment A
    if spring_i(1)==1
        An(:,i) = [0;0] + (eval(['ax' num2str(i)])*I + eval(['ay' num2str(i)])*R)* ...
            qn(:,spring_i(1));
    else
        An(:,i) = Jn(:,spring_i(1)-1) + (eval(['ax' num2str(i)])*I + eval(['ay' ...
            num2str(i)])*R)* qn(:,spring_i(1));
    end
    %Distal attatchment B
    Bn(:,i) = Jn(:,spring_i(2)-1) + (eval(['bx' num2str(i)])*I + eval(['by' ...
        num2str(i)])*R)* qn(:,spring_i(2));
end

% COM location coordinates S
for i = 2 : n_links
    Sn(:,i) = Jn(:,i-1) + (eval(['sx' num2str(i)])*I + eval(['sy' num2str(i)])*R)* ...
        qn(:,i);
end

%% %%%%%%%%%%%%%%%%%%%%%%%%%% Plot scematics %%%%%%%%%%%%%%%%%%%%%%%%%%%%%%

%Figure 1: links and springs
figure(99);

clf
hold on
axis equal

%links
for i = 1:n_links-1

    if i ==1; i_cc = 4;
    else i_cc = 1;
```

```
62      end
63
64      plot(Jn(1,[i i+1]), Jn(2,[i i+1]),'color',cc(i_cc,:),'linewidth',2)%130)
65  end
66
67  %spring attatchment to COM
68  for i = 1:n_springs
69      if eval(['k' num2str(i)]) ≠0 && springs(i,2) >2
70          plot([Sn(1,springs(i,2)), Bn(1,i)],[Sn(2,springs(i,2)), ...
                Bn(2,i)],'color',cc(1,:),'linewidth',2);end
71  end
72
73  for i = 1:n_springs
74      if springs(i,1) ≥2
75          plot([Sn(1,springs(i,1)), An(1,i)],[Sn(2,springs(i,1)), ...
                An(2,i)],'color',cc(4,:),'linewidth',2);
76      end
77      if springs(i,2) ==2
78          plot([Sn(1,springs(i,2)), Bn(1,i)],[Sn(2,springs(i,2)), ...
                Bn(2,i)],'color',cc(4,:),'linewidth',2);
79      end
80  end
81
82  %springs
83  % for i = 1:1
84  %     if eval(['k' num2str(i)]) ≠0
85  %         plot([An(1,i), Bn(1,i)],[An(2,i), Bn(2,i)],'color',cc(4,:),'linewidth',2);end
86  % end
87  for i = 1:n_springs
88      if eval(['k' num2str(i)]) ≠0
89          plot([An(1,i), Bn(1,i)],[An(2,i), Bn(2,i)],'color',cc(2,:),'linewidth',2);end
90  end
91
92  % hinges
93  for i = 1:n_links-1
94  plot(Jn(1,i), Jn(2,i),'ok','linewidth',4)
95  % plot(J2(1),J2(2),'ok','linewidth',4)
96  end
97
98  % spring attatchments
99  for i = 1:n_springs
100 plot(An(1,i), An(2,i),'+g','linewidth',1)
101 end
102
103
104 % %spring attatchment to Jv-1
105 % for i = 1:n_springs
106 %     if eval(['k' num2str(i)]) ≠0
107 %         plot([Jn(1,springs(i,2)-1), Bn(1,i)],[Jn(2,springs(i,2)-1), ...
        Bn(2,i)],'color',cc(1,:),'linewidth',2);end
108 % end
109 %
110
111 %COM
112 for i =2:n_links
113     plot(Sn(1,i), Sn(2,i),'+m','linewidth',1)
114
115 end
116
117 % text
118 for i = 1:n_springs
119 text(An(1,i),An(2,i),['A' num2str(i)], 'VerticalAlignment','bottom', ...
        'HorizontalAlignment','right')
120 text(Bn(1,i),Bn(2,i),['B' num2str(i)], 'VerticalAlignment','top', ...
        'HorizontalAlignment','left')
121 end
```

G.5. DESIGN EQUATIONS IN PARAMETERS OF PAPER 2

Using this script the design equations are rewritten to be in the form of paper 2.

```
%% NEW PARAMETERS
clearvars -except L8 %except a symbolic parameter, prevents symbolic toolbox to ...
    restart every run
% clear all
clc

springs = [1,3;1,3];
Methode_xy_fun;
clc
CSc = eval(subs(CS,{ax1,ax2,by1,by2,sy2,sy3},[0,0,0,0,0,0]));
CSc = CSc(find(CSc≠0))

syms b1 b2 c1 c2 b c d k s2 s3
CSd = eval(subs(CSc,{ay1,ay2,sx2,sx3,bx1,bx2},[d+c1,d-c2,s2,s3,b1,b2]))
CSe = ...
    eval(subs(CSd,{c1,c2,b1,b2},[c*k2/(k1+k2),c*k1/(k1+k2),b*k2/(k1+k2),-b*k1/(k1+k2)]))

CSd = simplify(simple(CSe))
```

G.6. STEP BY STEP FLOATING JOINT LINKAGE

This script shows step by step spring split up possibilities to obtain a floating point joint mechanism.

```
%% %%%%%%%%%%%%%%%%%%%%%%%%%% STEP 1: Moment balanced linkage %%%%%%%%%%%%%%%%%%%%%%%%%%
clearvars -except L8 %except a symbolic parameter, prevents symbolic toolbox to restart
% make constraint equations
springs = [1,3;1,3];
Methode_xy_fun

% Constant parameters
m2 = 2; m3 = 2;
L2 = 0.3; L3 = 0.3;
sx2 = double(L2/2); sx3 = double(L3/2);
sy2 = 0; sy3 = 0;
g=9.81;

% Variabel S2
r = sx2

% angle beta
beta =0/180*pi %%%%%%%%%%%%%%%%%%%%%%%%%%%%%%%%%%%%%%%%%%%%%%%%%%%%%%%%%%%%

Rot_beta = [cos(beta), -sin(beta);sin(beta), cos(beta)]

S2new = Rot_beta*[r;0]
sx2 = S2new(1)
sy2 = S2new(2)

% angle alpha
alpha = 0/180*pi; %%%%%%%%%%%%%%%%%%%%%%%%%%%%%%%%%%%%%%%%%%%%%%%%%%%%%%%%%%%%
Rot = [cos(alpha), -sin(alpha);sin(alpha), cos(alpha)];
B1 = Rot*[0.05;0] % point B1 rotated with angle alpha

% parameters
ax1 =   0
ay1 =    0.08
ax2 =   0
% ay2 =   -0.1

bx1 =    0.04%B1(1)
by1 =     0%B1(2)%0.0

bx2 =   -0.03%-bx1
by2 =     0%-by1

%%%
Methode_xy_evalsubs
% plots
plot_links_xy

%plot Z1 and Z2
A1 = [ax1;ay1]
A2 = [ax2;ay2]
A3 = [ax3;ay3]
A4 = [ax4;ay4]

Z1 = (A1*k1+A2*k2)/(k1+k2)
Z2 = Z1 - [0;m3*g/(k1+k2)]  % Z2(2)*(k1+k2) = 9.81 N !!!!!!!!!!!!!!!!!!!!

plot(Z1(1), Z1(2),'og','linewidth',3)
plot(Z2(1), Z2(2),'or','linewidth',3)

%% %%%%%%%%%%%%%%%%%%%%%%%%%% STEP 2: Moment balanced linkage + Force free point by ...
    adding 2 spring %%%%%%%%%%%%%%%%%%%%%%%%%%
clearvars -except L8 %except a symbolic parameter, prevents symbolic toolbox to restart
% make constraint equations
springs = [1,3;1,3;1,2;1,2];
Methode_xy_fun

```

```
% Constant parameters
m2 = 2; m3 = 2;
L2 = 0.3; L3 = 0.3;
sx2 = double(L2/2); sx3 = double(L3/2);
sy2 = 0; sy3 = 0;
g=9.81;

% Variabel S2
r = sx2

% angle beta
beta =0/180*pi %%%%%%%%%%%%%%%%%%%%%%%%%%%%%%%%%%%%%%%%%%%%%%%%%%%%%%%%%%%%

Rot_beta = [cos(beta), -sin(beta);sin(beta), cos(beta)]

S2new = Rot_beta*[r;0]
sx2 = S2new(1)
sy2 = S2new(2)

% angle alpha
alpha = 0/180*pi; %%%%%%%%%%%%%%%%%%%%%%%%%%%%%%%%%%%%%%%%%%%%%%%%%%%%%%%%
Rot = [cos(alpha), -sin(alpha);sin(alpha), cos(alpha)];
B1 = Rot*[0.05;0] % point B1 rotated with angle alpha

% parameters
ax1 =   0
ay1 =    0.08
ax2 =   0
% ay2 =   -0.1

bx1 =    0.04%B1(1)
by1 =     0%B1(2)%0.0

bx2 =   -0.03%-bx1
by2 =     0%-by1

% k1 = 147.15
% k2 = 147.15

%%% New springs
% spring 3
k3 = k1 +k2

ax3 = 0
ay3 = 0
bx3 = -0.3
by3 = 0

% spring 4

ax4 = 0
ay4 = 0.08
bx4 = 0
by4 = 0

k4 = (m2 * g * (L2-sx2)/L2)/ay4


%%%
Methode_xy_evalsubs
k3 = eval(subs(k3))
% plots
plot_links_xy

%plot Z1 and Z2
A1 = [ax1;ay1]
A2 = [ax2;ay2]
A3 = [ax3;ay3]
A4 = [ax4;ay4]


```

```
Z3 = (A1*k1+A2*k2+A3*k3+A4*k4-[0;(m2+m3)*g])/(k1+k2+k3+k4)
Z4 = (A1*k1+A2*k2+A3*k3+A4*k4)/(k1+k2+k3+k4)

plot(Z3(1), Z3(2),'oc','linewidth',3)
plot(Z4(1), Z4(2),'oy','linewidth',3)


%% %%%%%%%%%%%%%%%%%%%%%%%% STEP 3: Replace spring 3 by 2 other springs ...
    %%%%%%%%%%%%%%%%%%%%%%%%%%%%
clearvars -except L8 %except a symbolic parameter, prevents symbolic toolbox to restart
% make constraint equations
springs = [1,3;1,3;1,2;1,2;1,2];
Methode_xy_fun


% Constant parameters
m2 = 2; m3 = 2;
L2 = 0.3; L3 = 0.3;
sx2 = double(L2/2); sx3 = double(L3/2);
sy2 = 0; sy3 = 0;
g=9.81;

% Variabel S2
r = sx2

% angle beta
beta =0/180*pi %%%%%%%%%%%%%%%%%%%%%%%%%%%%%%%%%%%%%%%%%%%%%%%%%%%%%%%%%%%

Rot_beta = [cos(beta), -sin(beta);sin(beta), cos(beta)]

S2new = Rot_beta*[r;0]
sx2 = S2new(1)
sy2 = S2new(2)

% angle alpha
alpha = 0/180*pi; %%%%%%%%%%%%%%%%%%%%%%%%%%%%%%%%%%%%%%%%%%%%%%%%%%%%%%%%
Rot = [cos(alpha), -sin(alpha);sin(alpha), cos(alpha)];
B1 = Rot*[0.05;0] % point B1 rotated with angle alpha

% parameters
ax1 =   0
ay1 =    0.08
ax2 =   0
% ay2 =   -0.1

bx1 =    0.04%B1(1)
by1 =     0%B1(2)%0.0

bx2 =   -0.03%-bx1
by2 =     0%-by1

% k1 = 147.15
% k2 = 147.15


%%% New springs
% former spring 3, now split in new spring 3 and 5

ax3 = 0
ay3 = -0.08
bx3 = -0.15
by3 = 0

ax5 = 0
ay5 = -ay3
bx5 = -0.15
by5 = 0

k3 = (k1 +k2)*-L2/(2*bx3)  % factor 1/2 as form 1 to 2 springs, factor -L2/bx3 ...
    because changed bx2
k5 = (k1 +k2)*-L2/(2*bx3)
```

```
206
207
208 % spring 4
209
210 ax4 = 0
211 ay4 = 0.08
212 bx4 = 0
213 by4 = 0
214
215 k4 = (m2 * g * (L2-sx2)/L2)/ay4
216
217
218 %%%
219 Methode_xy_evalsubs
220 k3 = eval(subs(k3))
221 k5 = eval(subs(k5))
222
223
224
225 % plots
226 plot_links_xy
227
228 %plot Z1 and Z2
229 A1 = [ax1;ay1]
230 A2 = [ax2;ay2]
231 A3 = [ax3;ay3]
232 A4 = [ax4;ay4]
233 A5 = [ax5;ay5]
234
235
236 Z3 = (A1*k1+A2*k2+A3*k3+A4*k4+A5*k5-[0;(m2+m3)*g])/(k1+k2+k3+k4+k5)
237 Z4 = (A1*k1+A2*k2+A3*k3+A4*k4+A5*k5)/(k1+k2+k3+k4+k5)
238
239 plot(Z3(1), Z3(2),'oc','linewidth',3)
240 plot(Z4(1), Z4(2),'oy','linewidth',3)
241
242
243
244 %% %%%%%%%%%%%%%%%%%%%%%%%% STEP 4: Replace spring 4 and 5 by new spring 4 ...
        %%%%%%%%%%%%%%%%%%%%%%%%%%
245 clearvars -except L8 %except a symbolic parameter, prevents symbolic toolbox to restart
246 % make constraint equations
247 springs = [1,3;1,3;1,2;1,2];
248 Methode_xy_fun
249
250 % Constant parameters
251 m2 = 2; m3 = 2;
252 L2 = 0.3; L3 = 0.3;
253 sx2 = double(L2/2); sx3 = double(L3/2);
254 sy2 = 0; sy3 = 0;
255 g=9.81;
256
257 % Variabel S2
258 r = sx2
259
260 % angle beta
261 beta =0/180*pi %%%%%%%%%%%%%%%%%%%%%%%%%%%%%%%%%%%%%%%%%%%%%%%%%%%%%%%%%%%%
262
263 Rot_beta = [cos(beta), -sin(beta);sin(beta), cos(beta)]
264
265 S2new = Rot_beta*[r;0]
266 sx2 = S2new(1)
267 sy2 = S2new(2)
268
269 % angle alpha
270 alpha = 0/180*pi; %%%%%%%%%%%%%%%%%%%%%%%%%%%%%%%%%%%%%%%%%%%%%%%%%%%%%%%%
271 Rot = [cos(alpha), -sin(alpha);sin(alpha), cos(alpha)];
272 B1 = Rot*[0.05;0] % point B1 rotated with angle alpha
273
274 % parameters
275 ax1 =   0
```

```
ay1 =    0.08
ax2 =   0
% ay2 =   -0.1

bx1 =    0.04%B1(1)
by1 =     0%B1(2)%0.0

bx2 =   -0.03%-bx1
by2 =     0%-by1

% k1 = 147.15
% k2 = 147.15


%%% New springs
% former spring 3, now split in new spring 3 and 5

ax3 = 0
ay3 = -0.08
bx3 = -0.15
by3 = 0

% ax5 = 0
% ay5 = -ay3
% bx5 = -0.15
% by5 = 0
%
k3 = (k1 +k2)*-L2/(2*bx3)  % factor 1/2 as form 1 to 2 springs, factor -L2/bx3 ...
    because changed bx2
% k5 = (k1 +k2)*-L2/(2*bx3)


% spring 4

ax4 = 0
ay4_old = 0.08
ay4 = 0.08
% bx4 = 0
by4 = 0

k4_old = (m2 * g * (L2-sx2)/L2)/ay4_old

k4 = k4_old + k3
bx4 = k3/(k3+k4_old)*bx3
% by4 = 0
% ax4=0
% ay4 = 0.08

%%%
Methode_xy_evalsubs
k3 = eval(subs(k3))
k4 = eval(subs(k4))
bx4 = eval(subs(bx4))



% plots
plot_links_xy

%plot Z1 and Z2
A1 = [ax1;ay1]
A2 = [ax2;ay2]
A3 = [ax3;ay3]
A4 = [ax4;ay4]


Z3 = (A1*k1+A2*k2+A3*k3+A4*k4-[0;(m2+m3)*g])/(k1+k2+k3+k4)
Z4 = (A1*k1+A2*k2+A3*k3+A4*k4)/(k1+k2+k3+k4)

plot(Z3(1), Z3(2),'oc','linewidth',3)
plot(Z4(1), Z4(2),'oy','linewidth',3)
```

```
346
347 %% %%%%%%%%%%%%%%%%%%%%%%%% STEP 5: Variate values %%%%%%%%%%%%%%%%%%%%%%%%%%
348 clearvars -except L8 %except a symbolic parameter, prevents symbolic toolbox to restart
349 % make constraint equations
350 springs = [1,3;1,3;1,2;1,2];
351 Methode_xy_fun
352
353 % Constant parameters
354 m2 = 2.15; m3 = 1.87;
355 L2 = 0.32; L3 = 0.29;
356 sx2 = 0.144; sx3 = 0.1864;%double(L3/2);
357 sy2 = 0; sy3 = 0;
358 g=9.81;
359
360 % Variabel S2
361 r = sx2
362
363 % angle beta
364 beta =0/180*pi %%%%%%%%%%%%%%%%%%%%%%%%%%%%%%%%%%%%%%%%%%%%%%%%%%%%%%%%%%%%
365
366 Rot_beta = [cos(beta), -sin(beta);sin(beta), cos(beta)]
367
368 S2new = Rot_beta*[r;0]
369 sx2 = S2new(1)
370 sy2 = S2new(2)
371
372 % angle alpha
373 alpha = 0/180*pi; %%%%%%%%%%%%%%%%%%%%%%%%%%%%%%%%%%%%%%%%%%%%%%%%%%%%%%%%%
374 Rot = [cos(alpha), -sin(alpha);sin(alpha), cos(alpha)];
375 B1 = Rot*[0.05;0] % point B1 rotated with angle alpha
376
377 % parameters
378 ax1 =   0
379 ay1 =    0.08
380 ax2 =   0
381 ay2 =   -0.08
382
383 % bx1 =    0.03%B1(1)
384 by1 =     0%B1(2)%0.0
385
386 bx2 =   -0.03%-bx1
387 by2 =     0%-by1
388
389 % k1 = 147.15
390 % k2 = 147.15
391
392
393 %%% New springs
394 % former spring 3, now split in new spring 3 and 5
395
396 ax3 = 0
397 ay3 = -0.08
398 bx3 = -0.08
399 by3 = 0
400
401 % ax5 = 0
402 % ay5 = -ay3
403 % bx5 = -0.15
404 % by5 = 0
405 %
406 k3 = (k1 +k2)*-L2/(2*bx3)  % factor 1/2 as form 1 to 2 springs, factor -L2/bx3 ...
        because changed bx2
407 % k5 = (k1 +k2)*-L2/(2*bx3)
408
409
410 % spring 4
411
412 ax4 = 0
413 ay4_old = 0.08
414 ay4 = 0.08
415 % bx4 = 0
```

```
by4 = 0

k4_old = (m2 * g * (L2-sx2)/L2)/ay4_old

k4 = k4_old + k3
bx4 = k3/(k3+k4_old)*bx3
% by4 = 0
% ax4=0
% ay4 = 0.08

%%%
Methode_xy_evalsubs
k3 = eval(subs(k3))
k4 = eval(subs(k4))
bx4 = eval(subs(bx4))



% plots
plot_links_xy

%plot Z1 and Z2
A1 = [ax1;ay1]
A2 = [ax2;ay2]
A3 = [ax3;ay3]
A4 = [ax4;ay4]


% Z1 = (A1*k1+A2*k2)/(k1+k2)
% Z2 = Z1 - [0;m3*g/(k1+k2)]
Z3 = (A1*k1+A2*k2+A3*k3+A4*k4-[0;(m2+m3)*g])/(k1+k2+k3+k4)
Z4 = (A1*k1+A2*k2+A3*k3+A4*k4)/(k1+k2+k3+k4)
% plot(Z1(1), Z1(2),'og','linewidth',3)
% plot(Z2(1), Z2(2),'or','linewidth',3)

plot(Z3(1), Z3(2),'oc','linewidth',3)
plot(Z4(1), Z4(2),'oy','linewidth',3)


[k1,k2,k3,k4]
```

BIBLIOGRAPHY

[1] J. L. Herder, *Energy-free Systems; Theory, conception and design of statically balanced spring mechanisms,* Ph.d. thesis, Delft University of Technology (2001), iSBN 90-370-0192-0.

[2] B. M. Wisse, W. D. van Dorsser, R. Barents, and J. Herder, *Energy-free adjustment of gravity equilibrators using the virtual spring concept,* in *Rehabilitation Robotics, 2007. ICORR 2007. IEEE 10th International Conference on* (IEEE, 2007) pp. 742–750.

[3] J. Gallego Sánchez, *Statically Balanced Compliant Mechanisms: Theory and Synthesis* (TU Delft, Delft University of Technology, 2013).

[4] G. Endo, H. Yamada, A. Yajima, M. Ogata, and S. Hirose, *A passive weight compensation mechanism with a non-circular pulley and a spring,* in *Robotics and Automation (ICRA), 2010 IEEE International Conference on* (IEEE, 2010) pp. 3843–3848.

[5] C.-W. Hou and C.-C. Lan, *Functional joint mechanisms with constant-torque outputs,* Mechanism and Machine Theory **62**, 166 (2013).

[6] K. Kobayashi, *Comparison between spring balancer and gravity balancer in inertia force and performance,* Journal of Mechanical Design **123**, 549 (2001).

[7] R. Sapper, *Lamp with an articulated support,* (1974), uS Patent 3,790,773.

[8] J. Wang and C. M. Gosselin, *Static balancing of spatial three-degree-of-freedom parallel mechanisms,* Mechanism and Machine Theory **34**, 437 (1999).

[9] H. Hilpert, *Weight balancing of precision mechanical instruments,* Journal of Mechanisms **3**, 289 (1968).

[10] S. K. Banala, S. K. Agrawal, A. Fattah, V. Krishnamoorthy, H. Wei-Li, J. Scholz, and K. Rudolph, *Gravity-balancing leg orthosis and its performance evaluation,* Robotics, IEEE Transactions on **22**, 1228 (2006).

[11] P.-Y. Lin, W.-B. Shieh, and D.-Z. Chen, *A theoretical study of weight-balanced mechanisms for design of spring assistive mobile arm support (mas),* Mechanism and Machine Theory **61**, 156 (2013).

[12] P.-Y. Lin, W.-B. Shieh, and D.-Z. Chen, *A stiffness matrix approach for the design of statically balanced planar articulated manipulators,* Mechanism and Machine Theory **45**, 1877 (2010).

[13] P.-Y. Lin, W.-B. Shieh, and D.-Z. Chen, *Design of statically balanced planar articulated manipulators with spring suspension,* Robotics, IEEE Transactions on **28**, 12 (2012).

[14] Y.-Y. Lee and D.-Z. Chen, *Determination of spring installation configuration on statically balanced planar articulated manipulators,* Mechanism and Machine Theory **74**, 319 (2014).